Drilling of Uni-directional Carbon Fibre Reinforced Plastics with Diamond Tools: Experiment and Finite Element Study

A thesis submitted in fulfilment of the requirements for the degree of Doctor of Philosophy

Sinan Jamal Al-Wandi

B.Eng. (Production Eng.), University of Technology

M.Eng. (Production Eng.), University of Technology

School of Engineering

College of Science, Engineering and Health

RMIT University

April 2018

Abstract

Carbon fibre reinforced plastics (CFRP) are increasingly being used in aerospace, automobile and sporting goods due to its high strength to weight ratios, high resistance to corrosion and low thermal expansion coefficient. One of the most extensively used processes in assembling CFRP components is drilling operation. Different challenges are faced when drilling CFRP, among which Peel-up and Push-out are two distinguishable delamination mechanisms associated with drilling of composite laminates, due to the extremely abrasive nature of the fibres. It is economically significant to have composite components free of delamination and a long drill life.

Owing to the ultra-hardness and superior wear resistance of diamond, polycrystalline diamond (PCD) tools are being used widely as one of the main solutions for drilling CFRP. In addition to the well known fact that diamond is the hardest material ever found or made, PCD has outstanding properties such as high thermal conductivity, low coefficient of friction and low thermal expansion. All of these properties are critical in drilling CFRP.

In addition to cost, there is lots of time wasted when investigating the drilling process experimentally due to the large number of parameters included such as tool types, material type and machining conditions. One of the advantages of utilizing Finite Element Method (FEM) is obtaining mechanical results and thermal behaviour of the drilling tool and workpiece used without investing lots of time and money with the experimental work. Hence manufacturing time and costs are reduced dramatically especially when the input values for the FEM are accurate.

In this research, a new 3D finite element model was developed in ANSYS-Explicit by implementing the ply-based modeling technology to simulate the drilling of unidirectional CFRP using PCD twist drill and a special diamond coated double point angle drill tool without using a back-up plate, and also for predicting the thrust force and torque at planned feed rate and speed combinations. The ply-based modeling technology was used to model the laminates and to validate if the meso-scale approach used in this research would be the ideal solution to characterize the drilling induced damage.

Hole quality has been investigated through delamination factors in this research experimentally and by finite element analysis, as they are calculated and compared to study the effect of operating parameters for twist drill and double point angle drill on the drilling induced damage. The delamination factor F_d and the adjusted delamination factor F_{da} have been used in the research, a new approach to measure the equivalent adjusted delamination factor F_{eda} was developed, all of these delamination factors have been compared.

Results show that the F_{eda} obtained is suitable to estimate the drilling induced damages, and feed rate is regarded as one of the parameters highly affect the drilling induced damage indicated from the experimental and simulation derived results.

Experimental drilling validation process was implemented by utilizing a CNC machining centre, force-torque dynamometer and charge amplifier to measure drill torque and forces. While a Philips XL30 scanning electron microscopy (SEM) and a Leica optical microscope were used in obtaining the images of the delaminated vicinity of entrance of the holes drilled, software "Image J" was utilized to process the image of delaminated areas.

Declaration

I certify that except where due acknowledgment has been made, the work is that of the author alone; the work has not been submitted previously, in whole or in part, to qualify for any other academic award; the content of the thesis is the result of work which has been carried out since the official commencement date of the approved research program; any editorial work, paid or unpaid, carried out by a third party is acknowledged; and, ethics procedures and guidlines have been followed.

I acknowledge the support I have received for my research through the provision of an Australian Government Research Training Program Scholarship.

Sinan Al-Wandi

April 2018

Acknowledgments

First and foremost, I would like to thank and sincerely show my gratitude for the grateful support of my supervisors Dr. Songlin Ding and Prof. John Mo. Their expertise, input and advice have been ordinarily valuable for my whole research program.

I would like to express my gratitude towards RMIT University, the personnel at Advanced Manufacturing Laboratory and at the Microscopy and Microanalysis Facility (RMMF) for providing me with facilities to undertake this Ph.D program.

Furthermore, this thesis work is dedicated to my wife, Sura, who has been a constant source of support and encouragement during the entire study, I am truly thankful for having her in my life, also would like to dedicate this work to my children Sama and Samer.

This work is also dedicated to my mother and late father (Prof. Jamal Hussein Al-Wandi), whom they have always encouraged me to study and their good examples have taught me to work hard for the things that I aspire to achieve.

Lastly I would like to dedicate this work to my brothers and in-laws for their support and encouragement as well.

Publications

The following publications are associated with this research:

1. Al-wandi, S., Ding, S., & Mo, J. (2017). An approach to evaluate delamination factor when drilling carbon fiber-reinforced plastics using different drill geometries: experiment and finite element study. The International Journal of Advanced Manufacturing Technology, Vol. 93(9), pp. 4043-4061. doi:10.1007/s00170-017-0880-2.

2. Al-wandi, S., Pan, W., Ding, S., & Mo, J. (2016). Meso-scale modeling of the drilling of carbon fibre reinforced plastic: geometry and numerical Analysis. Universal Journal of Mechanical Engineering, Vol. 4, pp. 75-82. doi:10.13189/ujme.2016.040401.

3. Al-wandi, S., Ding, S., & Mo, J. (2015). Drilling of uni-directional carbon fibre reinforced plastics with PCD tools: experiment and finite element study. Journal of Advanced Research in Applied Mechanics, Vol. 8(1), pp. 32-42.

4. Al-wandi, S., Ding, S., & Mo, J. (2015). Drilling of uni-directional carbon fibre reinforced plastics with PCD tools: experiment and finite element study. World Virtual Conference on Applied Sciences and Engineering Applications, Johor Bahru, Malaysia, 27 – 29 March 2015.

5. Al-wandi, S., Pan, W., Ding, S., & Mo, J. (2016). Meso-scale modeling of CFRP: geometry and numerical analysis". The 4th Annual Conference on Engineering and Information Technology, Kyoto, Japan 29 – 31 March 2016.

6. Al-wandi, S., Ding, S., & Mo, J. Investigation of CFRP drilling without back-up plate using ply-based modeling technology. Proceedings of the Institution of Mechanical Engineers, Part B: Journal of Engineering Manufacture (In review).

7. Al-wandi, S., Ding, S., & Mo, J. Experiment and FEM comparative study to minimize delamination when drilling CFRP composites using design experiments. Journal of reinforced plastics and composites (In Writing).

Contents

List of Figures

List of Tables

NOMENCLATURE

$CFRP$	Carbon fibre reinforced plastics
$UDCFRP$	Uni-directional carbon fibre reinforced plastics
PCD	Polycrystalline diamond
FE	Finite element
FEM	Finite element method
F_d	Delamination factor
F_{da}	Adjusted delamination factor
F_{ed}	Equivalent delamination factor
F_{eda}	Equivalent adjusted delamination factor
CNC	Computer numerical control
SEM	Scanning electron microscope
HSS	High speed steel
Al	Aluminum
Ti	Titanium
WC	Tungsten carbide
FRP	Fibre reinforced plastics
MMC	Metal matrix composite
CMC	Ceramic matrix composite
ALE	Arbitrary lagrangian eulerian
RVE	Representative volume element
CD	Conventional drilling
UAD	Ultrasonically assisted drilling
OC	Orthogonal cutting
AIZ	Affected interface zone
Tg	Glass transition temperature
NDT	Non-destructive test
CT	Computerized tomography
σ	Normal stress
C	Stiffness tensor
ϵ	Normal strain

τ	Shear stress
E	Modulus of elasticity
γ	Shear strain
G	Shear modulus
υ	Poisson's ratio
Q	Reduced stiffness
$FSDT$	First-order shear deformation theory
$\overline{C}_{ij}$	Components of the 3-dimensional stiffness matrix
P	Particular part of the differential equation
u, v, w	Displacements in the cylindrical coordinate system
δ_m^f	Mixed-mode displacement at complete failure
δ_m^{max}	Maximum value of the mixed-mode displacement
δ_m^0	Effective displacement at the damage initiation
Gc	Energy dissipation
D_{max}	Maximum diameter
D_{nom}	Nominal hole diameter
A_{max}	Area related to the maximum diameter
A_{nom}	Area of nominal hole
F_a	Two dimensional delamination factor
A_d	Delaminated area
D_e	Equivalent delamination diameter
FEA	Finite element analysis
F_{tt}	Critical thrust force for twist drill
F_{dd}	Critical thrust force for double point angle drill
F_{tt1}	Thrust force for twist drill
F_{tt2}	Thrust force for double point angle drill
η	Effect of thrust force on delamination factor
F_{crit}	Critical thrust force for the onset delamination
G_{Ic}	Interlaminar fracture toughness in mode I
h	Uncut plate thickness
F_{dr}	Refined delamination factor
A_H	Heavy damage area
A_M	Medium damage area
A_L	Low damage area
F_{red}	Refined equivalent delamination factor
D_{re}	Refined equivalent diameter
f	Circularity of damaged zone around the drilled hole
P	Perimeter of the drilled hole
N_W	Numbers of the white pixels

N_B	Numbers of the black pixels
N_{BH}	Number of black pixels representing the drilled hole area

Chapter 1

Introduction

1.1 Introduction

Expanding request for high-performance, lightweight structures have stimulated a vigorous expanding development of fibre reinforced polymer composite laminates in a variety of industries such as aircraft, spacecraft, automobile, marine, chemical processing equipment and sporting goods [1]. CFRP have also been increasingly used in wind turbine blades especially for longer and wider blades to improve efficiency of wind turbine energy capture [2][3]. For the most part, components composed of composites are produced to a near-net shape, yet extra machining operations are frequently required to facilitate component assembly. Joining of composite parts to a structure regularly requires drilling openings in them, keeping in mind the end goal is to place rivets or bolts. Commonly drilling is utilized as a machining process to manufacture these holes [4].

However, the defects and damages, such as delamination, burr, microcracking, swelling, splintering and fiber pullout, are commonly visible after drilling. The delamination at hole vicinity on entrance and exit sides of workpiece are the most critical defects, this will result in reducing the bearing strength and therefore needs extra manufacturing operations to fix so as to extend the service life of the composite workpiece under fatigue loads. Several studies concluded that thrust force is the major factor for resulting drilling induced delamination as it mostly relies on several factors such as drill geometry, feed rate and drill materials [5].

The direct experimental approach to study machining processes is expensive and time consuming, especially when a wide range of parameters is included: tool geometry, materials, cutting conditions, etc. The alternative approaches are mathematical simulations where numerical methods are applied. Amongst the numerical procedures, the finite-element methods (FEMs) are the most frequently used [6]. There have been many different geometry drill bits such as twist drill, step drill, brad point drill, slot drill, straight-flute and core drill and made of different tool materials such as high speed steel (HSS), uncoated cemented carbides, coated cemented carbides, diamond coated and PCD, have been used to understand the drilling processes of composite laminates. Diamond drills have long been the preferred solution for the drilling of CFRP.

Due to the manufacturing requests, a solution for drilling a combination of different materials such CFRP stacked with aluminum (Al) and CFRP stacked with titanium (Ti) in one single drill operation is required with extra accuracy, minimal exit burr, minimal coolant usage and best surface finish, all this is required through the course of hundreds or thousands of holes in the least amount of time possible [7].

In this study a 3D finite element model for simulating the drilling process is developed to investigate the relative significance of the drilling parameters on thrust force and torque. Also we will characterize and quantify the drilling induced damage and do comparative analysis of different drills. This PhD project combines finite element analysis and experimental testing which are both performed in a step-wise process as shown by the flow-chart below (Figure1.1), as it can be seen CFRP layers were prepared first experimentally and in FE then drill bits are chosen for the drilling process, results are then obtained and compared between experimental work and FE.

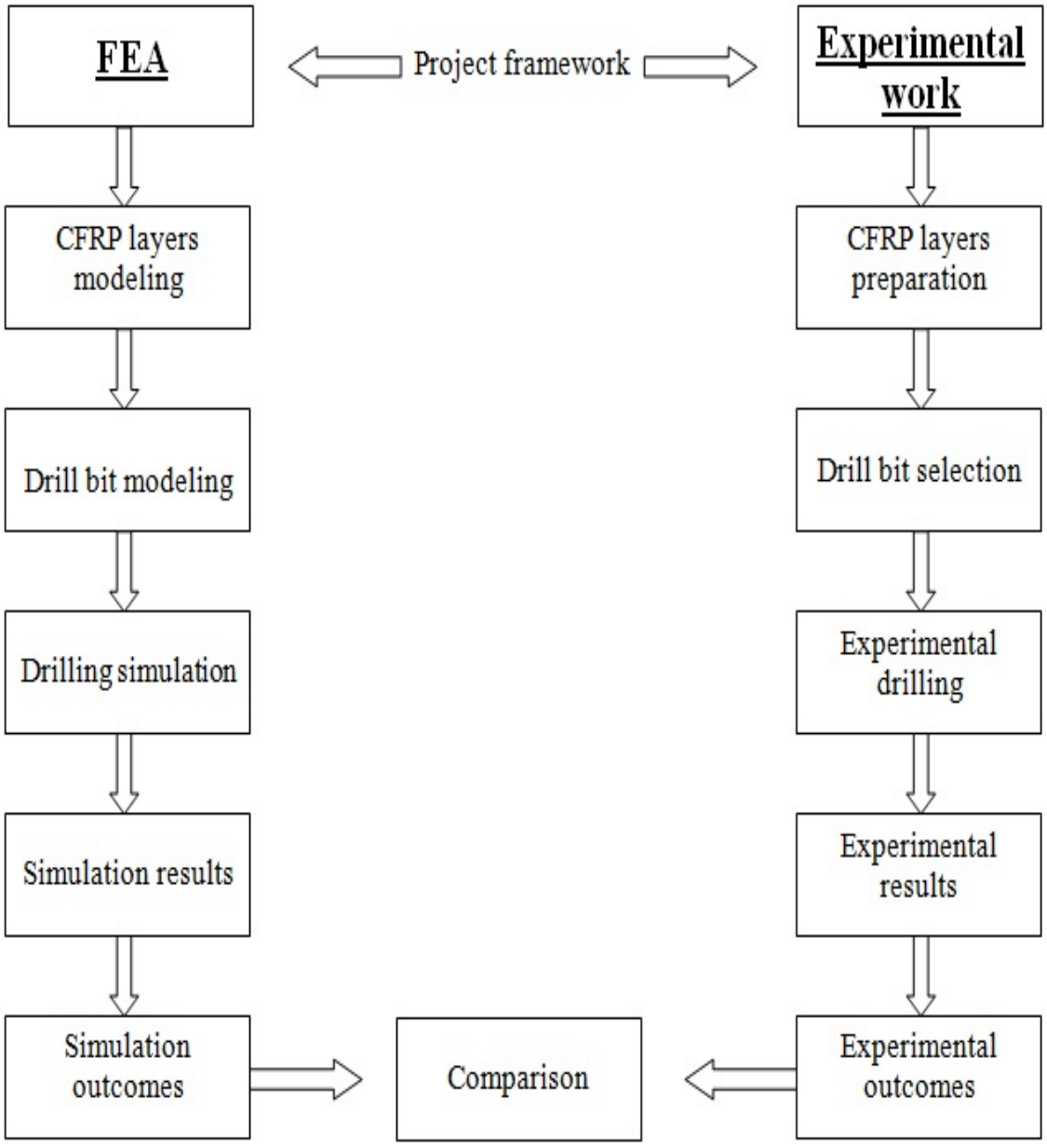

Figure 1.1: Flow-chart of the research.

1.2 Research gap and questions

The growing demand for composite materials such as CFRP due to its outstanding properties makes the machining of CFRP components a multi-billion dollar industry, but machining of composites is considered a dynamic, non-linear and very complex process and a significant percentage of the machined composite components are rejected in manufacturing process due to delamination induced during drilling and can be omitted when using the appropriate cutting tools and parameters. And the approach of utilizing non-destructive assessment is costly, tedious and often can't be implemented on structures placed in service due to the unavailability of hardware required to perform the test.

Also, another important factor which affects drilling of CFRP is the availability or absence of the back-up plate during drilling, as the absence of the back-up plate makes the drilling more complicated as the force applied from the drill bit acts as a punch especially when using high feed rates and not many researchers have eliminated the back-up plate during their study of drilling composites, so the question we raised in this case was what is the effect of the back-up plate absence when using different drill geometries during drilling.

Currently numerical modeling is utilized as a tool for a superior comprehension of machining of these composites, and numerical methods such as the finite element method uses elements from analytical models as constitutive relationships to develop detailed models of machining. These methods can provide detailed information on the drilling process and for this information to be accurate, it is important to setup the appropriate constitutive relationships which can be very labour intensive sometimes. Numerical methods are becoming effective tools to study manufacturing processes, therefore utilizing the correct finite element method is very critical, as there are several modeling methods have been implemented and studied but there is still a gap in finding the optimized modeling method which can give accurate data with less time consuming, hence one of the questions raised in this study was what is the best modeling approach.

Delamination not only affects the quality of hole but also sometimes leads to entire composite part failure under load, and calculating delamination factor is another research gap which has not been studied and several delamination factors have been proposed by many researchers but still there is no a standout delamination factor equation is used, as several researchers have used different delamination factors and had different outcomes, therefore the question raised was how to obtain better results when quantifying edge defects in CFRP Drilling.

The hypothesis of this research is that finite element modeling is significantly effective in studying and understanding the drilling process of CFRP without using the backup plate. Developing a new finite element model and a new delamination factor will enhance the analysis of drilling process and quantifying delamination factor.

1.3 Research objectives

The objective of this research is to study and analyze the drilling processes of carbon fibre reinforced laminates experimentally and analytically. The study was conducted to achieve the following objectives:

(i) Developing finite element model for simulating the drilling process, by modeling of composite layers using ANSYS and modeling the drill bit using Autodesk Inventor software. The finite element method can provide detailed information of the drilling process such as stress-strain behavior, temperature variations and crack propagation.

(ii) Investigating the relative significance of the drilling parameters on the thrust force and torque. Drilling induced damage can be reduced by optimizing the process parameters such as cutting speed and feed rate affecting the thrust force and torque.

(iii) Characterize and quantify the drilling induced damage, and propose a new approach for quantifying delamination factor. Visual examination is used initially to get an idea about the damaged area around the drilled hole. With the development of advanced methods and techniques of image based methods such as SEM and optical microscope, it is possible to quantify the damage in terms of certain geometrical features.

(iiii) Comparative analysis of different geometry drills made of diamond material, including analyzing the effect of critical thrust forces on drill bits.

1.4 Innovation and contributions

The main innovation and contributions of this thesis are summarized as follows:

(i) Developed a new FE model in simulation analysis of drilling of CFRP by applying ply-based modeling and meso-scale concept, and incorporating the flexibility of drill tool body to represent the actual changes of the materials physical properties during machining. The model makes the preparation and

definition of composite layups be shared and updated faster when product design changes are required.

(ii) Developed a new delamination factor called the equivalent adjusted delamination factor F_{eda} to obtain better delamination factors and make it suitable for hole entry delamination. Firstly we have implemented the equivalent delamination factor F_{ed} instead of the conventional delamination factor F_d and therefore it has a better discrimination of delamination damage results, and secondly to overcome the null critical cases of minimum or maximum delamination area arising from the adjusted delamination factor F_{da}.

(iii) For the first time, double point angle drill without using a backup plate was analyzed through FE simulation and validated with experimental results, the results show the significant affect of tool geometries on delamination.

1.5 Organisation of thesis

The thesis is organised as follows:

Chapter 2, highlights the literature review on CFRP and the various works done in the field of drilling composite laminates experimentally (with and without a backup plate) and through finite element analysis, the important types of drilling tools and their geometry which influences the machining of CFRP is discussed. Hole quality and drilling induced damage is presented in this chapter, a brief introduction on tool wear is also highlighted.

Chapter 3, a complete description of modeling and meshing of CFRP and drills using ANSYS Explicit is highlighted, as well as presenting the importance of using the ply-based modeling technique used to simulate the drilling process by utilizing the meso-scale method.

Chapter 4, presents the CFRP specimens, drilling tools (PCD twist drill and diamond coated double point angle drill) and the necessary equipments used in the drilling experiment which includes a CNC machining center and a digital signal processor (dynamometer), it also presents the equipments used in the microscopic observation of delamination (scanning electron microscopy SEM and optical microscope).

Chapter 5, damage methodology and an analysis on delamination is presented, while the types of delamination factors used in the studies are introduced. Also the proposed equivalent adjusted delamination factor F_{eda} has been presented and explained.

Chapter 6, discusses the results obtained from the drilling simulations and the experiments for PCD twist drill and diamond coated double point angle drill. It discusses the FE model validation for both drills by calculating the effects of feed rate and spindle speed on thrust force and torque during drilling of CFRP, also it highlights the results and effect of delamination factors used and compared in this study. FE stress analysis for workpiece and drill bits used have been discussed as well as workpiece displacement analysis has been presented, finally the effect of critical thrust force on drilling CFRP is highlighted.

Chapter 7, Summarizes the significant outcomes and contributions of this thesis, also possible future research works are discussed.

Chapter 2

Literature Review

2.1 Introduction

This chapter presents a review on CFRP and using diamond tools as machining process and focusing on the current technology methods in utilizing finite element method in simulating the drilling of CFRP.

The review in this chapter provides a scope on the characteristics and manufacturing of CFRP laminates, followed by the fundamental mechanical drilling of composites to understand the cutting mechanisms and the machining process. Thrust forces, torque and drilling induced delamination are also reviewed.

Finite element method is a unique tool to perform linear and non-linear analysis of reinforced composites to investigate the several aspects of responses when subjected to external loads, therefore, the current researches on the experimental and finite element studies on the drilling of fibre reinforced composites will be presented.

2.2 Carbon fibre reinforced plastics (CFRP)

The popularity of carbon fibre reinforced plastics (CFRP) in the aerospace industry has been increasing thanks to their desirable mechanical and physical properties. They show high resistance to corrosion and have low thermal expansion coefficient. In addition, CFRP is light and durable which allows manufacturers to produce lighter airplanes that consume less fuel [8]. In today's engineering world many classes of composite materials have emerged, including fibre reinforced plastics (FRP), natural fibre composites, metal matrix composites (MMC) and ceramic matrix composites (CMC). Composite materials in general exhibit inhomogeneity, anisotropy and non-ductile behavior. The inherent challenge in the machining of these composites is the attendant excessive tool wear and subsequent damage in the material sub-surface [9].

Although the methods used in studying the machining of composites have been diverse, generally they can be divided into three categories: experimental studies focusing on the macro/microscopic machinability of composites, simple modeling using conventional cutting mechanics and numerical simulations that treat the composite as a macroscopically anisotropic material or concentrate on reinforcement–matrix interaction microscopically. The macroscopic models normally ignore many fundamental characteristics of composites subjected to cutting and usually cannot provide the details of cutting mechanics and material behavior, while those focusing on micro-effects,including the analysis based on the finite element method, are tedious to implement. A sensible way would be to combine the merits of these methods to

develop realistic models that not only depict the material removal mechanisms in cutting, but also provide simple, predictive solutions for applications [10] [11].

2.2.1 Types of reinforcement in CFRP

Composite materials are usually classified according to the type of reinforcement used. Two broad classes of composites are fibrous and particulate. Each has unique properties and application potential, and can be subdivided into specific categories. A fibrous composite consists of either continuous (long) or chopped (whiskers) fibres suspended in a matrix material. A particulate composite is characterized as being composed of particles suspended in a matrix and have dimensions that are approximately equal in all directions. Particles can have virtually any shape, size or configuration such as concrete and particle board [12].

The reinforcing phase provides the strength and stiffness. In most cases, the reinforcement is harder, stronger, and stiffer than the matrix. Particulate composites tend to be much weaker and less stiff than continuous fibrous composites, but they are usually much less expensive. Particulate reinforced composites usually contain less reinforcement (up to 40 to 50 volume percent) due to processing difficulties and brittleness. Examples of continuous reinforcements include unidirectional, woven cloth, and helical winding (Figure 2.1(a)), while examples of discontinuous reinforcements are chopped fibres and random mat (Figure 2.1(b)). [13].

A fibre has a length that is much greater than its diameter. In the case of fibres length and diameter, their dimensions are characterized by the aspect ratio l/d, where l is the fibre length and d is the diameter [14]. Continuous fibres have long aspect ratios, while discontinuous fibers have short aspect ratios, continuous fibre composites normally have a preferred orientation, while discontinuous fibres generally have a random orientation.

2.2.2 Material classification

Materials can be classified as either isotropic or anisotropic. Isotropic materials have the same material properties in all directions, and normal loads create only normal strains. By comparison, anisotropic materials have different material properties in all directions at a point in the body. There are no material planes of symmetry, and normal loads create both normal strains and shear strains. A material is isotropic if the properties are independent of direction within the material [13].

Figure 2.2 shows the anisotropic composite ply which has properties that vary with

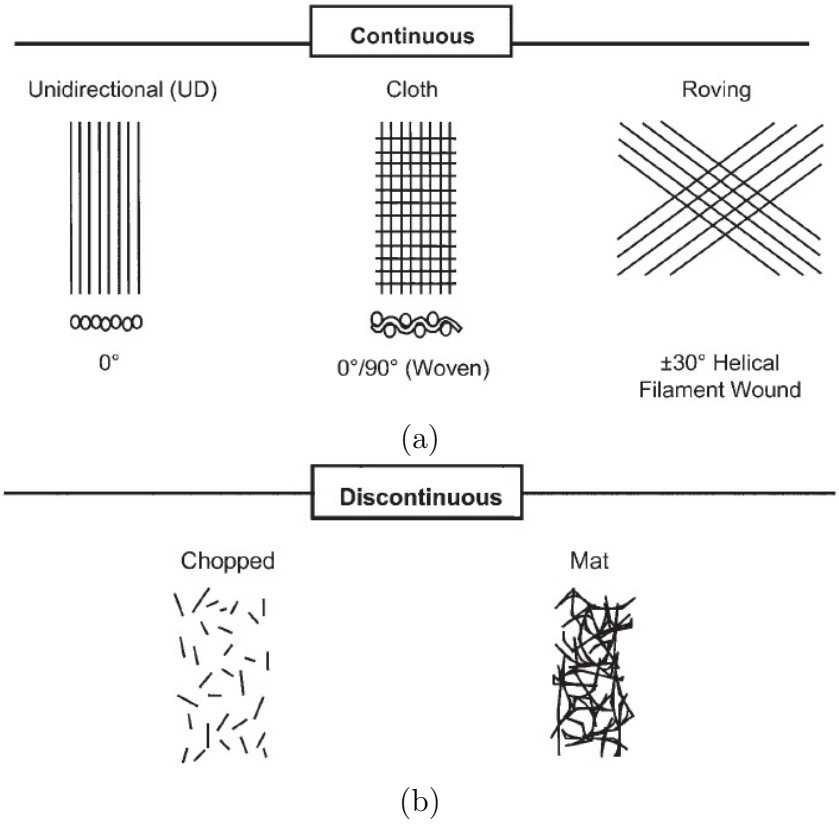

Figure 2.1: Typical reinforcement types in composites.

direction within the material. In this example, every modulus is different in each direction ($E0^o \neq E45^o \neq E90^o$). While the modulus of elasticity is used in the example, the same dependence on direction can occur for other material properties, such as ultimate strength, Poisson's ratio, and thermal expansion coefficient.

Most composites are a subclass of anisotropic materials that are classified as orthotropic. Orthotropic materials have properties that are different in three mutually perpendicular directions. They have three mutually perpendicular axes of symmetry, and a load applied parallel to these axes produces only normal strains. However, loads that are not applied parallel to these axes produce both normal and shear strains. Therefore, orthotropic mechanical properties are a function of orientation.

When the plies are stacked at various angles, the lay-up is called a laminate. If all of the layers or plies are stacked in the same orientation, the lay-up is called a lamina. Continuous fiber composites are normally laminated materials. It is usually necessary to balance the load-carrying capability in a number of different directions, such as the 0^o, $+45^o$, -45^o, and 90^o directions [15].

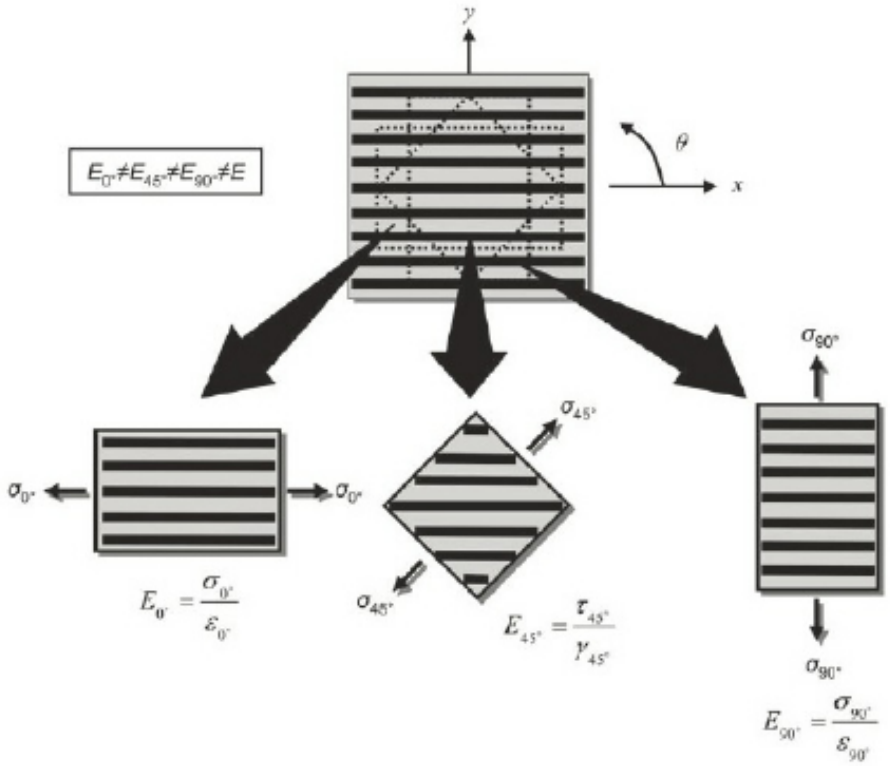

Figure 2.2: Element of composite ply material under stress.

2.2.3 Manufacturing of composites

There are many manufacturing, fabricating, processing, and forming processes for composites. There are seven major processes by which polymer matrix composites are formed: (1) molding, (2) casting, (3) thermoforming, (4) expansion, (5) coating, (6) fabrication, and (7) radiation, and within each of these processes different techniques can be used.

For example, in the category of molding, there are 9 sub processes containing 16 subsets: Injection, coinjection, reaction injection, compression, caldenering, blow (extrusion-blow molding, injection-blow molding, stretch-blow molding, multilayer-blow molding), extrusion, laminating, reinforcing (match-die molding, hand layup, spray-up molding, vacuum bag molding, filament winding, continuous reinforcing, cold molding, cold forming/stamping, sintering, liquid-resin molding, vacuum-injection molding, thermal expansion resin transfer). The process selected for the production of a component depends on many variables and can influence the final product [12].

The simplest technique, and probably the first used to make a modern composite structure, utilizes manual placement of the fibres and is called layup, layup molding, or wet layup. Wet layup is the method of laying the dry reinforcement (most oftena

fabric or a mat) into the mold and then applying the resin is the oldest and, perhaps, the most common means of wet layup. The wet composite is rolled by hand to evenly distribute the resin and to remove air pockets. Another layer of reinforcement is laid on top. Then more catalyzed resin is poured, brushed, or sprayed over the reinforcement. This sequence is repeated until the desired thickness is reached. The layered structure is then allowed to harden (cure) (Figure 2.3) [16].

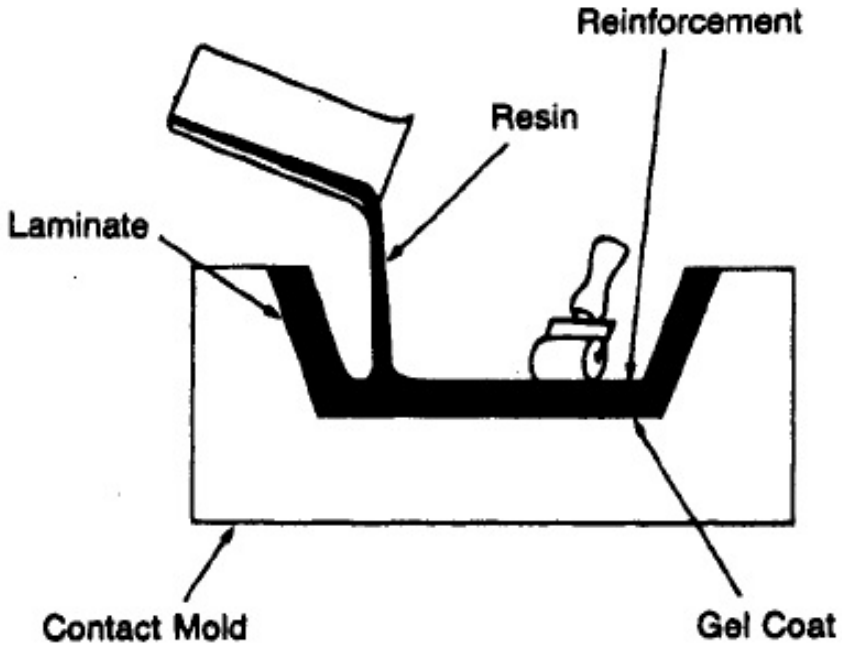

Figure 2.3: Wet Layup [16].

2.2.4 Prepreg technology

In the early 1980's prepregs were considered specialty materials, accounting for around 5% of an aircraft design and used only for non-critical secondary structures. Today prepregs are baseline for aircraft primary structures and constitute more than 50% of the airframe of the Airbus A350 XWB and Boeing 787. The growth in aerospace and other industries including wind energy, automotive, sports goods and industrial machinery has followed. More recent applications benefitting from prepreg include subsea tubes for oil and gas exploitation and high pressure vessels. This growth in the use of prepreg composites over metal has been driven by higher strength to weight performance, better fatigue strength and potential to offer greater freedom of design [17]. A pre-preg can be made incorporating a variety of reinforcement fabrics and fiber types. Although it can be produced by the component fabricator, it is normally purchased from a materials-supply company, mainly woven hi-directional cloth pre-preg and Unidirectional pre-preg are material forms are available as carbon/epoxy pre-pregs.

Unidirectional pre-preg is made by spreading and collimating many fiber tows (typically around 104 fibers in each tow) into a uniform sheet of parallel fibers typically 0.125-0.25 mm thick and 300 or 600 mm wide. This is immediately pre-impregnated. Unidirectional pre-preg is the cheapest to make, and it provides laminates with the best mechanical properties.

The pre-preg with its non-stick backing films is then inspected for resin content, which is typically between 34% and 42% by weight for carbon prepregs, wound onto a roll, and sealed to prevent the absorption of water vapor as illustrated in Figure 2.4 [18].

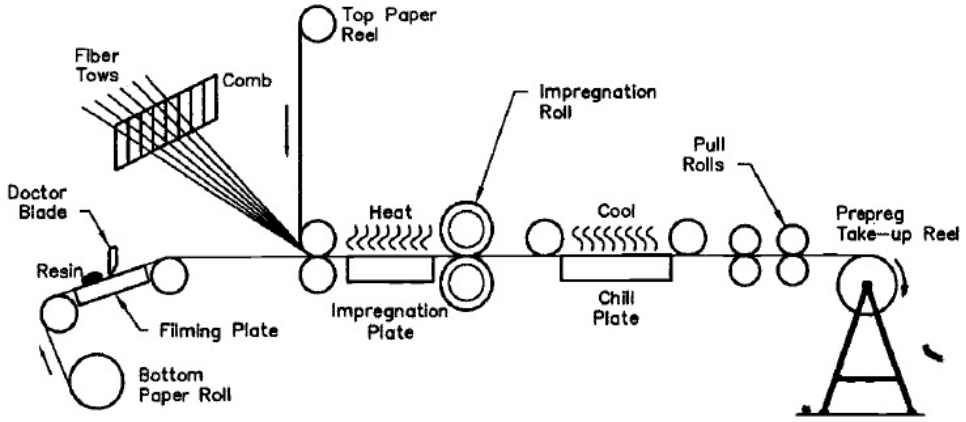

Figure 2.4: Schematic illustration of Hot-Melt film Pre-Pregging process [18].

2.2.5 Vacuum bag/oven or autoclave

Vacuum bag/oven and autoclave processing are the two main methods for the manufacture of components from prepreg. The processing method is determined by the quality, cost and type of component being manufactured. The vacuum bag technique involves the placing and sealing of a flexible bag over a composite lay-up and evacuating all the air from under the bag (Figure 2.5).

The removal of air forces the bag down onto the lay-up with a consolidation pressure of up to 1 atmosphere (1 bar). The completed assembly, with vacuum still applied, is placed inside an oven or on a heated mould with good air circulation, and the composite is produced after a relatively short cure cycle.

The autoclave technique requires a similar vacuum bag (Figure 2.6) but the oven is replaced by an autoclave. The autoclave is a pressure vessel which provides the curing conditions for the composite where the application of vacuum, pressure, heat up rate and cure temperature are controlled. High processing pressures allow the moulding of thicker sections of complex shapes. Long cure cycles are required

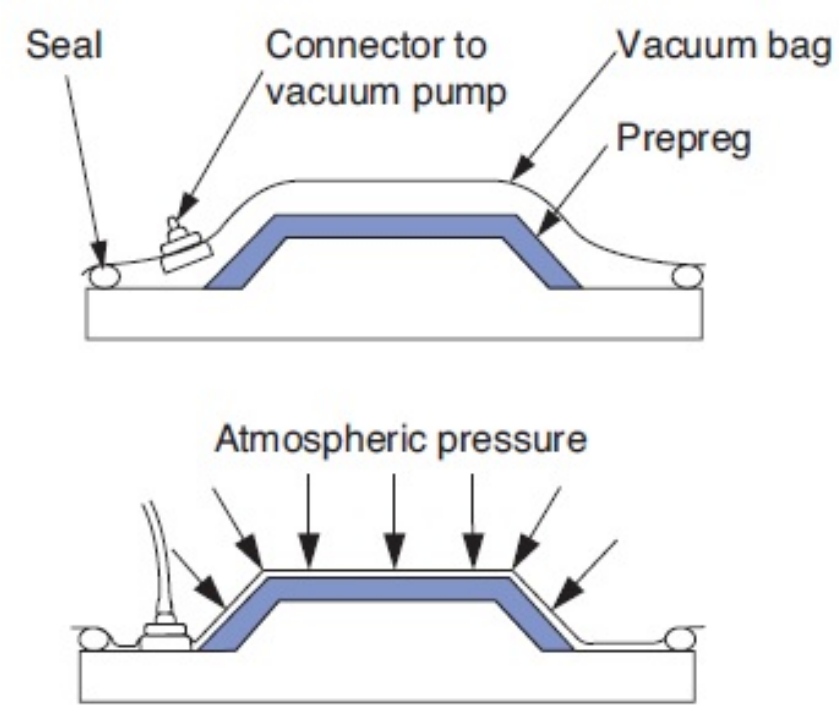

Figure 2.5: Sealing flexible bag over lay-up and applying vacuum to the system [17].

because the large autoclave mass takes a long time to heat up and cool down. Sometimes slow heat up rates are required to guarantee even temperature distribution on the tooling and composite components [17].

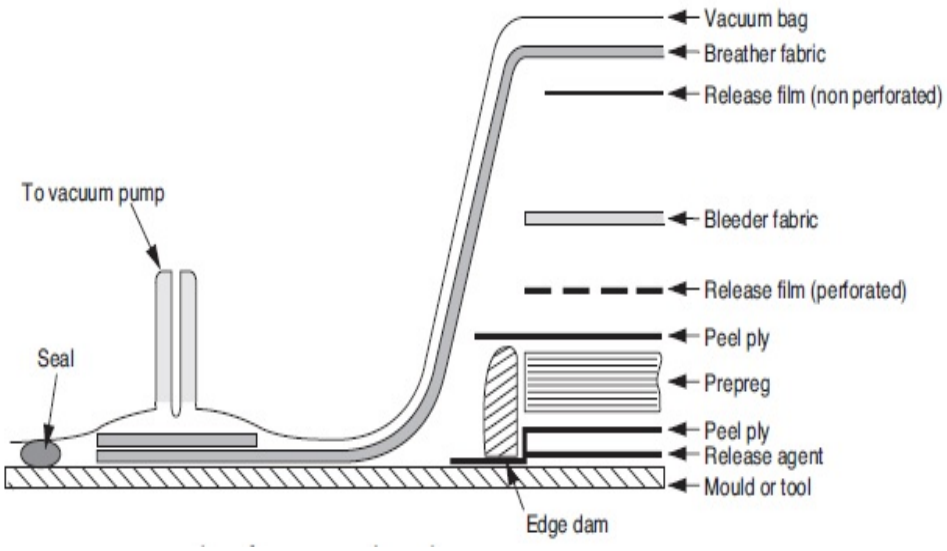

Figure 2.6: Example of vacuum bag lay-up [17].

2.3 Drilling of carbon fibre reinforced polymers

As parts in composite materials are to be usually assembled in complex structures, joining of these parts is always needed. Drilling is the most common machining operation in industry. Drilling is a complex process, characterized by the existence of extrusion and cut mechanisms. The former is performed by the drill chisel edge that has null or negligible linear speed and the latter by the existence of rotating cutting lips at a certain speed. The most common drill is the conventional conical point drill. The cutting process is unique and can be divided into two distinct regions: chisel edge and cutting lips. In a common drill, there is a small region around the centre of the chisel edge, called the indentation zone, where the tool does not cut the material, but extrudes it instead. At the region outside the indentation zone, called the secondary cutting edge area, the rake angle is highly negative. As fibre reinforced plastics are more brittle than metals, it is unlikely that extrusion really takes place [19].

Drilling of these composite materials, irrespective of the application area, can be considered a critical operation owing to their tendency to delaminate when subjected to mechanical stresses. With regard to the quality of machined component, the principal drawbacks are related to surface delamination, fibre/resin pullout and inadequate surface roughness of the hole wall. Among the defects caused by drilling, delamination appears to be the most critical.

In order to overcome these difficulties it is necessary to develop procedures to select appropriate cutting parameters, due to the fact that an unsuitable choice could lead to unacceptable work material degradation.

Figure 2.7 shows that factors such as cutting parameters and tool geometry/material must be careful selected aiming to obtain best performance on the drilling operation, i.e., best hole quality, which represents minimal damage to the machined component and satisfactory machined surface [20].

Rakesh et al. [21] developed a finite element model in order to investigate the drilling behavior of FRPs, they have concluded the drill point geometry plays a significant role in defining the damage characteristics while drilling in FRP laminates.

A judicious selection of the drill point geometry on the basis of work-piece material will lead to production of damage free holes. Strenkowski et al. [22] described a three-dimensional drilling model to determine the thrust force and torque in drilling process. They predicted the forces can be readily coupled with solid models, so that complex drill geometries can be accurately represented. Barschke et al. [23] presented simulations of the behavior of composite materials based on kinematic

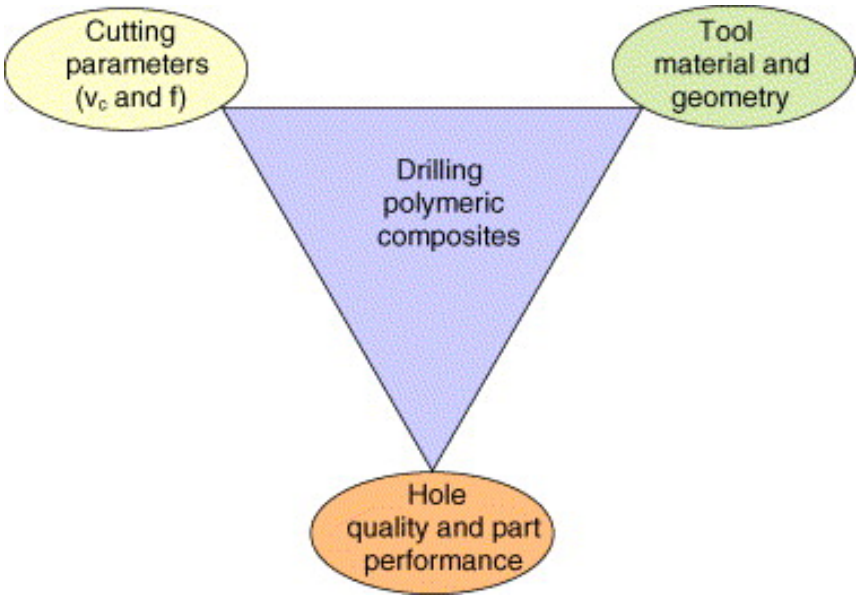

Figure 2.7: Principal aspects to be considered when drilling fibre reinforced plastics.

restrictions among the fibers themselves and among fibers and the surrounding resin, the approach was used to obtain the material properties for a two layered material which can be applied to a three dimensional structures.

Durao et al. [24] studied the effect of two variables on the drilling process of composite materials: the tool material and the tool geometry. Two tool materials – tungsten carbide (WC) and PCD – with the same twist drill geometry were evaluated; and three different tool geometries of the WC drills – twist, Brad, and step, were assessed, results show that feed rate is the most important factor for delamination reduction, followed by tool geometry. Zhou et al. [25] carried out a two-dimensional orthogonal cutting experiments and simulation analysis on the machining of SiCp/Al composites with a polycrystalline diamond tool, the results indicate that the cutting speed and depth have significant effects on the cutting force, and the predicted cutting force is in agreement with that of the experiment.

Persson et al. [26][27] investigated the effects of hole machining defects on static strength and fatigue life of carbon/epoxy composite laminates. Traditional drilling processes were implemented using polycrystalline diamond-tipped drill (PCD) and cemented carbide drill with a sharp tip angle (Dagger drill). They reported that hole machining defects significantly reduced the static strength of pin-loaded PCD specimens about 11% compared to defect-free holes specimens, while this reduction percent become 2–3% for Dagger specimens. The fatigue strength at 106 cycles was, respectively, reduced to about (19–27%) and (9–11%) for PCD and Dagger specimens compared to defect-free holes specimens.

2.4 Drilling tools

There have been many different geometry drill bits made of different tool materials used in drilling of composite laminates, as shown in (Figure 2.8) below. It has been found that drilling induced damage can be reduced by modifying the drill point geometry, the drill bits used could be divided into six categories (1)Twist drill bit, (2) Step drill bit, (3) Brad point drill bit, (4) Slot drill bit, (5) Straight-flute drill bit, and (6) Core drill bit. Different drill bits such as high speed steel (HSS), uncoated cemented carbides (ISO grades K10, K20, etc.), coated cemented carbides, and PCD, have been used to understand the drilling processes of composite laminates [1].

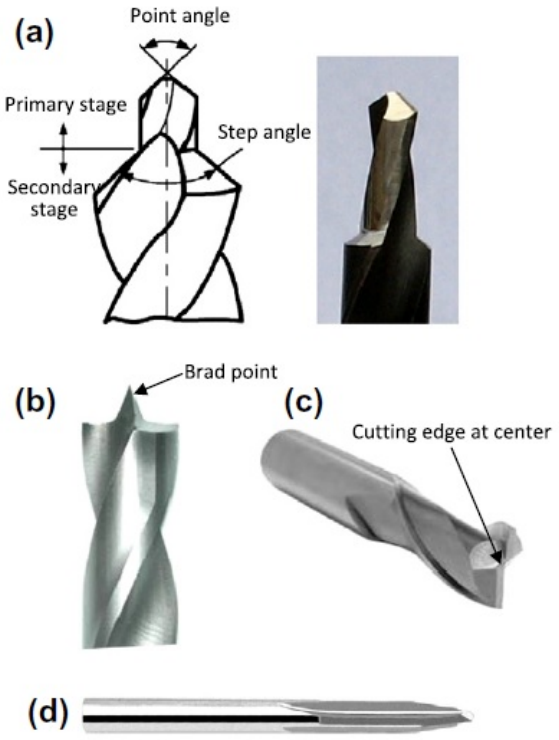

Figure 2.8: (a) Step drill bit. (b) Brad point drill bit. (c) Slot drill bit. (d) Straight-flute drill bit. [1] [28] [29].

2.4.1 Twist drill geometry

Drilling is among the most difficult machining processes because of chip-flow restrictions, poor heat dissipation, and rapid wear, which severely limits the productivity. Drilling constitutes about 40% of all metal-cutting operations, and 50 to 70% of all production time is spent on making holes [30].

The drill bit is a complicated structure and among all the elements of drill geometry (Figure 2.9), the most important are lips, chisel edge, web, helix angle, point angle,

chisel edge angle and clearance angle. The lips do the main cutting action, while the web together with the chisel edge does the extrusion action during drilling. Helix angle practically determines the rake angle at the cutting edge of the drill. The helix angle is chosen such that there is a compromise between the strength of the cutting edge and efficient chip ejection through the flutes. Point angle is the angle formed by the two flank surfaces with that of the axis of the drill. The chisel edge angle is the angle between the chisel edge and the cutting lip as viewed from the end of the drill. The clearance angle at any point on the lip is the angle between the tangent to the flank and the tangent to the surface of revolution at that point [31].

Even today, more than 200 years from the date of invention, the design of an efficient and powerful twist drill is still a very difficult task. The complex geometry compared to other types of cutting tools incorporates numerous conflicts of design objectives such as low cutting forces, wear resistance, torsional and axial stability, chip evacuation capability and more. Handling those interdependencies requires a high level of experience from the tool designer. Most approaches of simulation-based drill design focus on a limited number of geometrical aspects such as optimization of cross section geometry or optimization of drill point grinding parameters [32].

2.4.2 Double point angle drill geometry

An example of the geometry of the double point angle drill is shown in Figure 2.10, it shows the helix angle θ, the rake angle ρ, and the clearance angle γ of the drill, it also shows the differential cutting dFc, thrust dFz and tangential dFt forces acting on the drill. Multiplying the differential cutting force and the distance from the center gives the differential torque. Adding together all differential thrust forces and torques along the cutting edges yields total torque and thrust force during drilling [33].

2.5 Tool wear

Tool wear in CFRP machining is quite different than that in conventional metal machining. In conventional metal machining, crater and flank wear were the dominant wear types. In contrast, the primary tool wear type is edge rounding when machining CFRP. To understand the edge rounding wear in CFRP machining is to discuss the reason for not having edge rounding wear in conventional metal machining. In metal machining the edge of a cutting tool, is covered by the work material, known as the stagnation zone, which protects the cutting edge from the excessive mechan-

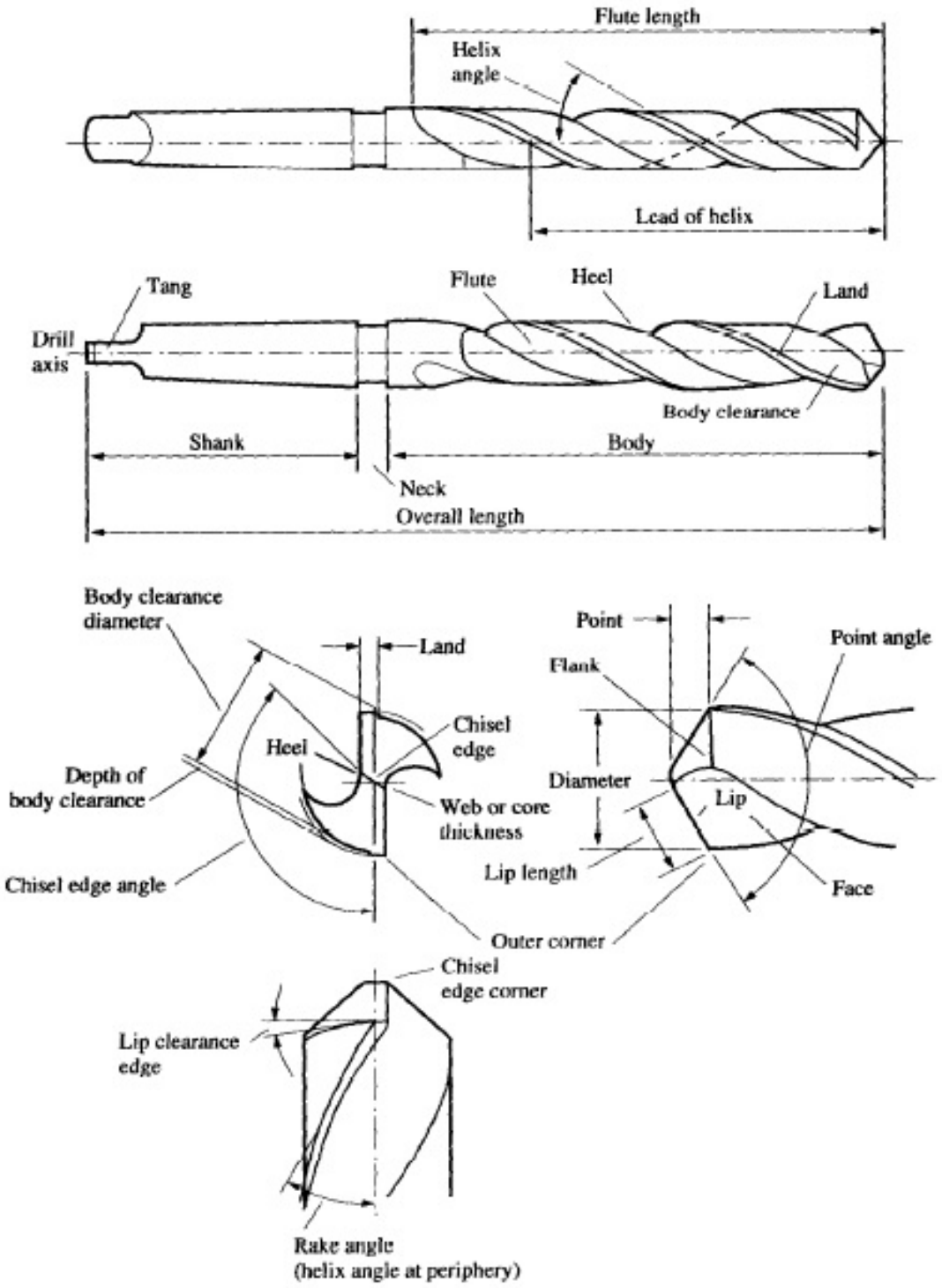

Figure 2.9: Twist drill geometry [31].

ical wear. Depending on the friction and other parameters during machining, the stagnation zone may contain a "dead metal" that sticks on the top of the cutting edge, the work material is being separated around the stagnation point either to form chip or to become the new surface of the work piece [34].

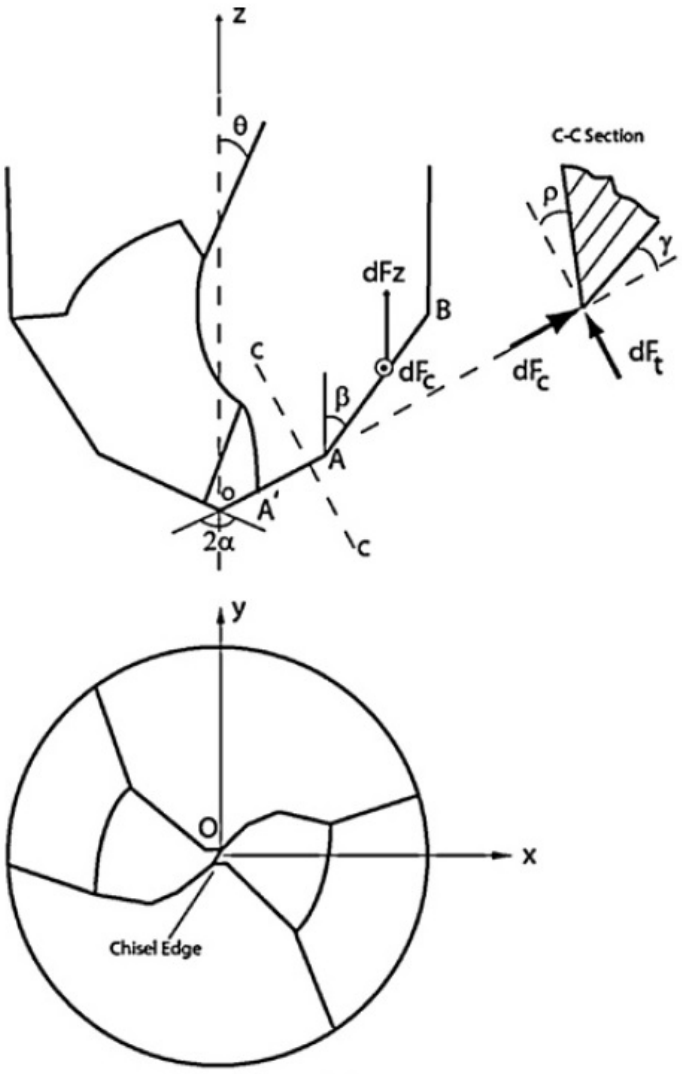

Figure 2.10: Double point angle drill geometry [33].

CFRP is a highly abrasive material, which, depending on the direction of the fibre in the matrix will produce severe tool wear. Unlike metals, CFRP cutting involves not only tool edge chipping but also excessive abrasive wear due to the hard carbon fibres [35, 36, 37, 38, 39]. Thus, the choice of the cutting tool and the optimal cutting parameters is very important when cutting this kind of materials. The machining process affects significantly these materials leading to various modes of damages. This damage consists of various fibre breakage, matrix cracking, fibre–matrix debonding and plies delamination [40].

PCD tools have high wear resistance to abrasive materials due to its high hardness, and hence they are generally preferred and used when cutting composites [41, 42, 43, 44]. Because of the low of wear rate of PCD drills, the composite material will have a better hole quality when compared with High Speed Steel (HSS) and Tungsten Carbide (WC) drills when drilling CFRP composites. It was also concluded that there will be little amount of microchipping exists when drilling CFRP composites

when utilizing a PCD drill [45], but due to its superior wear resistance, PCD drills have been the preferred tool for drilling CFRP even though if it has high cost and as long as the chipping is reduced [7].

2.6 Hole quality, drilling induced delamination and delamination detection methods

2.6.1 Hole quality

The quality of the drilled holes depends on drill geometry and process parameters (cutting speed and feed rate of the drill). The geometry of the drill plays an important role in deciding the hole quality. Very rapid tool wear due to abrasive carbon fibres is the primary reason for poor hole quality. Tool wear also results in frequent tool changes affecting the cycle time and raising the production cost. The need therefore arises to thoroughly investigate drill bit performance to produce good quality holes [46].

Hole quality in composite drilling consists of a number of output parameters including material integrity, hole diameter, surface texture, delamination, exit burrs of drilled holes. Delaminations and exit burrs can be classified as exit hole damage which is very critical in structural durability of the composite structures [47].

The inhomogeneity of FRPs caused by the difference in properties of the fibre and the matrix materials will result in a machined surface that is less regular and is usually rougher in comparison with machined metal surfaces. Therefore, the evaluation of the quality of drilled fastener holes must include both the general geometry of the hole and the condition of the hole surface [48].

Shyha et al. [49] outlined the analysis of hole quality/integrity following drilling of titanium/CFRP/aluminium stacks with uncoated and coated CVD diamond and hard metal tungsten carbide drills. The results showed that the delamination of CFRP laminates were considerably decreased due to the Al and Ti supported layers, only few damage areas was observed around the hole edges of the CFRP caused by sharp Ti exit burrs. Brinksmeier et al. [50] discussed the thermal and mechanical impact of orbital drilling and conventional drilling techniques on the borehole surface in multi-layer materials (aluminum, CFRP, and titanium materials). The orbital drilling of Al/CFRP/Ti composites showed better quality results than CFRP composites when using conventional drilling at boreholes in regards to surface integrity.

2.6.2 Drilling induced delamination

Delamination during drilling in composite laminates can be an outcome of two types of damage mechanisms that are different in their causes and effects, usually known as peel-up delamination and push-down delamination [51] as shown in Figure 2.11.

The former is a consequence of the drill entering the upper plies of the plate and the cutting edge of the drill abrades the laminate. The material spirals up along the flute before being effectively cut. This action can be avoided with the use of low feeds. On the other hand, the latter mechanism is a result of the indentation effect caused by the quasi-stationary drill chisel edge, acting on the uncut plies of the laminate. The cause of this damage mechanism is the compressive thrust force, measurable during the drilling process, exerted by the drill on the uncut plies of the plate. As the uncut thickness approaches zero, the mechanical resistance of the plate decreases. At some point, this load exceeds the interlaminar fracture toughness of the laminate and the plies tend to be pushed away from the plate, causing the separation of two adjacent plies of the laminate and, consequently, delamination takes place [24].

In the literature, Durao et al. [19] studied the delamination assessment techniques based totally on radiographic information compared or correlated with mechanical test outcomes. They have concluded that an adequate feed rate and tool geometry combination should be used in order to eliminate delamination effects when drilling holes. Tsao et al. [5] described a novel method for reducing delamination through the use of active backup force during drilling of composites. The utilized backup force majorly suppressed the growth of delamination at drilling exit by $60-80\%$. To investigate the influence of tool geometry and cutting parameters on delamination, Grilo et al. [52] carried out an experimental assessment and found that both delamination factor and adjusted delamination factor were appropriate for delamination assessment in drilling CFRP.

To determine the optimal process parameter levels and to analyze the effect of parameters on delamination factor, Gaitonde et al. [53] introduced the methodology of Taguchi optimization approach for reducing the delamination at the hole entrance of CFRP composites when using high speed drilling, the results show that the most significant factor was the point angle then feed and spindle speed.

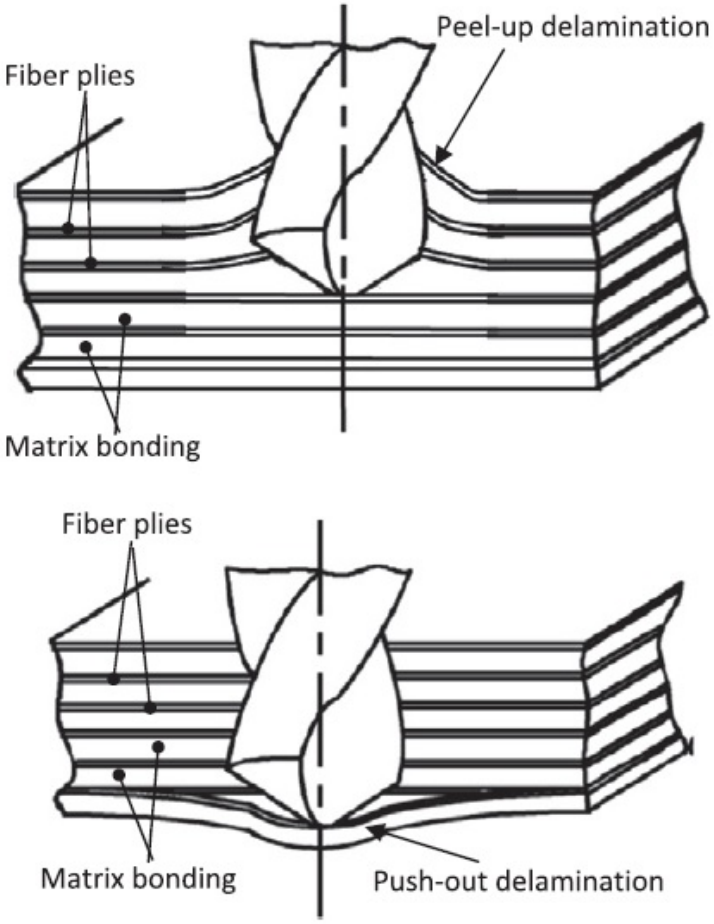

Figure 2.11: Mechanism of drilling induced delamination in CFRP a- Peel-up delamination b- Push-out delamination [1].

2.6.3 Delamination detection methods

Due to the negative impact of delamination on the structure of composite, non-destructive testing (NDT) of drilling induced delamination has been of great interest. Several methods such as visual inspection by low-magnification microscopy (partially combined with digital image processing), acoustic emission, X-Ray radiography, computed tomography (CT), ultrasonic testing (US) [54], eddy current technique (ECT), thermography, optical fibre sensors, digital image correlation (DIC), lamb waves and microwave techniques [55] are employed for the detection of size, shape and location of delamination damage.

The common methods to measure the extent of delamination have been summarized by Babu et al. [56]. The measurements are used to develop assessment factors, both dimensional and non-dimensional, for comparing delamination damage resulting from different machining methods and parameters.

2.7 Drilling of CFRP with and without a backup plate

One of the familiar ways of reducing delamination induced damages is to use a backup plate (supporting plate) under the bottom ply of the CFRP and therefore the critical thrust force will be increased, the backup plate can be also predrilled in the zone area where the hole will be drilled, using backup plates is a good way of reducing delamination but sometimes it becomes complex and not always feasible [57], Figure 2.12 shows an example of supported and unsupported drilling.

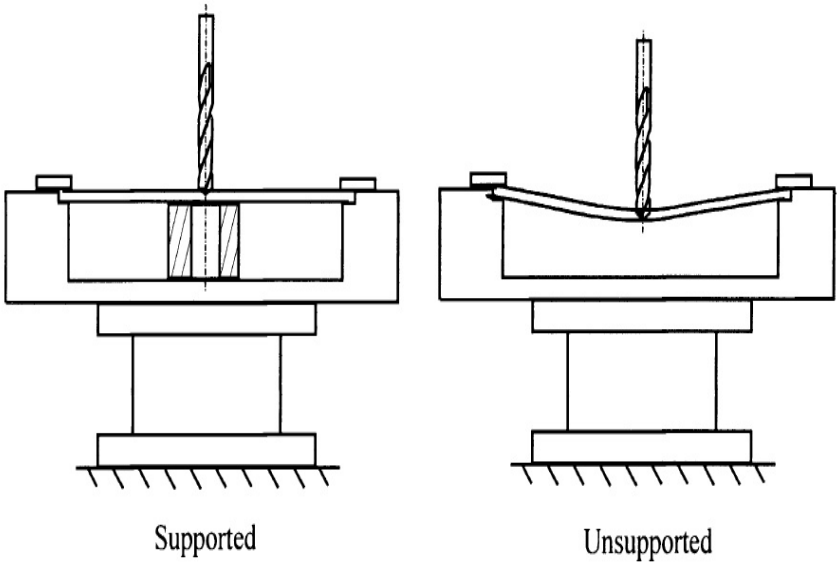

Figure 2.12: Supported and unsupported drilling [57].

At the beginning of drilling process when using a backup plate the thrust force intends to push and deflect the composite laminate downwards, while the backup plate intends to counteract the bending deflection by reacting as a uniform upward load applied underneath the workpiece, but this will not completely stop the bending deflection as a slight deflection will occur although the backup plate has much higher stiffness than the composite laminate.

During drilling the internal reaction force associated with the downward bending of the uncut laminate in the laminate will lift up the laminate from the outskirt of the circular crack, leaving the bottom side of workpiece in approximately point contact with the back-up material, this will lead to the uniform load changing to a concentrated load applied on the bottom center of the workpiece [58].

2.8 Finite element modeling

The finite element method is the computational tool most widely used to validate the performance of structures. It provides the analysis required for the design process. Typically it can be used to define the displacements, stresses, vibration, and buckling characteristics of a structure composed of metal or composite materials under a defined set of loads and displacement boundary conditions. It can either be applied at the macroscopic level to analyze the stiffness and strength of the complete structure, or it can be applied at the microscopic level to study the interface between fibre and resin. Finite element analysis procedures are either embedded inside the geometric modeling systems that carry the geometry database or are stand-alone packages capable of special analysis, such as post-buckling behavior or response to shock loading. The finite element analysis can be applied to assess structural performance, to form the geometric model to which an optimization algorithm is applied, or to provide simulations of molding processes and manufacturing strategies [18]. An accurate and reliable FE simulation of drilling enables good predictions of strain and stress distributions; cutting forces and torque; and discrete damage modes in composites by taking into account the complex drill geometry and process parameters. With the advent of high power computing facilities, simulation of the drilling process using FE analysis provides an excellent tool for this challenging problem in applied mechanics [59].

To analyze machining process in the experimental approach is considered tedious and costly especially when several parameters are included such as cutting conditions, tool geometry and materials. The finite element analysis (FEA) method is an alternative approach which is able to provide an insight of the cutting process, and is very much required for a reliable prediction and optimal stress and damage results [60].

Diamond tipped tools have been used in micro-scale cutting to withstand tool wear and ensure a successful machining process. While experimental investigation of micro-scale cutting is necessary for improving the process and developing new knowledge in ultra-precision machining, numerical study is also important and FEM has been successfully utilized to simulate micro-scale and nano-scale cutting in several studies. The purposes of these studies were to investigate the chip formation mechanism and to re-examine the cutting process in general [61, 62].

2.8.1 Finite element model formulations

Progresses in computational power prompted the improvement of numerical techniques and modeling tools [4]. Model formulations refers to the way in which the FE mesh is 'associated' with the workpiece material. There are three main formulations proposed in FEM and they are the Eulerian, Lagrangian, and the arbitrary Lagrangian–Eulerian (ALE) [63].

In a Lagrangian formulation, the mesh is attached to the workpiece. The tool or workpiece is advanced through predefined displacement increments, and the finite element solution is obtained. The displacement increment will be a function of the time step in explicit solution methods and it can be related to the material removal rate during cutting. For Eulerian finite element formulations, The workpiece material is assumed to flow through a meshed control volume (Cutting zone). Two basic formulations have been used in the Eulerian approach, namely, a penalty method (velocity used as primary variable) or a mixed method (velocity and pressure used as primary variables). In arbitrary Lagrangian-Eulerian the models utilize both Lagrangian and Eulerian methods during solution iterations. Hence, there is a need to relate the stationary (Eulerian) frame to the moving frame (Lagrangian) [64].

Isbilir et al. [65, 66] developed three-dimensional (3D) FE model using the commercial finite element software ABAQUS/Explicit for drilling CFRP based on pure Lagrangian contact algorithm used for the penetration, so the surface of the tool is set to be the master object and the surface of the work piece is assumed to be the slave object. The model aims to simulate the drilling process, to calculate the damage initiation and evolution in the work piece material; to predict induced cutting forces, torque, stress distribution in the work piece throughout the drilling process; and to predict the delamination at the entrance of the hole. Thermal issues are not accounted for in the model since high amount of coolant is used in the experiments. The results showed the model indicates that delamination and other workpiece defects could be controlled by selection of suitable drill geometry. Hence the 3D model could be used as a design tool for drill geometry for minimization of delamination in CFRP drilling.

Most simulations in research use Lagrangian descriptions for the deforming material, there is an exception in the work done by Dandekar et al. [67] were they have utilized a multiphase finite element model using the commercial finite element package ABAQUS/EXPLICIT for simulating the orthogonal machining of unidirectional fibre reinforced composite materials. In the simulation, a numerical damping of 0.5 was used in combination with the arbitrary Lagrangian–Eulerian ALE method. The value for the numerical damping ensures that the solution is accurate to the second

order time integration. The model is successful in predicting cutting forces and damage at the front and rear faces with respect to the fibre orientation. A successful prediction of fiber pullout is also demonstrated in the study. While the study done by Hsu et al. [68] were a computer simulation method is proposed to study burr formation, an Lagrangian–Eulerian ALE finite element model was developed for the burr formation simulations. The model uses Eulerian elements to model the workpiece and Lagrangian elements to model the cutting tool, the simulation results obtained are reasonably good in both the stable cutting stage and burr formation stage.

2.8.2 Multi-scale modeling

Many natural and man-made materials exhibit an internal structure at more than one length scale. These internal structures may be of a translational nature, where the structure is more or less invariant with respect to a translation corresponding to the smallest length scale. Materials with internal structure may show also multi-scale features. The material behaviour is controlled by the physical phenomena which take place at the various scales and by the interaction of these phenomena across scales. Single-scale models, usually at a macro scale, make use of constitutive equations which should reflect the behaviour of the underlying finer scales. These constitutive equations are generally of a phenomenological type. An alternative to the use of constitutive equations at a single (macro) scale is provided by multiscale modelling [69], in which the material behavior at the nanoscale or mesoscale often crucially depends on the bridging of these scales through the integration of multiscale components and multiphysical science [70].

As pointed out by Mishnaevsky [71], the following scale levels are applied in the analysis of material behavior:

(i) Macro-scale (or a specimen scale) (Figure 2.13(a)), of the order of more than 1mm. Material behavior at this scale level is analyzed using continuum mechanics methods.

(ii) Micro-scale (Figure 2.13(c)) and meso-scale (or a microstructure scale) (Figure 2.13(b)), between 1μm and 1mm. Material behavior at this scale level falls into the area of materials science, and is analyzed using methods of both physics and mechanics of materials, including micromechanics and fracture mechanics.

(iii) Nano- and atomistic scales, less than 1μm. Material behavior at this scale level falls into the area of the physics of materials.

In literature, Niezgoda et al. [72] proposed a global-local (meso) modeling technique

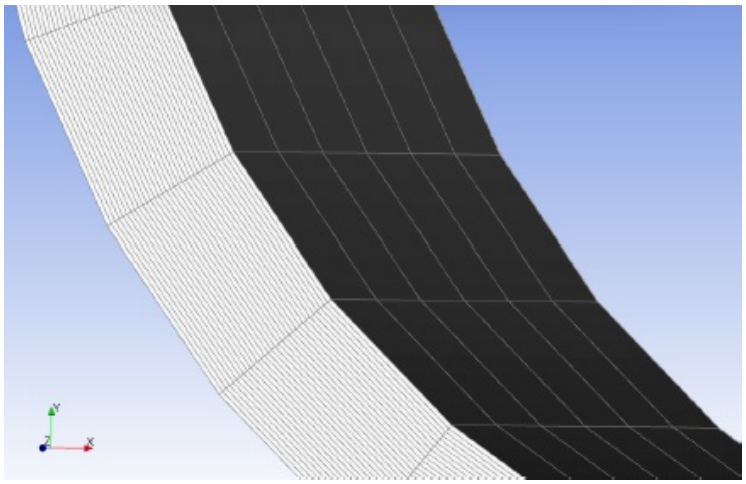

(a)

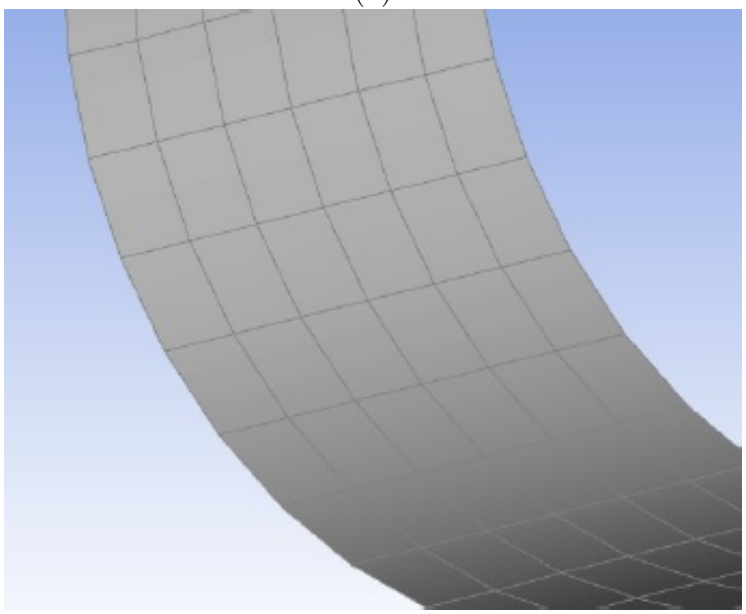

(b)

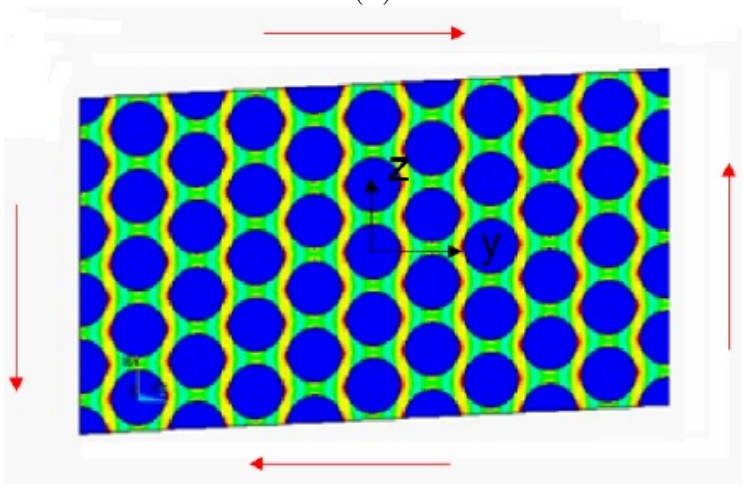

(c)

Figure 2.13: Illustration of (a) Macro-scale (b) Meso-scale (c) Micro-scale.

to minimize the computational effort in assessing composite structures. The amount of nodes and elements utilized in the meso-scale approach is around 60% less than in the micro-scale approach, this will allow assessing a 3D composite structure with different fibre orientations in a sensible amount of time. To analyze the hypervelocity impact damage in composite laminates, Cherniaev et al. [73] developed a numerical meso-scale approach of a laminate composite totally based on detailed representation of meso-scale technique. The material models in regards to laminate structure including resin-rich areas and fibre-reinforced layers are appropriate for explicit modeling. Stier et al. [74] modeled a meso-scale representative volume element (RVE) of a twill weave CFRP ply comprised of the yarn part, and the surrounding matrix region. The modeled material represented distinctive yield strengths in the compressive and tensile directions and in addition to pressure dependence. The results for experiment and numerical tests for large shear strains at large deformations were different from each other, however at small deformations were in good agreement. Lubineau et al. [75] proposed a pragmatic approach for the depiction concerning the degradation of composites laminates under certain cyclic loading, which also includes the impact of oxidation primarily based on hybrid meso-scale and micro-scale modeling of the included degradation and propagates the classical micromechanical approach under static loading, the results obtained are promising but additional research stays vital for the model to totally become quantitative and predictive. By using finite element analysis, Han et al. [76] analyzed the failure modes to determine the material failure subjected to loading for a type III hydrogen pressure vessel distinguishing it's structural solidity, utilizing the ply-based approach to model the composite laminates of the pressure vessel. Their results showed accurate stress distribution in the layers of the composite provided by the ply-based modeling approach, and despite that couple of layers showed delamination or matrix failure, the general structure was reliable under service condition.

2.8.3 Failure Criteria

Failure mechanisms for composites are very different from those of traditional metallic structures. The combination of various interfaces (fibres, matrix, layers) at a macro scale level requires a local dedicated analysis to establish the initiation of failure mechanisms of a fibre, a crack in the matrix or a delamination between two different layers. Hence, further advances in the use of laminated composites are subordinate to a better understanding of their failure mechanisms. On the other hand, the analysis and simulation of the failure of composite laminated structures are quite cumbersome tasks [77]. Generally speaking, the failure behaviour of composites depends on the heterogeneity, anisotropy, and on the various possible failure

modes of the composite [78].

Failure occurs when either of the stress components reaches the yield stress, and in this case we can observe the occurrences of damage and progressive failure. While damage can advance in several directions in the model near and around the weakest elements, "Matrix Cracking" is usually the first damage to happen as the matrix has the lowest stress for failure [21]. When panels and plates during service are subjected to in-plane multi axial stress, then failure is prompted and significantly affected by the in-plane shear stress depending on the sequence of the stacking. To estimate the damage initiation and evolution, we must first identify the type of group it falls into, as there are two groups of failure criteria exist.

(i) Independent failure criteria: The interactions between several stress components are neglected.

(ii) Polynomial failure criteria: The interactions between several stress components are considered.

Independent failure criteria include the maximum stress criteria and the maximum strain criteria. The stress and strain components in these criteria don't have any dependence between them, this means that the components in the longitudinal, transverse and stacking directions do not affect each other. Polynomial failure criteria include Polynomial maximum stress criterion, Tsai-Wu, Tsai, Tsai-Azzi, Tsai-Hill, Polynomial maximum strain criterion, Hoffman criteria and Hashin criteria, the components in each direction depends on each other.

In literature, Phadnis et al. [79, 80] utilized an advanced drilling technique known as Ultrasonically Assisted Drilling (UAD) to demonstrate its several advantages over Conventional Drilling (CD) including a reduced thrust force. They developd a 3D finite element (FE) models simulating CD and UAD techniques for drilling in CFRP laminates using the general-purpose FE software ABAQUS/Explicit. The Hashin's failure criteria was used to model initiation and evolution of damage in long-fibre composites, the numerical results obtained with the FE model were found to be in a good agreement with the experimental data. Xu et al. [81] developed a finite element (FE) model to inspect the key mechanisms governing the induced damage formation when cutting hybrid carbon fiber reinforced polymer (CFRP)/Ti. The developed orthogonal cutting (OC) model aims to characterize the dynamic mechanisms of interface delamination formation and the affected interface zone (AIZ). The failure initiation law required to motivate damage among the interface layer is based on the quadratic stress criterion. The numerical results highlighted the pivotal role of AIZ in affecting the formation of interface delamination, and the significant impacts of feed rate and cutting speed on delamination extent and fiber/matrix failure.

Lasri et al. [82] studied the progressive failure of unidirectional glass fiber-reinforced polymer composites (FRP) using finite element analysis in orthogonal machining. Chip formation process and damage modes such as matrix cracking, fiber–matrix debonding and fibre breaking were modeled by degrading the material properties. Damage analysis was carried out using Hashin, Maximum stress and Hoffman failure criteria. The objective of this study is to better understand the chip formation process and to analyse the cutting induced damage from initiation stage until complete chip formation. The results were addressed in terms of cutting forces evolution and damage progression in the composite structure during machining. It was demonstrated that the use of the stiffness degradation concept with the appropriate failure criterion responds potentially in a predictable fashion to changes in chip formation process for machining of FRPs.

Chapter 3

Finite Element Analysis

3.1 Finite element analysis

The development of accurate and reliable machining process models has received considerable attention from both academic researchers and industry practitioners in recent years. Traditionally, the techniques used in industry are based on past experience, extensive experimentation, and trial-and-error. Such an approach is time consuming, expensive, and lack of a rigorous general scientific knowledge [83]. Alternative approaches are mathematical simulations where numerical methods are applied. Amongst the numerical procedures, the FEMs are the most frequently used [84], and can be defined as small interconnected geometrical entities connected to other elements through nodes (1D), boundary lines (2D), and boundary surfaces (3D). Finite element methods have the capability to predict the mechanical and thermal behavior of the material and the tool, without spending time and money with experimental work. Therefore, productivity can be improved and costs can be reduced at the same time. Progressive damage modeling of polymer matrix composites has received a great deal of attention in recent years as predictive capabilities for the complex nonlinear behavior of these materials are sought [60]. Generally, the term meso-scale is used to describe the intermediate level of material description between micro-scale (modeling the composite to the scale of the constituents such as fibre filament and matrix materials) and macro-scale (modeling the composite to the scale of smeared or homogenous shell/solid, with no detailed ply stresses or strains). In general, the micro-scale is computationally demanding scale whereas the meso-scale approach is treated as effective anisotropic materials and is more computationally efficient.

3.2 Meso-scale modeling

Meso-scale was first introduced by Panin et al. [85] as an approach of modeling properties (density, young modulus, shear modulus, poisson ratio, etc) and the deformation and failure mechanisms of structural and functional materials at different scale levels, with different loads [71], it's the intermediate level between micro-mechanics and macro-mechanics. It comprises the involvement of the main micro-mechanisms controlling the materials mechanical behaviour and failure and the applicability of the continuum mechanics equations [86]. Between these two scales, the meso-scale approach, commonly used in composite modeling [87, 88], seems to be the appropriate one, although it requires more detailed laws as compared to macroscale models, it nonetheless has the potential to capture most of the physical phenomena [87, 89]. Therefore it is used in this study to close the gap between the complex failure

mechanisms of the micro-mechanics analysis and the empirical and case specific of the macro-mechanics analysis. In meso-scale continuum mechanics size matters, as plastic flow processes in crystalline solids are inherently size dependent over a scale that ranges from a fraction of a micrometer to 100 mm. Such formulations are intermediate between a direct atomistic and an unstructured continuum description of deformation processes [90].

3.3 Ply-based modeling

Ply-based model and zone-based model are the two basic methodologies commonly employed to create composite models. Ply-based models are developed based on each ply in a composite; material properties and local orientations are assigned to each ply [91], while zone-based models discretize the composite into zones of effective properties, each zone is aligned a material property based on the ply-stacking and fabric deformation.

To describe an arbitrary composite layup, a ply-based concept is much more realistic than a zone-based concept because ply-based means manufacturing-based. In the ply-based concept it is simple to add or delete plies at any location. Figure 3.1 shows a simple plate made by four plies. Each ply has different size and orientation, particularly layer 4 is diagonally oriented. In a zone-based approach the plate has to be divided into 8 zones with different thickness and different fibre direction across the thickness [92], however, a ply-based approach only requires four plies to capture the behavior of the entire structure, this will significantly make modifying the model easier if it's required.

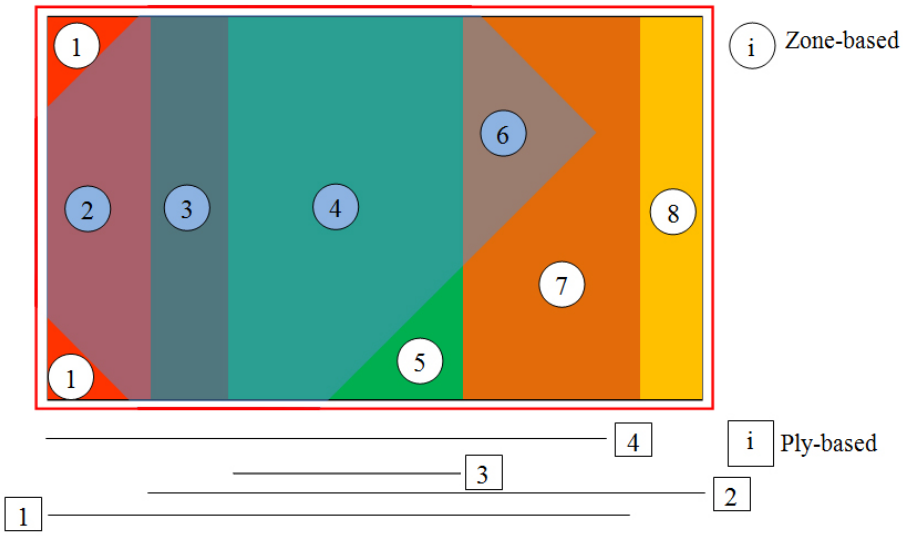

Figure 3.1: Zone-based vs ply-based.

Ply-based composite model preparation and definition of layup can be shared from existing composite layup and can be updated faster when product design changes are required and it's a comfortable way to generate layered composite structures using a ply-based = manufacturing-based concept which makes it much more realistic. Figure 3.2 shows an entire workflow for composite structure from design to final information production as a result [93].

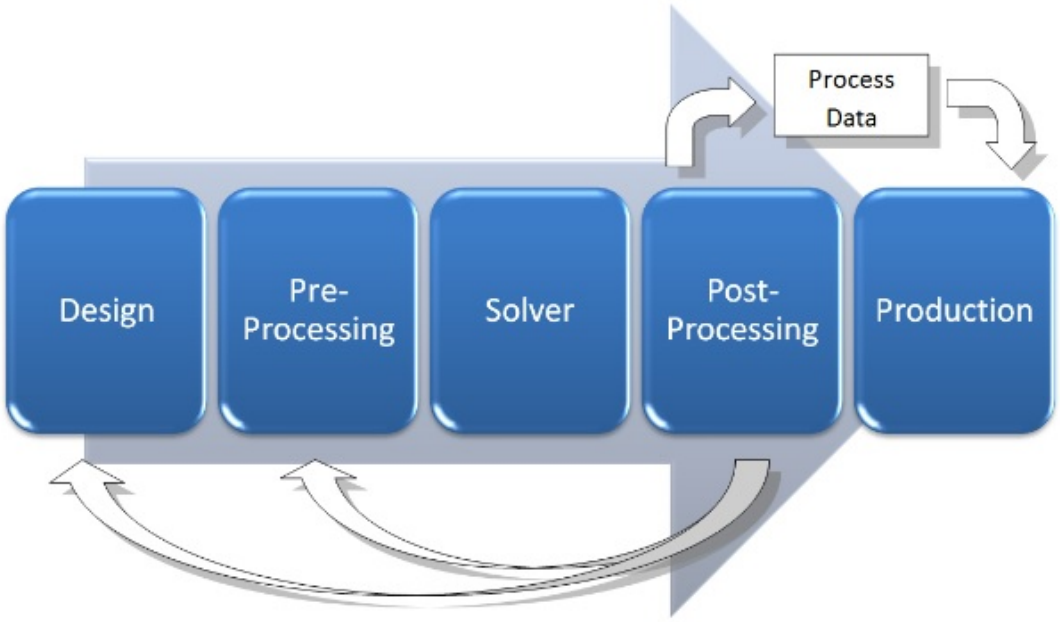

Figure 3.2: ACP composite workflow.

While there are manufacturing effects that need to be considered when laying up the laminates such as draping (the avoidance of kinking when wrapping material around curved shapes), as shown in Figure 3.3, the ply application on curved surfaces changes the theoretical fibre orientations and deformation occurs with the in-plane shear and up to certain deformation level and it's important to know how big this effect can be if it's considered. Ply-based modeling allows evaluating the draped fibre directions with angles can be visualized and are considered in all analysis resulting in more accurate evaluations. Hence the need for draping simulation is twofold. Firstly, the manufacturability of the composite product can be assessed, areas where the reinforcement cannot follow the surface are indicated and hence measures can be taken in design to avoid this. Secondly, the draping simulation gives the actual fibre orientations at any location in the model. This information is needed for accurate finite element analysis of the structure.

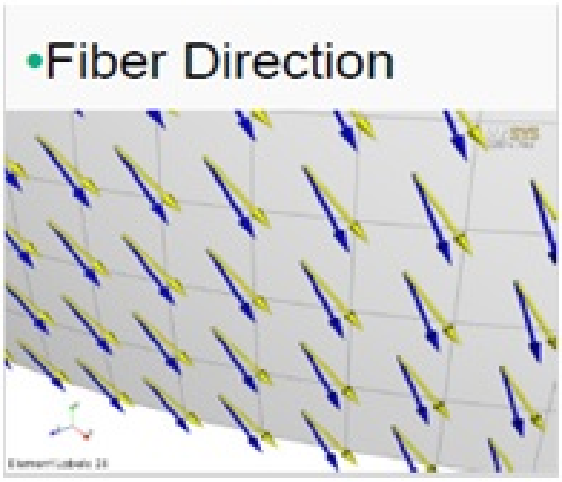

(a)

(b)

(c)

Figure 3.3: Draping process and its effect on composite layup (a) Fibre direction (b) Draping (c) curved shapes.

3.4 Modeling of tool and workpiece

Previously, simplified models of CFRP drilling were developed, owing to the advantage of reduced computational cost [94]. Modeling of drilling processes involves elevated difficulty, because of the need of simulating drill rotation and feed movement [95]. Common assumption in simplified models considers the drill acting like a punch that pierces the laminate, as per studies done by Durao et al. [96, 97] in drilling carbon/epoxy composites, the same approach was also done by Singh et al. [98] when studying GFRP drilling as they showed the influence of the drill point angle in the induced damage.

Modeling of the cutting tool is very important to FE simulation. The model must represent the dynamic change of the tool's physical properties during machining. A simplified rigid body cutting tool, which is currently used by the vast majority of researchers when drilling CFRP in their FE simulation, is not able to predict correctly the effect of process parameters on drilling CFRP. In this study we intend to capture and predict the dynamic effect of machining parameters on the CFRP workpiece as well as the inflected stresses on the cutting tool, hence the drill was modeled as a flexible body. The heat generated in the simulation process was not considered because high amount of coolant was used in the experiments.

3D Lagrangian formulation finite element (FE) models of CFRP composite and twist drill and double point angle drill (Figure 3.4) were developed using ANSYS-EXPLICIT and AUTODYN software, both drills were meshed with solid185 eight node linear tetrahedral elements. A uni-directional CFRP composite laminate with stack sequence of [(0/90)2]s which was used in the FE analysis has dimensions of 20mmx20mmx1.6mm and consists of 8 plies. The thickness of each ply was 0.2mm. The workpiece was meshed with shell181 four node linear quadrilateral elements.

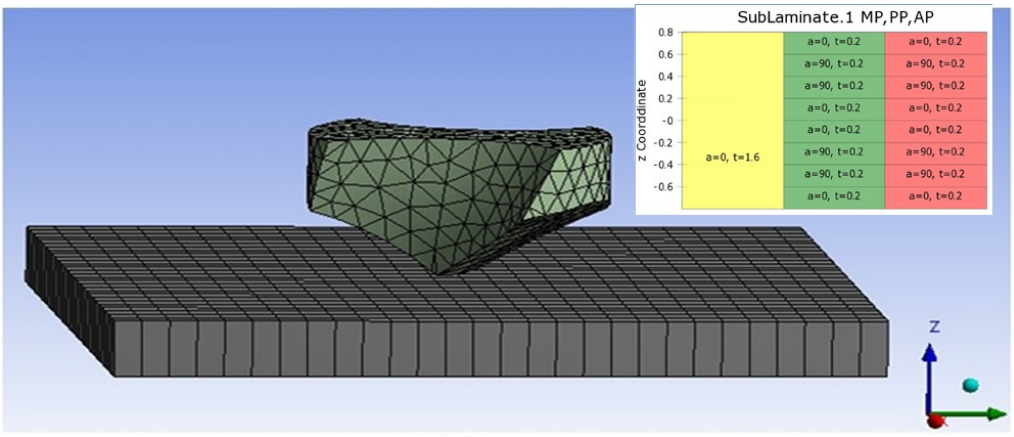

Figure 3.4: Finite element model of VTM264 CFRP laminate and PCD twist drill.

The boundary conditions were enforced on the drills and workpiece to enable simulation process. Both drills were located at the top centre of the workpiece and was made to rotate (angular velocity) around the Z axis (urz) and moved in the cutting direction (uz). The workpiece was fixed from the sides from moving (ux=uy=uz=0). The cutting parameters applied in the experiments are listed in Table 3.1.

Table 3.1: Cutting parameters used in drilling.

drilling parameter	magnitude
drill diameter (mm)	8
spindle speed (rpm)	2500, 5000, 7500, 10000
feed (mm/rev)	0.05, 0.10, 0.125
feed rate (mm/min)	125, 500, 1250

The material model used for the workpiece was orthotropic homogeneous elastic assigned according to the fibre orientation through a defined local coordinate system. Table 3.2 shows properties of the orthotropic unidirectional material VTM264 [99], Table 3.3 shows the strength properties of the unidirectional laminate while Table 3.4 shows the general properties of diamond used in the drilling tool.

Table 3.2: Mechanical properties of unidirectional VTM264 laminate.

E11	E22	E33	v12	v13
117GPa	7.47GPa	7.47GPa	0.33	0.02
v23	G12	G13	G23	cured ply thickness
0.33	4.07GPa	4.07GPa	2.31GPa	0.2mm

Table 3.3: Strength properties of unidirectional VTM264 laminate.

property	magnitude
0^o Tensile strength	2575 MPa
90^o Tensile strength	40 MPa
0^o Compressive strength	1235 MPa
90^o Compressive strength	182 MPa
In-plane shear strength (IPSS)	85.7 MPa
0^o Interlaminar shear strength (ILSS)	88.6 MPa

Table 3.4: General properties of diamond used in the drilling tool.

property	magnitude	units
Hardness	10,000	kg/mm^2
Strength, tensile	>1.2	Gpa
Strength, compressive	>110	Gpa
Fracture strength	400-800	MPa at <1mm thickness
Density	3.52	g/cm^3
Young's modulus	1200	Gpa
Poisson's ratio	0.2	Dimensionless
Thermal expansion cofficient	1.1-5.0 (300-1300K)	ppm/K
Thermal Conductivity	10-20	W/cm-k
Coefficient of friction	0.05 (dry)	Dimensionless

3.5 Constitutive material model of unidirectional CFRP

Progressive damage modeling of polymer matrix composites as a predictive capability for the complex nonlinear behavior of these materials has been used. Intralaminar and interlaminar damage mechanisms are the basis of fracture process of composites which include fibre breakage, matrix cracking and delamination. The most common fracture mode is interlaminar delamination, it is prompted by shear and normal stresses at the interface of adjoining layers in CFRP laminate [100]. Due to experimental difficulties caused by the typical extensive fibre bridging, which makes the insertion of initial defect difficult for the fracture toughness test. The following constitutive material in the FE model was used to find out how intralaminar delamination effects the first ply failure.

The orthotropic material model for shell layers developed can be expressed as in-plane stress-strain relationship [101]:

$$\sigma_i = c_{ij}\epsilon_j \tag{3.1}$$

Plane stress condition is applicable by setting:

$$\sigma_3 = 0, \quad \tau_{23} = 0, \quad \tau_{31} = 0 \tag{3.2}$$

The stress-strain relation in terms of reduced stiffness is:

$$\begin{bmatrix}\sigma_1\\ \sigma_2\\ \tau_{12}\end{bmatrix} = \begin{bmatrix}Q_{11} & Q_{12} & 0\\ Q_{12} & Q_{22} & 0\\ 0 & 0 & Q_{66}\end{bmatrix}\begin{bmatrix}\epsilon_1\\ \epsilon_2\\ \gamma_{12}\end{bmatrix} \tag{3.3}$$

Whereas in terms of engineering terms:

$$Q_{11} = \frac{E_1}{1 - v_{12}v_{21}}, Q_{22} = \frac{E_2}{1 - v_{12}v_{21}} \tag{3.4}$$

$$Q_{66} = G_{12}, Q_{12} = \frac{v_{12}E_2}{1-v_{12}v_{21}} = \frac{v_{21}E_1}{1-v_{12}v_{21}}$$

The stress-strain relationship becomes:

$$\begin{bmatrix}\sigma_{11}\\ \sigma_{22}\\ \tau_{12}\end{bmatrix} = \begin{bmatrix}\frac{E_1}{1-v_{12}v_{21}} & \frac{v_{21}E_1}{1-v_{12}v_{21}} & 0\\ \frac{v_{12}E_2}{1-v_{12}v_{21}} & \frac{E_2}{1-v_{12}v_{21}} & 0\\ 0 & 0 & G_{12}\end{bmatrix}\begin{bmatrix}\epsilon_{11}\\ \epsilon_{22}\\ \gamma_{12}\end{bmatrix} \tag{3.5}$$

Where σ is normal stress; C is stiffness tensor; ϵ is normal strain; τ is shear stress; E is modulus of elasticity; γ is shear strain; G is shear modulus; υ is poisson's ratio and Q is the reduced stiffness.

3.6 Intralaminar, interlaminar, and shear stresses

To reduce the computational time, and in the meantime, ensure the high accuracy of predictive outcomes, shell elements of layered composite structures is applied based on the first-order shear deformation theory (FSDT) in analyzing intralaminar, inerlaminar, shear stresses, and transverse shear stresses, Figure 3.5 shows a cylindrical coordinate system for describing an arbitrary doubly curved shell [102].

The differential equation of the through-the-thickness displacement is:

$$0 = w_{,rr} + w_{,r}(\frac{1}{r} + \frac{1}{r+r_d}) + w(\frac{\widehat{C}_{13} + \widehat{C}_{23} - 2\widehat{C}_{12}}{r(r+r_d)} - \frac{\widehat{C}_{11}}{r^2} - \frac{\widehat{C}_{22}}{(r+r_d)^2}) + P \tag{3.6}$$

$\widehat{C}_{ij} = \frac{\overline{C}_{ij}}{\overline{C}_{33}}$ *and* P *is*

$$P = u_{,\varphi}(\frac{\widehat{C}_{13} - \widehat{C}_{12}}{r(r + r_d)} - \frac{\widehat{C}_{11}}{r^2}) + u_{,\varphi r}\frac{\widehat{C}_{13}}{r} + \nu_{,\vartheta}(\frac{\widehat{C}_{23} - \widehat{C}_{12}}{r(r + r_d)} - \frac{\widehat{C}_{22}}{(r + r_d)^2}) + \nu_{,\vartheta r}\frac{\widehat{C}_{23}}{r + r_d} + \epsilon_i^F(\frac{\widehat{C}_{1i} - \widehat{C}_{3i}}{r} + \frac{\widehat{C}_{2i} - \widehat{C}_{3i}}{r + r_d}) \quad (3.7)$$

Where:

$\overline{C}_{ij}$ are the components of the 3-dimensional stiffness matrix expressed in reference coordinates. P is the particular part of the differential equation.
$r = R_1 + z,\ r_d = R_2 - R_1$ *and* $z = [-t/2, t/2]$
u,v,w are displacements in the cylindrical coordinate system.

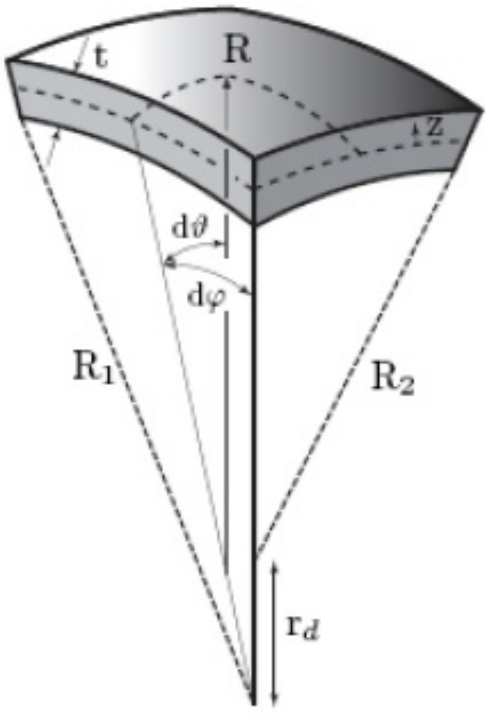

Figure 3.5: Doubly curved FE geometry

3.7 Constitutive damage initiation and evolution

Hashin [103] damage mechanism and failure criterion are used here to simulate the damage process of matrix and fibre. The failure criterion is formulated under tensile and compressive loads in longitudinal and transverse direction of fibre respectively and the interaction between the four failure modes shown in Equation 3.8 to Equation 3.11 are taken into account and therefore Hashin failure was used in the finite element analysis. One of the requirements for this criteria is to have the lamina properties and it can be experimentally determined easily. Moreover, it can give numerically solid results when the criteria is applied for first ply failure load in glass and carbon fibre composites.

Tensile Fibre Mode

$$(\frac{\sigma_{11}}{\sigma^f_{11t}})^2 + (\frac{\sigma_{12}}{\tau^f_{12}})^2 = 1 \qquad \sigma_{11} > 0 \tag{3.8}$$

Compressive Fibre Mode

$$(\frac{\sigma_{11}}{\sigma^f_{11c}})^2 = 1 \qquad \sigma_{11} \leq 0 \tag{3.9}$$

Tensile Matrix Mode

$$(\frac{\sigma_{22}}{\sigma^f_{22t}})^2 + (\frac{\sigma_{12}}{\tau^f_{12}})^2 = 1 \qquad \sigma_{22} > 0 \tag{3.10}$$

Compressive Matrix Mode

$$(\frac{\sigma_{22}}{2\tau^f_{12}})^2 + [(\frac{\sigma^f_{22c}}{2\tau^f_{12}})^2 - 1](\frac{\sigma_{22}}{\sigma^f_{22c}}) + (\frac{\tau_{12}}{\tau^f_{12}})^2 = 1 \quad \sigma_{22} \leq 0 \tag{3.11}$$

Where f denotes fibre; t is tension and c is compression.

When any Hashin's criteria have been fulfilled in any mode in the equations above, damage will be initiated.

Without damage initiation criteria, the damage evolution law has no effect on the material. The damage evolution law defines the way a material degrades following the initiation of damage and progressive damage generally refers to degradation of stiffness, the stiffness reduction takes a value of 0 to 1, where 0 is no damage and 1 is completely damaged.

The evolution law of the damage variable in the post-damage initiation phase can also be based on the fracture energy dissipated Gc during the damage process. The damage variable can be defined from the equation below [104]:

$$D = \frac{\delta_m^f(\delta_m^{max} - \delta_m^0)}{\delta_m^{max}(\delta_m^f - \delta_m^0)} \tag{3.12}$$

Where δ_m^f is the mixed-mode displacement at complete failure, δ_m^{max} refers to the maximum value of the mixed-mode displacement, and δ_m^0 is the effective displacement at the damage initiation.

The energy dissipation Gc can be found from the area under the triangle shown in Figure 3.6, whereas the failure displacement can be calculated as follows:

$$\delta_m^f = \frac{2Gc}{\sigma_m^0} \tag{3.13}$$

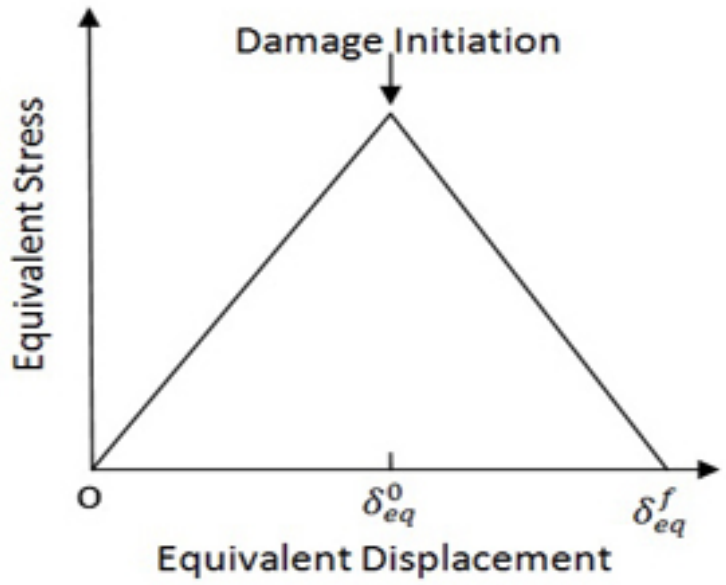

Figure 3.6: Damage initiation and evolution.

Figure 3.7 shows an example of the FE drilling process of CFRP using the twist drill, it also shows the delaminated areas and the dusty abrasive chips generated during drilling which causes an increased abrasiveness of the cutting tool.

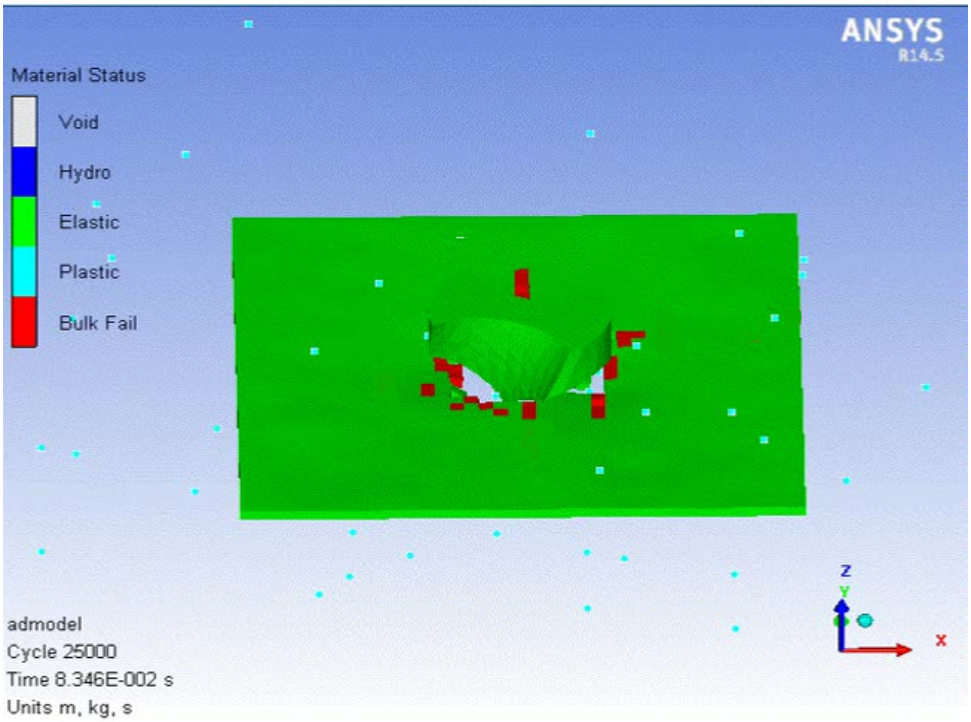

Figure 3.7: Example of FE drilling process of CFRP using twist drill.

Chapter 4

Experimental Setup

4.1 Introduction

To obtain the required experiment results from this research, several experimental investigations on the drilling process of uni-directional CFRP composites were conducted. The experimental procedure starts with fabrication of the CFRP laminates, followed by the online monitoring of drilling CFRP laminates using thrust force and torque, six signals were acquired during the drilling operation. Then followed by offline inspection and measurement procedure of drilling induced damage and defects at the entry of the drilled holes. In this chapter, experimental setup, drill tool materials used, workpiece materials, experimental procedures, measurement methods of signals, damage inspection will be presented.

4.2 Experimental setup

Drilling tests were carried out on 3 axis HAAS CNC machining centre with maximum spindle speed 10000RPM, spindle maximum rating 20HP and feed rate 1000IPM (25.4 m/min) as shown in (Figure 4.1), while Figure 4.2 show the schematic drawing and experimental setup of the system.

Figure 4.1: CNC machine used in experiment.

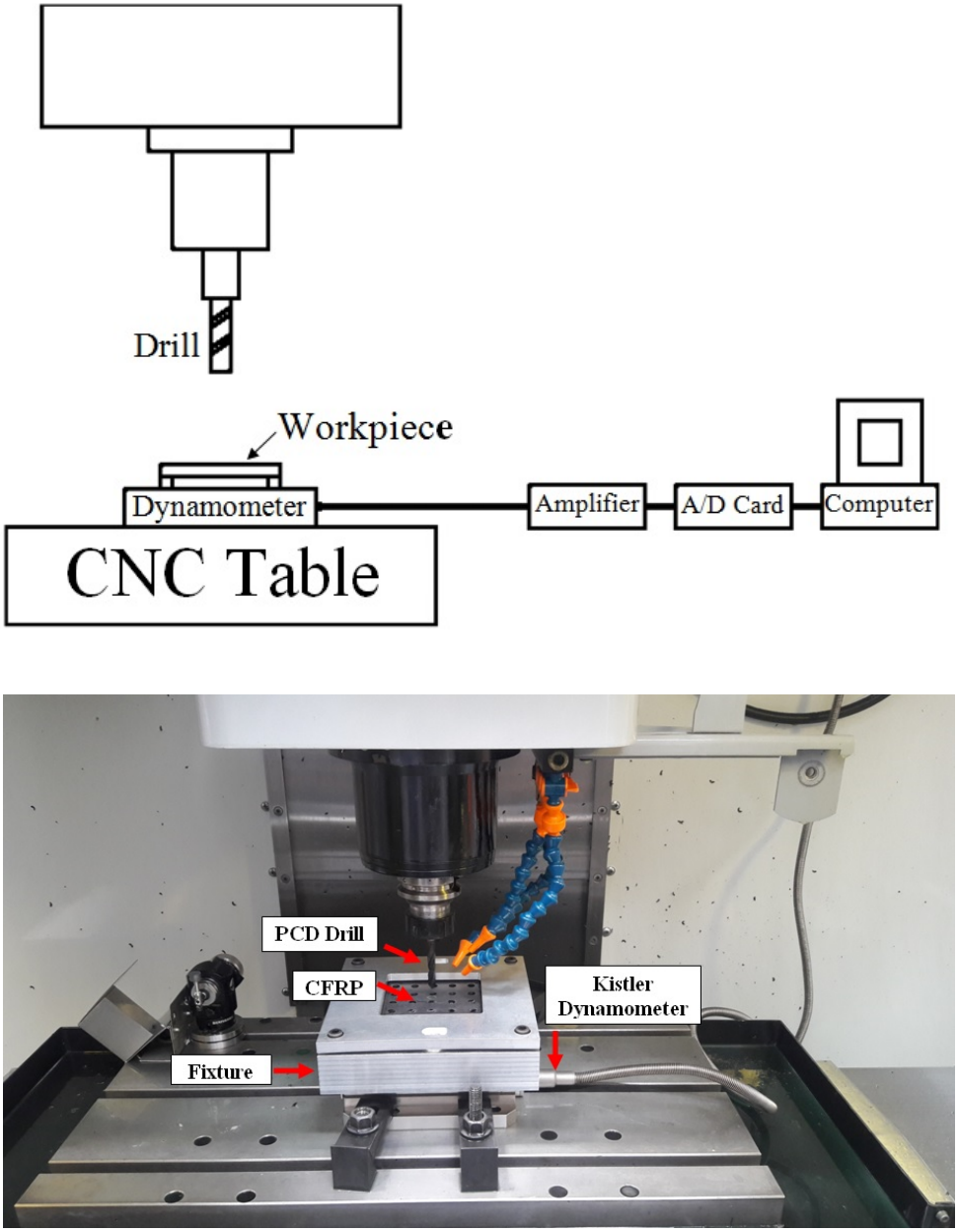

Figure 4.2: Experimental setup.

A fixture was designed to clamping the workpiece for the precise measurement of thrust force and torque. As shown in Figure 4.3, the fixture consists of three components: a top plate, a base plate, and a support block. A specimen was clamped by the top and base plates, which was fixed on the dynamometer with bolts. The support was an aluminum alloy solid with 25 through holes were drilled to eliminate vibration during drilling when fixed on the holder.

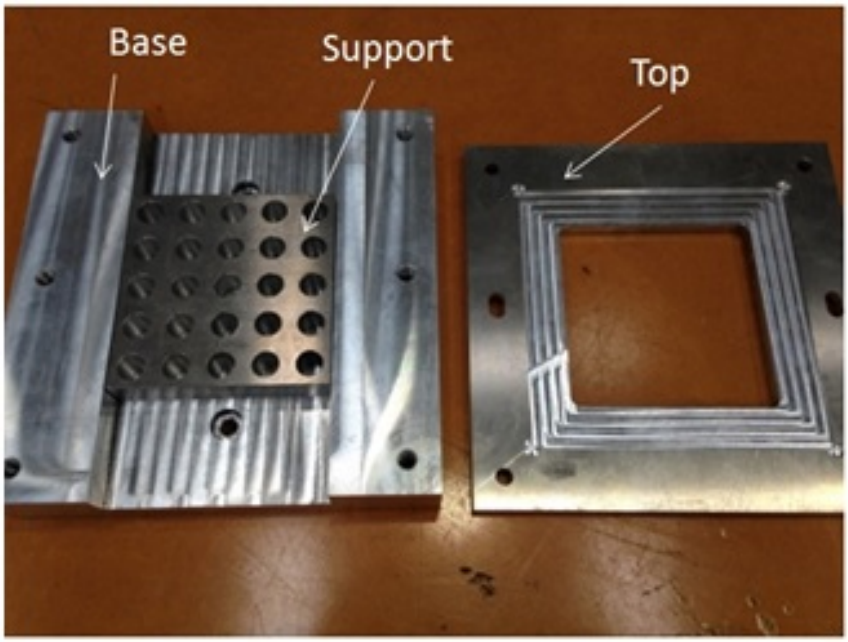

Figure 4.3: Fixture used in experiment.

4.3 Workpiece VTM 260 series

In this study the workpiece (Figure 4.4) which was used in the drilling experiment was a 4mm thickness of uni-directional CFRP VTM264 prepared using the hand lay-up process with stack sequence of [(0/90)5]s, dimensions of 20mmx20mm and consists of 20 plies, the thickness of each ply is 0.2mm . It features outstanding vacuum-only processing capability for the wildest scope of reinforcement formats, flexible curing capability, free standing postcure capability, excellent glass transition temperature Tg development, and suitable for full impregnation of light and medium weight unidirectional and fabric reinforcements, material type, cure cycle and test conditions as shown below and appendix (A) [105]:

Material: VTM264/T700-35%

Cure Cycle: 5 hours at 80^{o}C (176^{o}F), oven vacuum bag cure.

Test Conditions: Room temperature, dry.

4.4 Drill tool geometry and materials

Experimental studies have been pursued to better understand the relationships between process inputs, such as machining parameters and drill geometry, and process

Figure 4.4: VTM264 CFRP.

.

outputs such as cutting forces, torque, tool wear and drilled hole quality [33].

From experiments, the capabilities of the special drill bits compared to twist drill bit show it can [106]:

(i) Provide higher drilling feed rates without delamination by better distributed load and lower thrust force and delamination free drilling.

(ii) They can be used with plain composite or stacks with composite.

(iii) Outstanding surface quality.

(iiii) Outstanding size and shape of the hole.

(iiiii) Some tested to 2800 holes without size degradation (within 0.025mm tolerance).

(iiiiii) Smaller chisel edge can be used for minimization of delamination due to lower thrust force obtained.

Cutting tools used for machining should possess low affinity to workpiece, low friction coefficient, and high hardness which makes diamond tools the suitable choice due to the ability to reduce significantly the built-up edge formation and hence improve cutting performance [107, 108, 109].

In this study, two different types of Ø8mm two-flute diamond drill bits (PCD twist drill and diamond coated double point angle drill) made by "SECO" were utilized

in the experiment as shown in Figure 4.5, while Table 4.1 shows the geometric parameters of the drill bits.

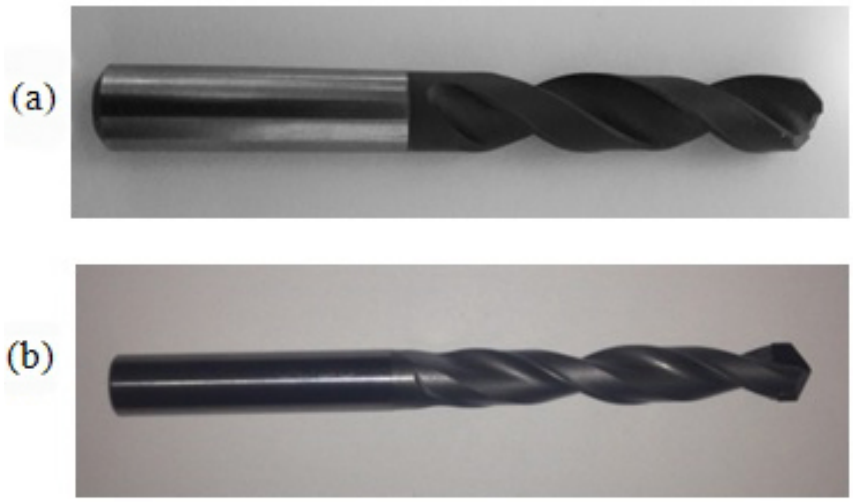

Figure 4.5: (a) PCD twist drill bit (b) Diamond coated double point drill bit.

Table 4.1: Geometric parameters of the drill bits.

Drill type	Drill diameter	Point angle	Helix angle	flutes
PCD twist drill	8mm	120^o	30^o	2
Diamond coated double point angle drill	8mm	$60^o - 130^o$	30^o	2

4.5 Digital signal processor (dynamometer)

In this study a six channel force-torque Kistler dynamometer type 9257B was used to measure the thrust force and torque. An eight channel Kistler charge amplifier type 5070A was used to amplify the signals which were transferred to the data acquisition card (NI DAQ E6213).

The multi component dynamometer provides dynamic and quasi-static measurement of the 3 orthogonal components of a force Fx, Fy, Fz acting from any direction onto the top plate. With the aid of optional evaluation devices the 3 moments Mx, My and Mz can be measured as well as shown in Figure 4.6 [110].

While the eight channel Kistler charge amplifier type 5070A instrument is ideal for multi-component force-torque measurement with piezoelectric dynamometers or force plates. Piezoelectric force sensors produce an electric charge which varies in direct proportion with the load acting on the sensor. The charge amplifier then converts the electric charge into a proportional voltage as shown in Figure 4.7 [111].

Figure 4.6: Dynamometer Type 9257B.

Figure 4.7: Multi-channel charge amplifier type 5070A.

4.6 Thrust force and torque measurements

While drilling the CFRP laminates, the thrust force and torque were measured with the Kistler dynamometer. A typical measurement signal while drilling is shown in Figure 4.8.

The noises or the oscillations of the signal were caused by the extremely high sampling frequency of the DAQ which was much higher than the rotating frequency of the spindle, in this study the signals have been processed to utilize the mean values

for force and torque.

As mentioned in several studies in literature before [112] [113], the drilling mechanism of CFRP consists of three stages, first stage is the entrance region when the drill starts entering the workpiece, second stage shows a steady state when the drill fully engages with the workpiece, in this stage the force and torque reach their peak values, the third stage starts with a drop in value until the drill exits the workpiece. Since the thickness for the CFRP plate used in the cutting experiment is only 4mm, which is very thin in comparison with the diameter of the tool and the value of the feed rate, therefore, the steady drilling process is very short.

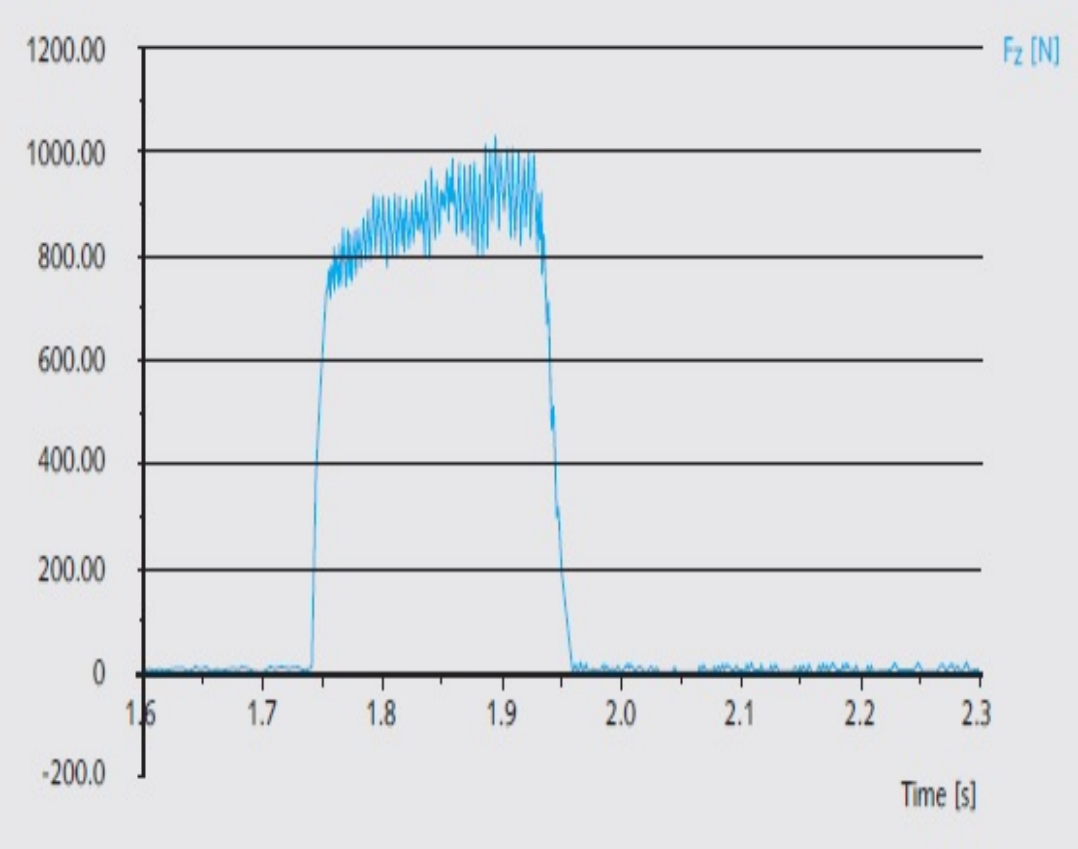

Figure 4.8: Typical measurement signal while drilling.

4.7 Microscopic observation of delamination

Peel-up delamination and push-down delamination are the two main types of damage that are different in causes and effects in drilling CFRP. Damage extension can be evaluated through Non-Destructive Test (NDT) such as acoustic emission, enhanced radiography, C-Scan, computerized tomography (CT) [4] and digital image correlation (DIC) [55]. In the majority of these methods, the objective is to acquire

images that outline the surrounding areas of the hole to further measure and analyze diameters and areas.

In this study, a compromise between the resolution and magnification was employed to obtain the required images of the delamination areas for the drilled holes, as we have used two different devices to evaluate the damages obtained experimentally at the hole entrance peripheral, the first device used is the PhilipsXL30 scanning electron microscopy (SEM) for the holes drilled by PCD twist drill as shown in Figure 4.9, On this system an acceleration voltage of 20 kV was used, which required the samples to be coated with a conductive metal (gold) to prevent charging effects, while the second device we used a Leica optical microscope when drilling the holes using the double point angle drill with diamond coating as shown in Figure 4.10, it was capable enough and faster in obtaining the images of the delaminated vicinity of entrance of the holes drilled. In both cases, the software "Image J" was utilized to process the image of delaminated areas. Both devices have been successful in acquiring the delaminated areas.

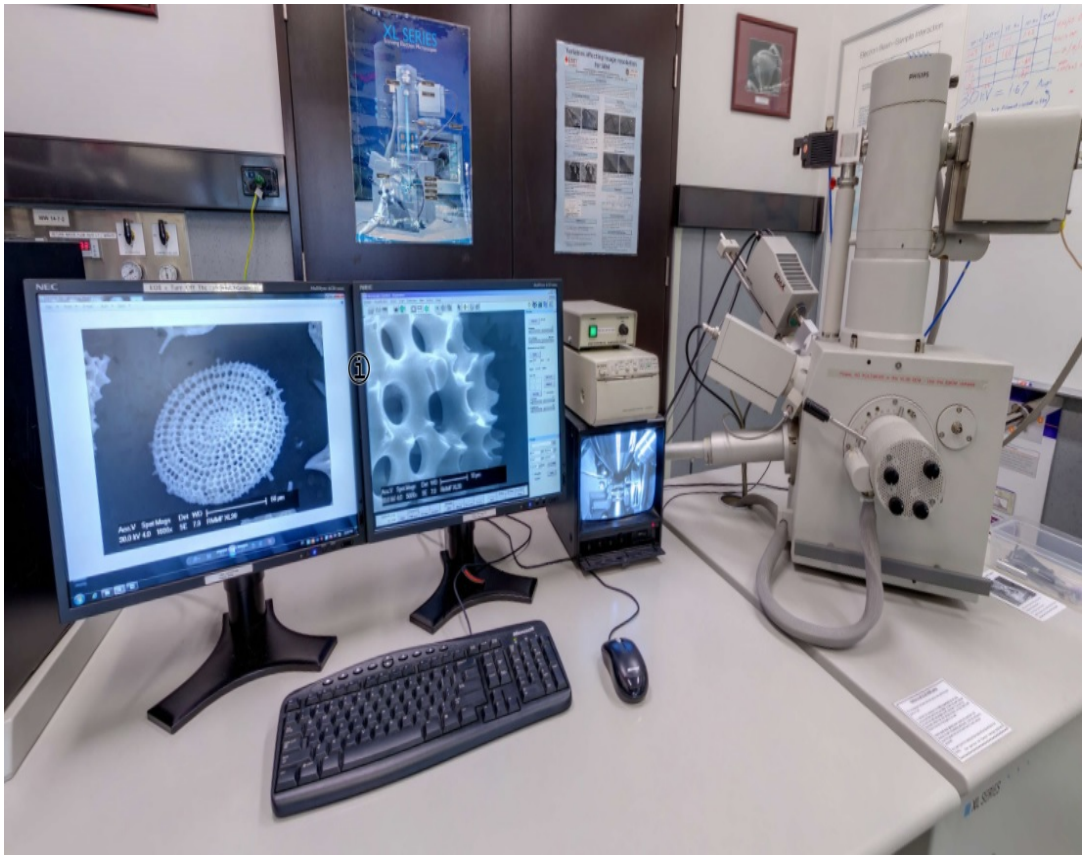

Figure 4.9: PhilipsXL30 scanning electron microscopy (SEM).

Figure 4.10: Leica optical microscope.

Results from a sample drilling and quality assessment with the holes inside being filtered from any noises for CFRP laminates using both drills are shown in Figure 4.11 and Figure 4.12.

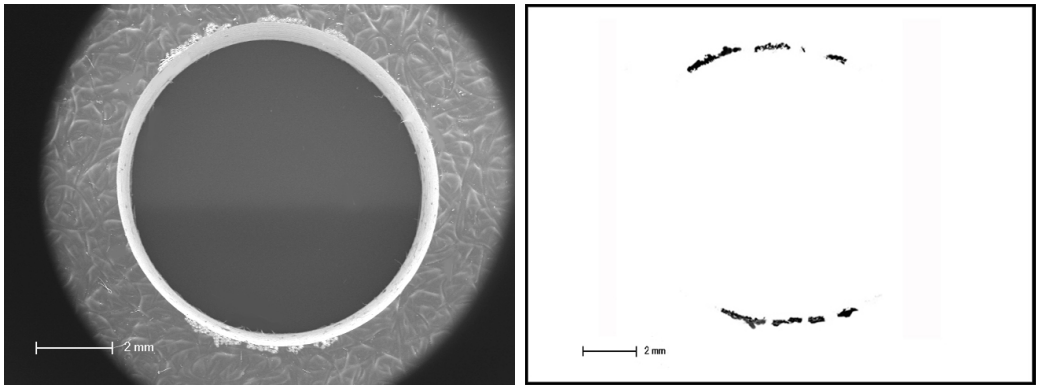

(a) (b)
(PCD twist drill) (Spindle speed: 5000 rpm) (Feed rate: 1250 mm/min)

Figure 4.11: Sample of drilling and delamination assessment (a) SEM image processing. (b) Experimental delamination areas after processing with "Image J" software.

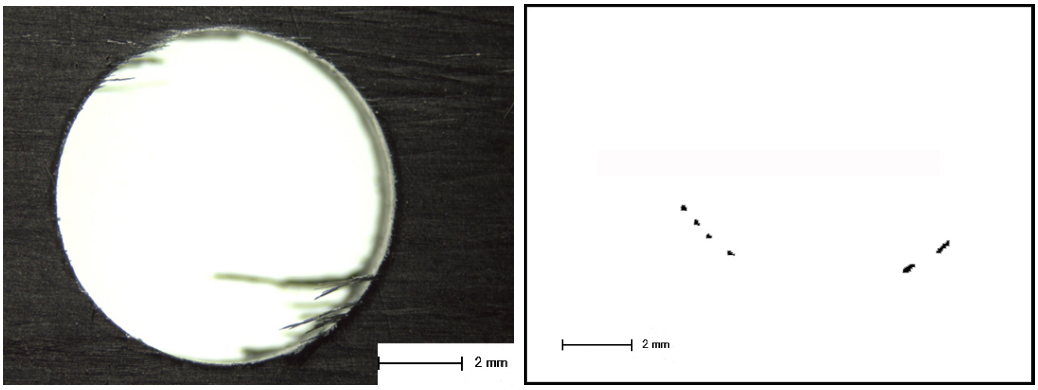

(a) (b)

(Double point angle drill) (Spindle speed: 5000 rpm) (Feed rate: 125 mm/min)

Figure 4.12: Sample of drilling and delamination assessment (a) Optical microscope. (b) Experimental delamination areas after processing with "Image J" software.

Chapter 5

Damage Methodology and Proposed Delamination Factor

5.1 Delamination Analysis

As mentioned previously delamination is considered one of the most severe damage process induced when drilling CFRP composite materials, and one of the problems which occurs during drilling of composite laminates are surface delaminations called peel-up delamination and push-out delamination [114].

Also during drilling of composite laminates, the drill starts to penetrate the laminates and the ability of these laminates to withstand the drilling thrust forces decreases when the drill bit approaches th exit plane, while the laminates are held together by their interlaminar bond throughout the composite material, these bondings can be broken when the loading of the drill bits exceeds the interlaminar strength and hence bottom laminates will be separated from their interlaminar bond around the hole periphery and delamination occurs [115].

Delamination intends to grow along the fibre direction and is developed in two phases, the first phase is called the chisel edge action phase while the second phase is called the cutting edge action phase as shown in Figure 5.1. The first phase starts when the thrust force of the chisel edge pushes onto the surface of the laminate composite and reaches a critical value and ends when the chisel edge just penetrates the laminate, at this phase it was found in previous studies that the chisel edge has a strong effect on the formation of the delamination, after the chisel edge penetrates the laminate composite then the second phase of the cutting edge action phase develops and the delamination damage initiated in the first phase further develops due to the continuous pushing and twisting of the cutting edge [116] [117].

There are several approaches and models have been developed to analyze delamination mechanisms during drilling, and one of the most used is the Linear Elastic Fracture Mechanics (LEFM) approach done by Hocheng-Dharan [118],

In this model (Equation 5.1), the critical thrust force for the onset of delamination is related with properties of the unidirectional laminate like the elastic modulus, the poisson ratio, the interlaminar fracture toughness in mode I and the uncut plate thickness [119].

$$F_{crit} = \mathit{\Pi}[\frac{8G_{Ic}E_1 h^3}{3(1 - v_{12}{}^2)}]^{0.5} \tag{5.1}$$

Where F_{crit} is critical force; E_1 is elastic modulus; v_{12} is poisson ratio; G_{Ic} is interlaminar fracture toughness in mode I; h is uncut plate thickness.

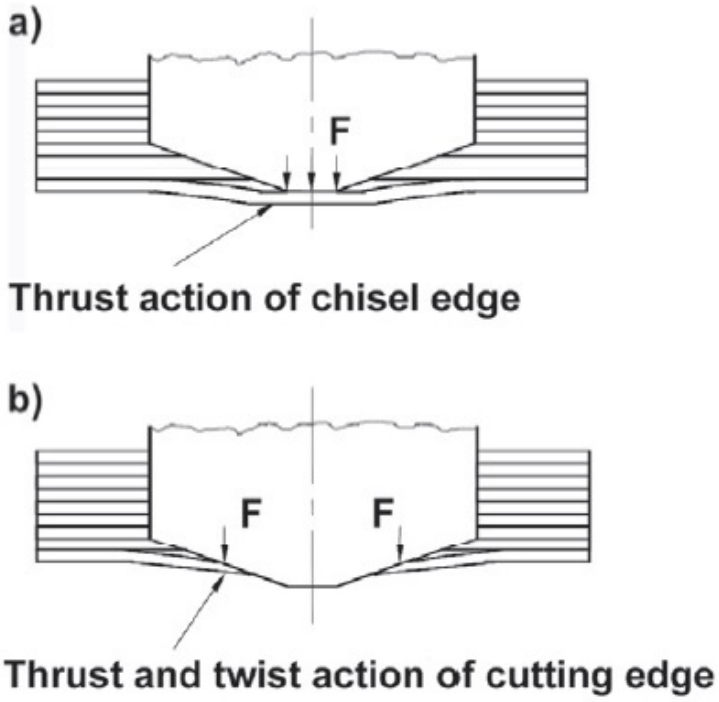

Figure 5.1: The phases of delamination development (a) Chisel edge action phase (b) Cutting edge action phase.

5.2 Conventional delamination factor F_d

There exists some major methods utilized for the assessment of the delamination levels around the drilled holes of the CFRP composites and hence the extension of the damaged zone should be quantified [120].

Chen et al. [39] proposed a comparing delamination factor F_d, and it's calculated from the ratio of the maximum diameter D_{max} of the delamination zone to the nominal hole diameter D_{nom} (Equation 5.2), is widely used to evaluate and characterize the level of delamination damage in composite materials. The conventional delamination factor F_d can be used where the damage is in regular form such as glass fibre reinforced plastics (GFRP) composites [121].

$$F_d = \frac{D_{max}}{D_{nom}} \tag{5.2}$$

Where F_d is conventional delamination factor; D_{max} is maximum diameter; D_{nom} is nominal hole diameter.

5.3 Alternative delamination factor F_a

The delamination criterion based on delamination factor F_d cannot be satisfactory because the extent of the delamination caused by just a few fibres, or fibre-bundles peeled up or pushed down to a distinct significant width will never predict truly the extent of the real characteristic delamination across the entire drilled hole periphery [36].

Mehta et al. [122] proposed a more accurate two dimensional delamination factor called the alternative delamination factor F_a (Equation 5.3). The alternative delmination factor F_a has been used in a very few studies due to complexity of the calculation of the area of an arbitrary damaged region at the hole periphery. However this delamination factor can be used where the damage is in irregular form and generally occurs in arbitrary shape, such as CFRP [121].

$$F_a = \frac{A_{max}}{A_{nom}} \tag{5.3}$$

Where F_a is alternative delamination factor; A_{max} is the area related to the maximum diameter of the delamination zone D_{max}, A_{nom} is the area of nominal hole D_{nom}. Figure 5.2 shows the scheme of delamination in drilling composite laminate.

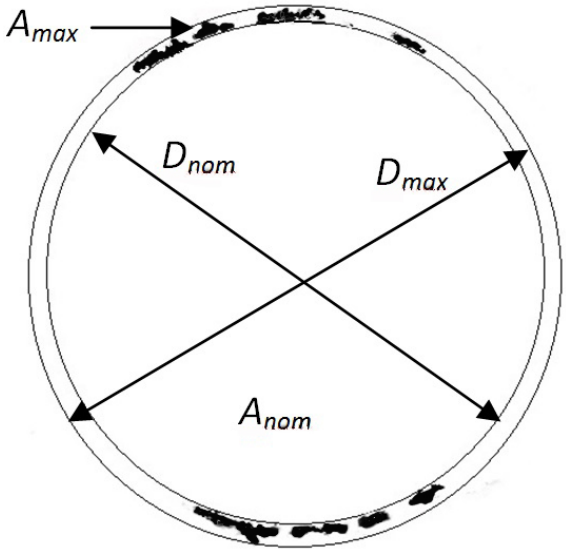

Figure 5.2: Scheme of delamination in drilling composite laminate.

5.4 Adjusted delamination factor F_{da}

Davim et al [123] presented a novel technique to measure the adjusted delamination factor F_{da} using digital analysis (Equation 5.4), it is used to process delaminations possessing an irregular pattern when machining CFRP, the adjusted delamination factor F_{da} can be described as follows:

$$F_{da} = F_d + \frac{A_d}{A_{max} - A_{nom}}(F_d^2 - F_d) \tag{5.4}$$

Thus.

$$\text{If} \begin{cases} A_d \to (A_{max} - A_{nom}) \Longrightarrow F_{da} \to F_d^2 \\ A_d \to 0 \Longrightarrow F_{da} \to F_d \end{cases}$$

Where F_{da} is adjusted delamination factor and A_d is the delaminated area in the region around the hole. In this study A_d was measured through a sequence of steps, firstly by using digital imaging processing which produced satisfactory pictures of the drilled holes and its surroundings, then the damaged area was obtained through processing the pictures using Image J software by selecting suitable parameters such as brightness intensity, noise suppression, image enhancement and edge detection to obtain an image with acceptable quality, and finally Image J software could be used to select the damaged areas and calculate the sum of areas. Figure 5.2 shows the delaminated areas in black colour.

The adjusted delamination factor F_{da} includes the effect of delamination area and shape, as the first part of Equation 5.4 represents the delamination factor or the size of the crack contribution, and the second part represents the damage area contribution.

5.5 Equivalent delamination factor F_{ed}

The adjusted delamination factor F_{da} is a better measure of delamination than F_d and F_a but the domination of damage area measured tends to exaggerate the factor value [124].

Tsao et al [125] proposed a delamination factor for a better measure of the delamination with a different two-dimensional criterion called the Equivalent Delamination Factor F_{ed}, Tsao concluded that whether the delamination area is minimum or maximum, F_{da} is not equivalent to F_d, also F_{da} is null for minimum and maximum

delamination area. Hence, F_{da} is similarly reasonable for regular delamination area. The Equivalent Delamination Factor F_{ed} is calculated as follows:

$$F_{ed} = \frac{D_e}{D_{nom}} \tag{5.5}$$

$$D_e = [\frac{4(A_d + A_{nom})}{\pi}]^{0.5} \tag{5.6}$$

Where F_{ed} is equivalent delamination factor; D_e is the equivalent delamination diameter. Figure 5.3 shows the scheme of F_{ed} delamination in drilling composite laminate.

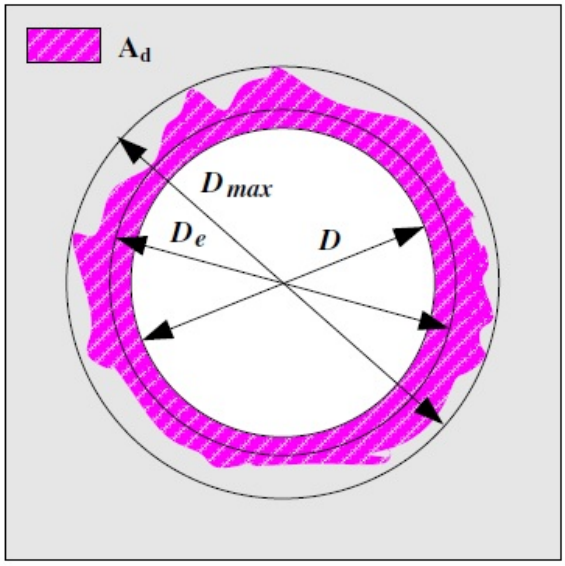

Figure 5.3: Scheme of F_{ed} delamination in drilling composite laminate [125].

5.6 Other delamination factors

Nagarajan et al. [126] proposed a delamination factor called the Refined Delamination Factor F_{dr} through extending the conventional delamination factor F_d and F_{da} and considers the severity of damage to characterize delamination.

They divided the total damage area into three sub divisions namely, heavy damage area A_H, medium damage area A_M, low damage area A_L and by using Buckingham's π theorem to develop Equation 5.7, they used seven steps to calculate D_{max} and the area of damage by generating a neural networks in MATLAB.

$$F_{dr} = \frac{D_{max}}{D_{nom}} + 1.783(\frac{A_H}{A_{nom}}) + 0.7156(\frac{A_M}{A_{nom}})^2 + 0.03692(\frac{A_L}{A_{nom}})^3 \quad (5.7)$$

Babu et al. [124] in their study evaluated the equivalent delamination factor F_{ed} in high speed drilling of a composite laminate to develop a Refined Equivalent Delamination Factor F_{red} (Equation 5.8) which always gives either an equal or a greater value than F_{ed}, the proposed method uses the area enclosed by the envelope of damaged zone and converts it in to a circle to determine the refined equivalent diameter, which includes any increase in hole diameter.

$$F_{red} = \frac{D_{re}}{D_{nom}} \quad (5.8)$$

Durao et al. [19], they suggested that the shape of the damaged area should be taken into account in the analysis of delamination,the shape is related with circularity (shape's compactness compared to a circle of equal perimeter) and defined as a function of the perimeter P and the area A of the damaged zone around the drilled hole as f (Equation 5.9).

$$f = 4\pi\frac{A}{P^2} \quad (5.9)$$

The value of circularity equals 1 for a perfect circle and decreases to zero for distended shapes as shown in Figure 5.4.

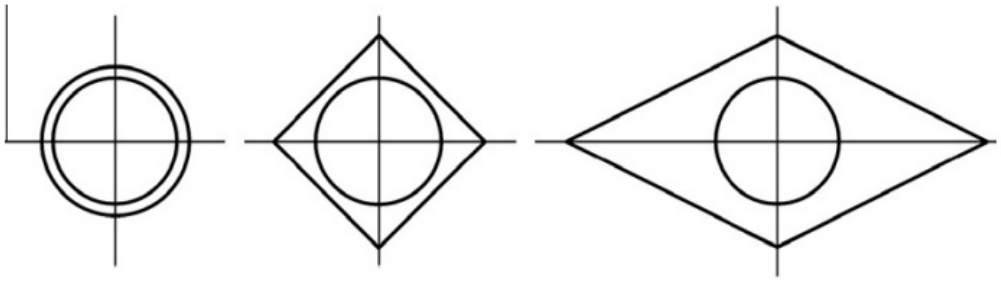

Figure 5.4: Circularity examples: (a) Circle ($f = 1$) (b) Square ($f = 0.79$) (c) Diamond shape ($f = 0.63$) [19].

Phadnis et al.[4] developed a delamination factor (Equation 5.10) by using a CT system to obtain the CT scan images of the drilled holes at drill entry and exit and transfer it to the MATLAB code developed in order to measure the extend of delamination at the entry and exit, Figure 5.5 shows the methodology of selecting delamination contours at drill entry and exit [4].

$$D = \frac{Damaged\ area}{Total\ intact\ area} = \frac{N_W}{N_W + N_B - N_{BH}} \tag{5.10}$$

where N_W is numbers of the white pixels, N_B is the numbers of black pixels and N_{BH} is the number of black pixels representing the drilled hole area.

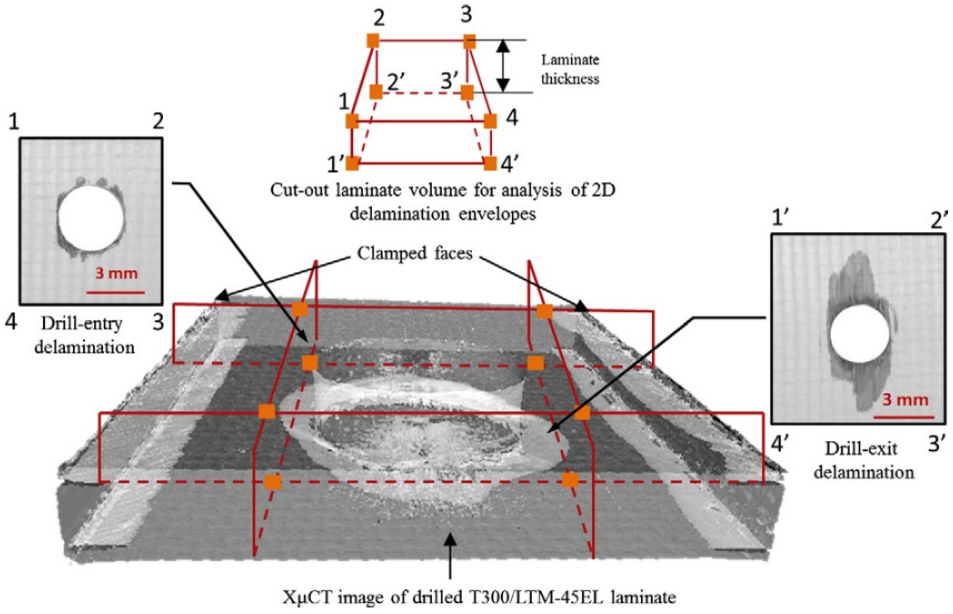

Figure 5.5: Methodology of selecting delamination contours at drill entry and exit [4].

5.7 Proposed delamination factor - equivalent adjusted delamination factor F_{eda}

In this study the back-up plate has been eliminated when drilling the unidirectional CFRP experimentally and in the FEM simulation. Hence, the delamination mechanism when drilling the workpiece without using the back-up plate becomes more complicated than drilling when using a back-up plate according to Capello [57], especially when conventional drilling is still considered the major drilling process used, therefore obtaining the delamination damage becomes more complicated and calculating the delamination factor at the hole entry is a challenge.

The study done by Tsao et al [125] shows F_{da} and F_{ed} had better recognition results regarding delamination damage when compared to F_d, moreover, the trend of F_d is almost identical to F_{da} and F_{ed}. The experimental results indicated that F_{ed} obtained through digital image processing is considered suitable for characterizing delamination. However, F_{da} is null for the minimum and maximum delamination area and also F_{da} had clearly larger values than F_{ed}.

In this study we have proposed a new delamination factor called the equivalent adjusted delamination factor F_{eda} as shown in Equation 5.11, the new delamination factor overcomes the null for minimum and maximum delamination areas and still can quantitatively estimate delamination areas possessing an irregular pattern to obtain better delamination factors and make it suitable for hole entry delamination.

$$F_{eda} = F_{ed} + \beta(F_{ed}^2 - F_{ed}) \tag{5.11}$$

Whereas:

$$\beta = \frac{A_{max} - A_{nom} - A_d}{A_{max}} \tag{5.12}$$

The new proposed delamination factor is a combination of the adjusted delamination factor F_{da} representation (size of the crack contribution and the damage area contribution) and the equivalent delamination factor F_{ed} representation (equivalent delamination diameter), as we have implemented F_{ed} instead of F_d because it has a better discrimination of delamination damage results.

While β is considered as a delamination free area ratio indicator, i.e., assuming A_{max} and A_{nom} are constant throughout the drilling process, hence whenever A_d increases then β decreases until β becomes zero which indicates that the whole area is delaminated. Also if the delamination area A_d equals zero or maximum then the second part of Eq. 19 results to zero leading to F_{eda} equaling F_{ed}.

Equation 5.2, Equation 5.4 and Equation 5.11 have been used in this research for comparison reasons.

Table 5.1 shows an example of the effect of delamination parameters on delamination factors highlighting the delamination free and maximal delamination area effects on delamination factors, it can be seen that F_{da} is null for these two cases whereas F_{eda} is equal to F_d and F_{ed}. This shows that the new delamination factor F_{eda} has overcome the null cases and can be used instead of F_{da} for delaminations possessing an irregular pattern while implementing the equivalent delamination diameter for F_{ed}.

Table 5.1: Example of the effect of delamination parameters on delamination factors.

D_{nom}	D_{max}	A_{nom}	A_{max}	A_d	F_d	F_{da}	F_{ed}	F_{eda}
8.000	8.000	50.265	50.265	0.000	1.000	DIV/0	1.000	1.000
8.000	8.112	50.265	51.683	0.091	1.014	1.015	1.001	1.001
8.000	8.406	50.265	55.497	1.147	1.051	1.062	1.011	1.012
8.000	8.792	50.265	60.711	1.623	1.099	1.116	1.016	1.018
8.000	9.000	50.265	63.617	13.352	1.125	1.266	1.125	1.125

Chapter 6

Results and Discussion

6.1 PCD Twist drill analysis

6.1.1 FE model validation

Thrust force and torque (5000rpm - 500mm/min)

Thrust force and torque measured in the drilling experiments were calculated and compared with the results obtained from the new FE model. Figure 6.2 and Figure 6.3 are examples of graphs for thrust force and torque measured obtained from experiment and FE analysis, it can be seen that the experiment and simulation graphs have different timelines due to the thickness of CFRP samples used in the experiments are less thicker than FE simulation samples so as to reduce simulation time, while Table 6.1 shows the force and torque measured in the drilling process when the spindle speed was 5000 rpm and feed rate was 500 mm/min.

It can be seen that the average thrust force measured in the experiments was 123.3 N whereas the FE result showed 118 N; the experimental torque was 0.39 N.m and FE torque was 0.36 N.m, the deviation in results ranges approximately between 4% to 8%.

Table 6.1: Experimental and FE thrrust force and torque measurements for spindle speed 5000 rpm and feed rate 500 mm/min.

Drill type	Exp.	FE	%Errors	Exp.	FE	%Errors
	Thrust force (N)	Thrust force (N)		Torque (N.m)	Torque (N.m)	
PCD twist drill	123.28	118	4.28	0.39	0.36	7.69

The data obtained from Figure 6.2 and Figure 6.3 can be summarized in Table 6.2 and Table 6.3. The deviation in results ranges from 1.5% to 16.5 for maximum value and 3.7% to 15.5% for minimum value, hence the accuracy between the experiment and the FE simulation results for average, maximum and minimum is concluded close and within acceptable range, which indicates the FE model is accurate.

Table 6.2: Experimental and FE maximum thrust force and torque measurements for spindle speed 5000 rpm and feed rate 500 mm/min.

Drill type	Exp.	FE	%Errors	Exp.	FE	%Errors
	Max. thrust force (N)	Max. thrust force (N)		Max. torque (N.m)	Max. torque (N.m)	
PCD twist drill	157	135	16.29	0.52	0.53	1.92

Table 6.3: Experimental and FE minimum thrust force and torque measurements for spindle speed 5000 rpm and feed rate 500 mm/min.

Drill type	Exp.	FE	%Errors	Exp.	FE	%Errors
	Min. thrust force (N)	Min. thrust force (N)		Min. torque (N.m)	Min. torque (N.m)	
PCD twist drill	91	79	15.18	0.28	0.27	3.70

Thrust force and torque (10000rpm - 1250mm/min)

Table 6.4 shows drilling force and torque of experiment and FE simulation at spindle speed of 10000 rpm and feed rate of 1250 mm/min, the experimental thrust force measured was 140.09 N whereas the FE result showed 134 N; the experimental torque was 0.45 N.m and FE torque was 0.42 N.m, the difference in results approximately ranges between 4.5% to 7.5%.

the deviations for FEA thrust force and torque when compared to experimental results for both validations shown above have occurred due to modeling affects such as the precise modeling of the drill bits or the constitutive properties, but mainly the accuracy between the experiment and the FE simulation results are concluded close and within acceptable range, which indicates the FE model is accurate.

To provide a bigger picture of %errors, Figure 6.1 shows a statistical comparison of the %errors for other cutting conditions used in this study for thrust force and torque using twist drill.

Table 6.4: Experimental and FE thrust force and torque measurements for spindle speed of 10000 rpm and feed rate of 1250 mm/min

Drill type	Exp.	FE	%Errors	Exp.	FE	%Errors
	Thrust force (N)	Thrust force (N)		Torque (N.m)	Torque (N.m)	
PCD twist drill	140.09	134.00	4.54	0.45	0.42	7.14

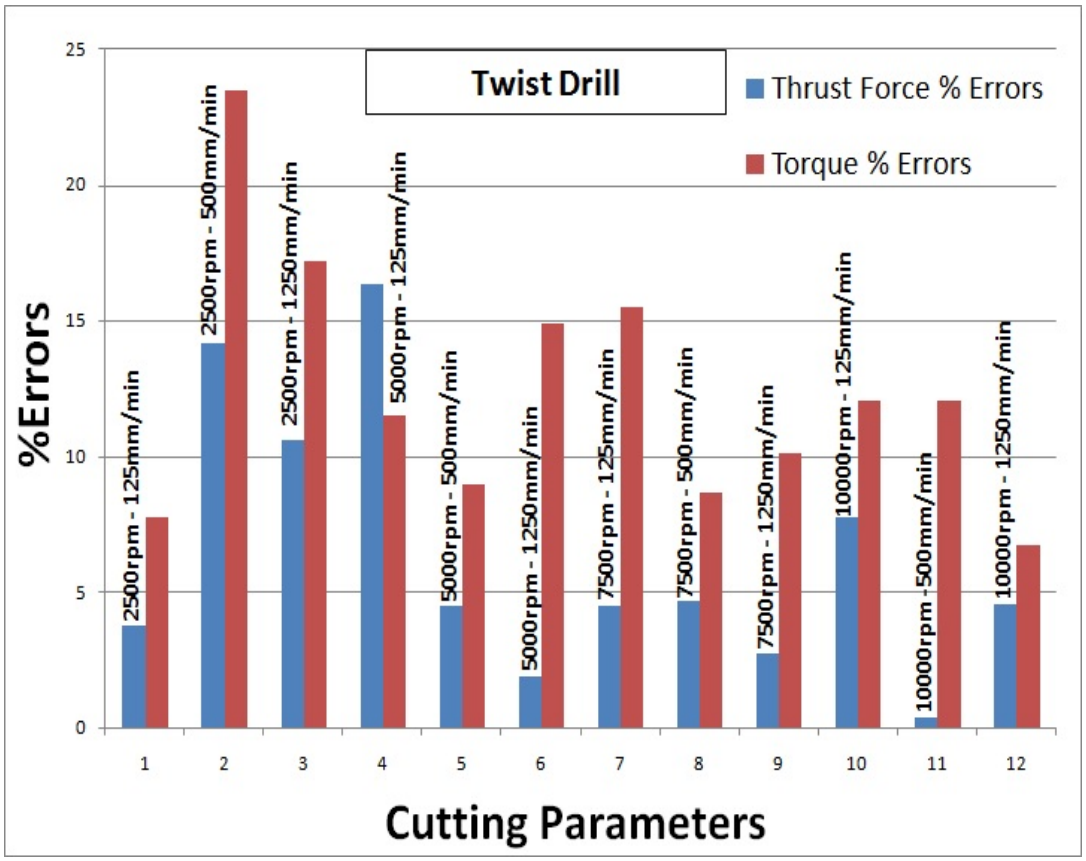

Figure 6.1: Statistical comparison of the %errors for thrust force and torque using twist drill.

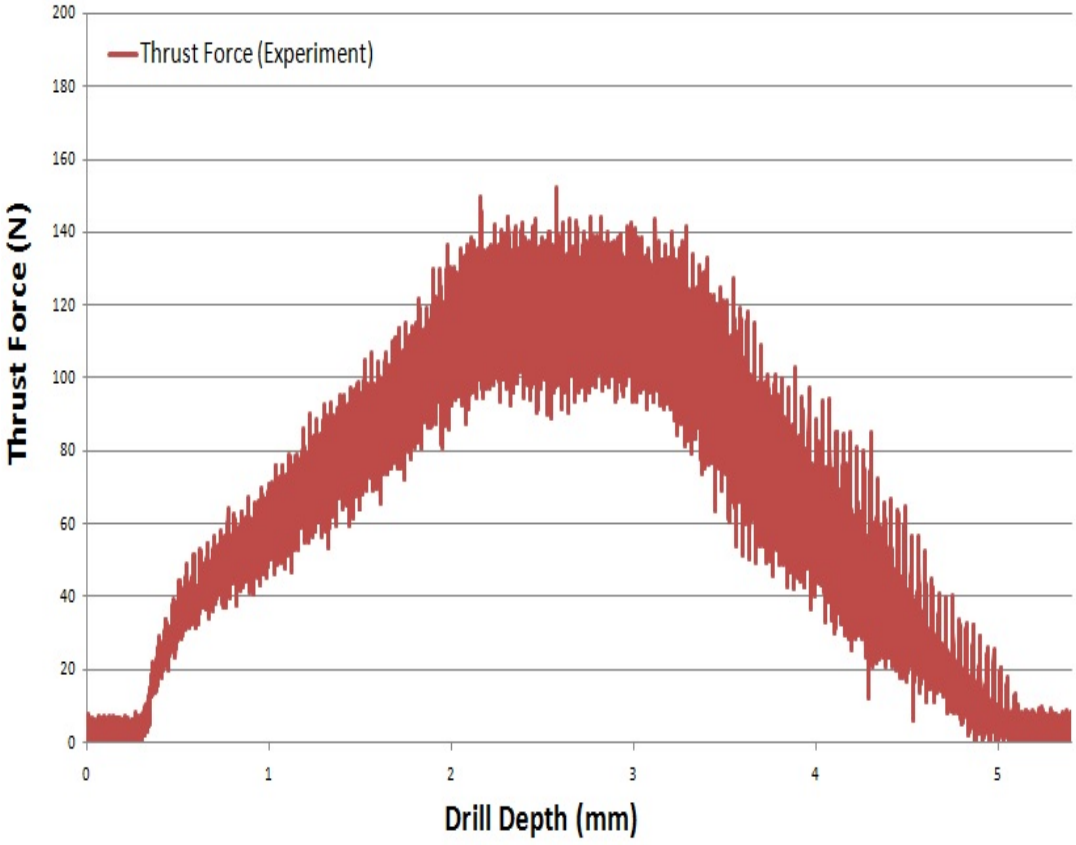

(a)

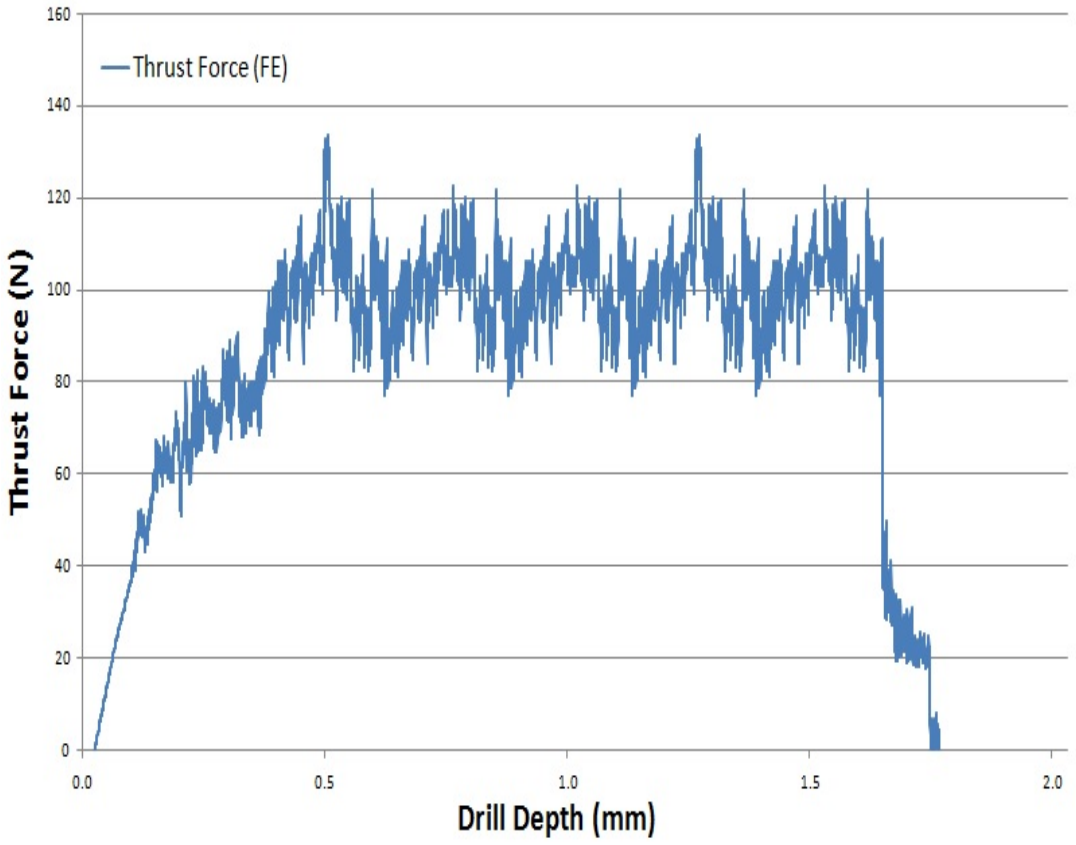

(b)

Figure 6.2: Example of (a) Experimental result of thrust force. (b) Simulation result of thrust force.

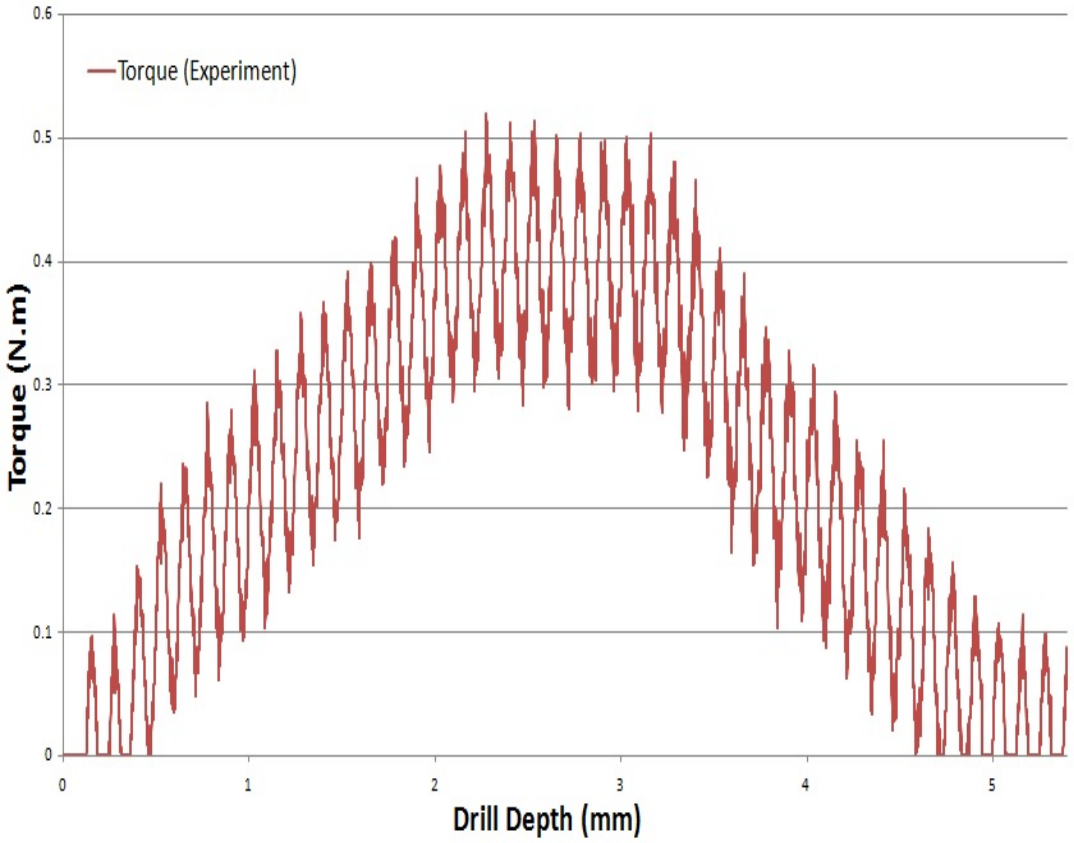

(a)

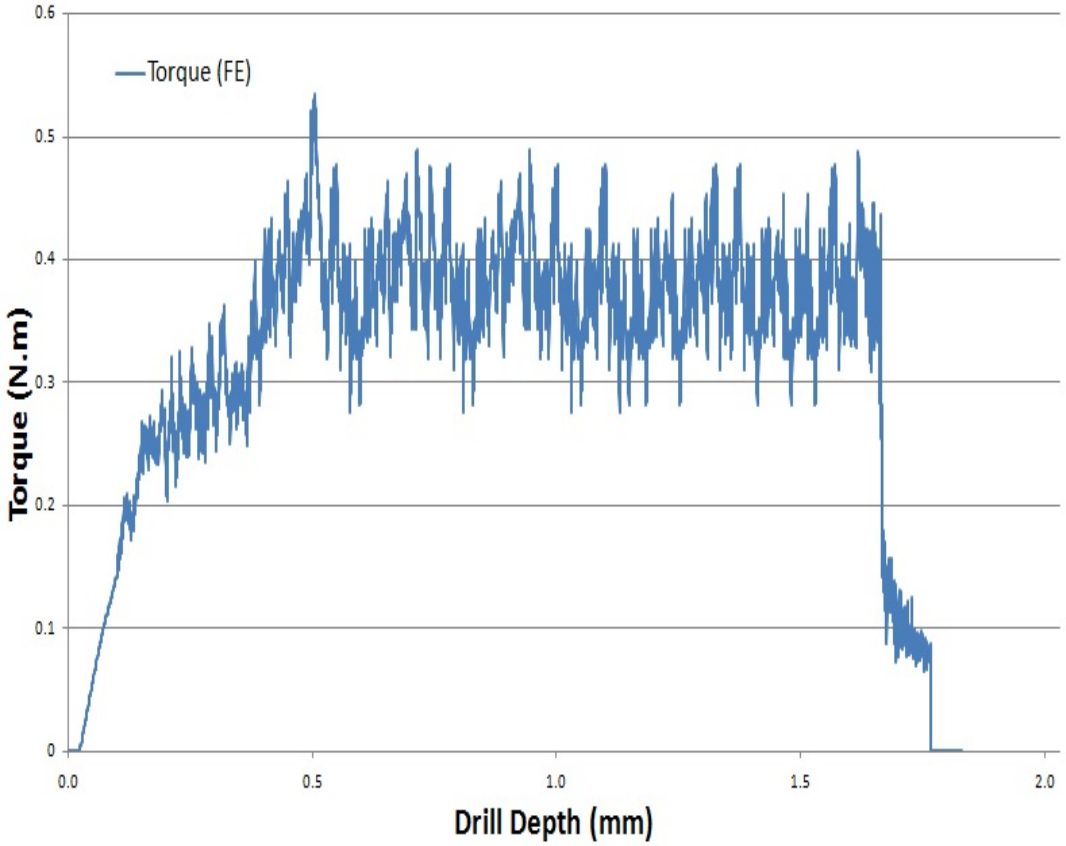

(b)

Figure 6.3: Example of (a)Experimental result of torque. (b) Simulation result of torque.

Effect of feed rate on thrust force and torque

Feed rate is one of the major parameters that affect drilling of composite materials. As shown in Figure 6.4(a) and 6.4(b), thrust force and torque went up with the increase of feed rate when spindle speed was constant 10000rpm. To be specific, thrust force in the experiment was 56 N at 125 mm/min feed rate, and the highest was 140 N at 1250 mm/min feed rate, whereas the FE simulation was estimated minimum of 52 N at 125 mm/min feed rate, and the highest was 134 N at 1250 mm/min feed rate. Whilst the torque in the experiment was 0.11 N.m at 125 mm/min feed rate, and the highest was 0.44 N.m at 1250 mm/min feed rate, whereas the FE was estimated 0.1 N.m at 125 mm/min feed rate, and the highest was 0.42 N.m at 1250 mm/min feed rate.

In terms of feed per revolution effect on thrust force and torque, it is evident that when spindle speed is constant and feed per revolution is increased then feed rate will increase leading to thrust force and torque increasing as well. On the other hand, if feed rate and spindle speed are increased proportionally then feed per revolution stays the same, however, if the spindle speed is increased, the cutting speed (the relative speed between the cutting edge and the workpiece) will be increased correspondingly, this will definitely cause the increase in cutting force without doubt.

Effect of feed rate and spindle speed on thrust force and torque

In order to predict the effects of feed rate and spindle speed on thrust force and torque in the drilling process, and by using the validated FE model, a combination of drill feed rates and spindle speeds were chosen from Table 6.5. The overall results (Figure 6.5) show that thrust force and torque increase with the increase in drill feed rate and decrease with the increase in spindle speed. It was found that thrust force increased by 158% when the drill feed rate increased from 125 mm/min to 1250 mm/min at spindle speed of 10000 rpm, torque increased by 320%. Also thrust force decreased by 35% when spindle speed increased from 2500 rpm to 10000 rpm at 125 mm/min, and the torque decreased by 61%.

In the case of predicting the influence of change of feed rate and spindle speed on thrust force and torque in each individual condition, it can be seen from Figure 6.5 there is more precipitous increase behaviour of graph in each condition when feed rate is increased compared to when spindle speed is increased, hence it can be concluded that feed rate has more effect than spindle speed and using low feed rates and high speed is recommended.

Table 6.5: Cutting parameters used in optimization study.

Spindle speed (rpm)	2500	5000	10000	10000	10000	7500	7500
Feed rate (mm/min)	125	500	1250	125	500	125	500

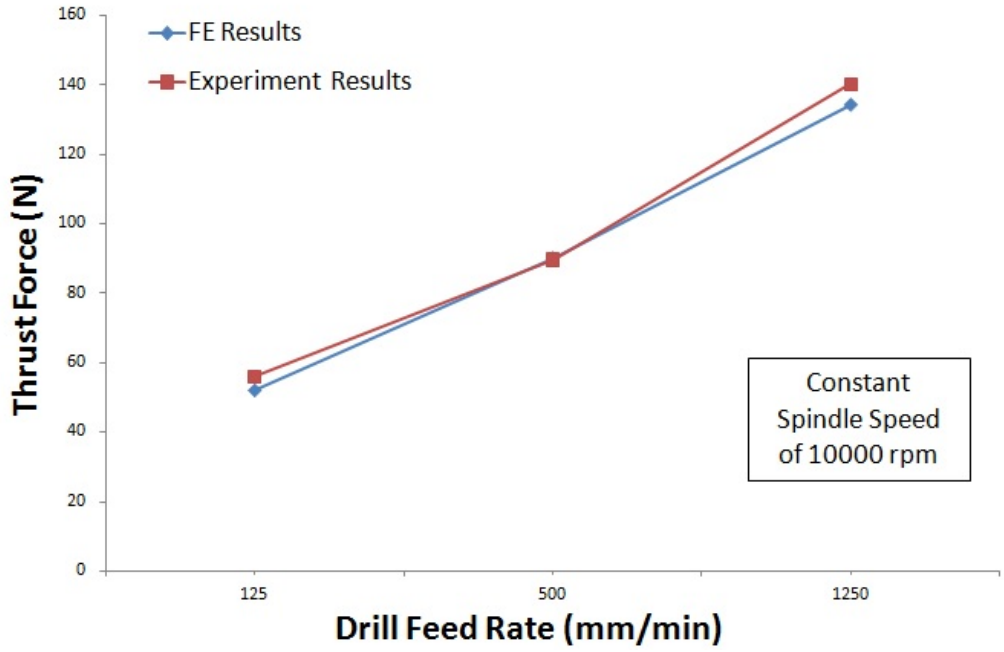

(a)

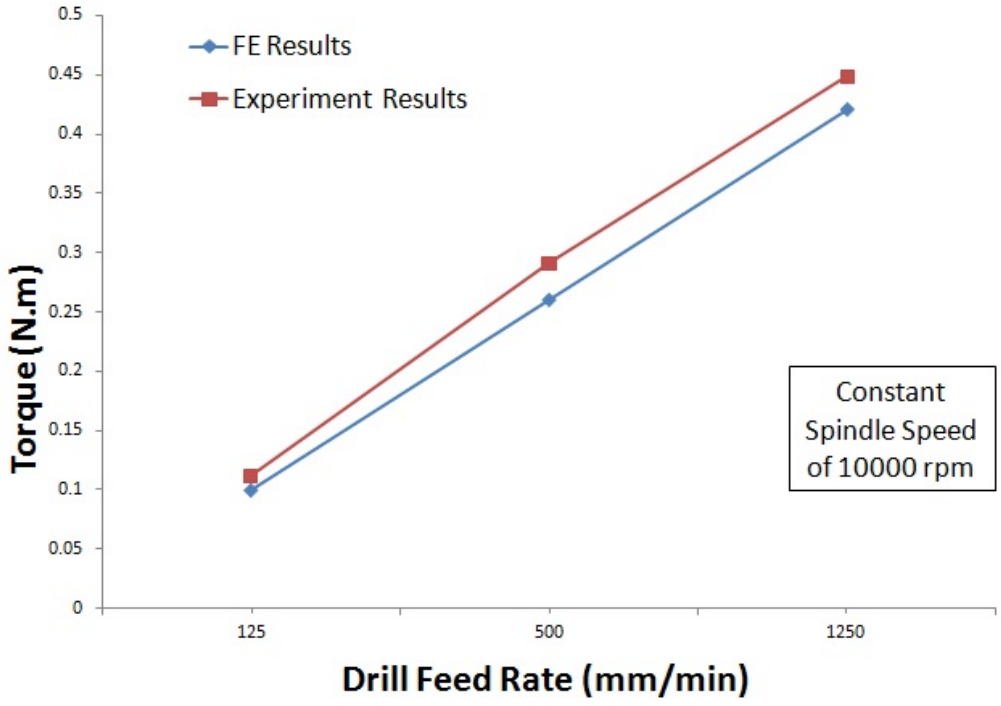

(b)

Figure 6.4: PCD twist drill (a) Thrust force analysis (Experiment and FE). (b) Torque analysis (Experiment and FE).

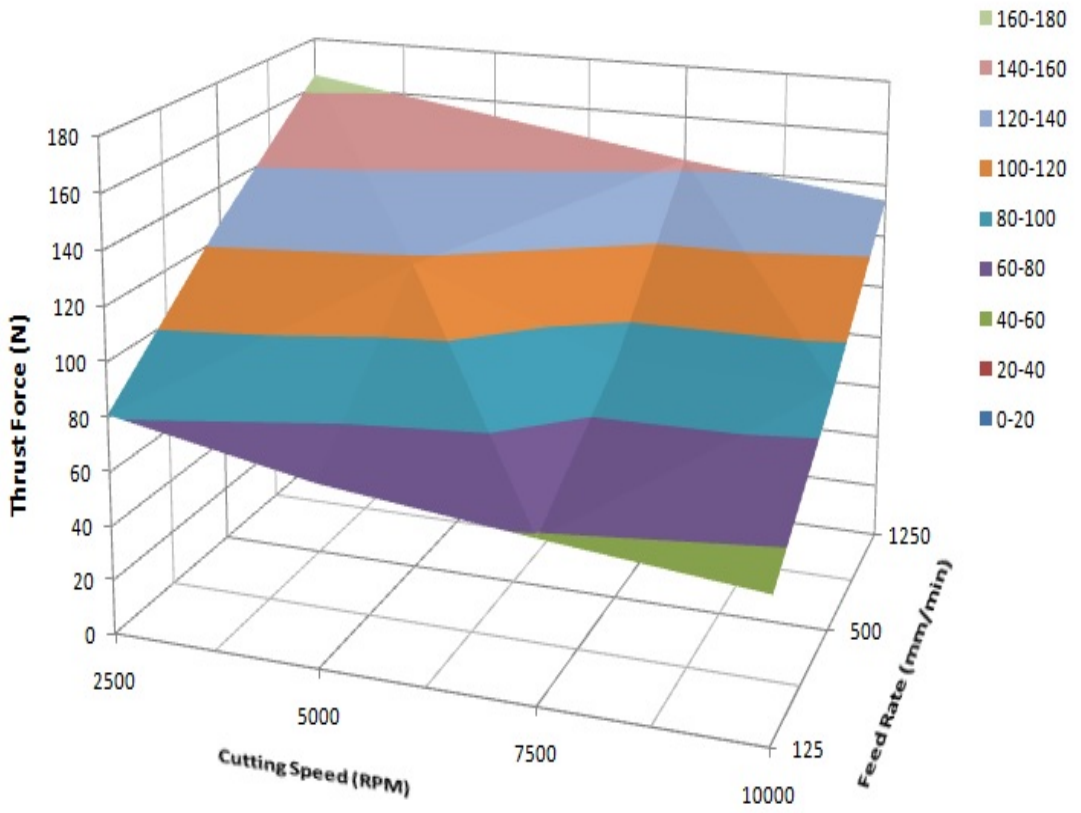

(a)

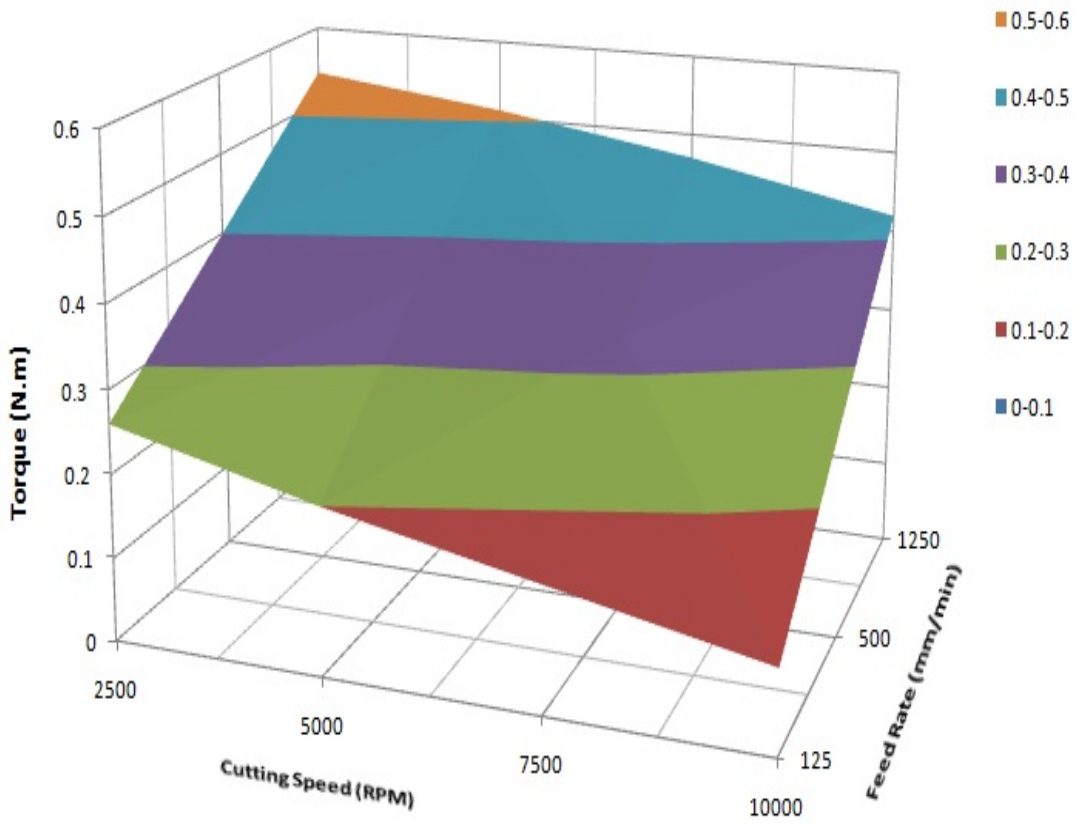

(b)

Figure 6.5: PCD twist drill (a) Effect of drill feed rate and spindle speed on thrust force. (b) Effect of drill feed rate and spindle speed on torque.

6.1.2 Delamination factor analysis

To investigate the effect of operating parameters for PCD twist drill on the drilling induced damage, the delamination factors obtained in the experimental drilling and finite element analysis were calculated and compared.

Figure 6.6 shows results of delamination occurred on the drilled hole entrance peripheral at different cutting parameters. Figures in (a) illustrate the SEM images of holes drilling in the experiments with noises inside the holes filtered, Figures in (b) show the acquired delamination areas of Figures in (a) after being processed with "Image J" software. Figures in (c) show the FEA simulation results of drilling induced damage. By comparing figures (b) and (c), it can be seen that the FEA prediction was well estimated and the general delamination trend is very similar to the experiment results.

Effect of spindle speed on experimental delamination factors

The experimental delamination factor F_d, the adjusted delamination factor F_{da} and the equivalent adjusted delamination factor F_{eda} are calculated and compared in each case against spindle speed; the results are shown in Figure 6.7. From these results it can be seen that F_{da} is highest value of the delamination factors, and due to the increase of number of cutting action in the cutting edges at each stage of feed, the trend of delamination factors decreases with the increase in spindle speed. It can be noted that when spindle speed increased 300%, F_d decreased between 0.63% to 4.1%, F_{da} decreased between 0.8% to 5.0% while F_{eda} decreased between 0.15% to 1.0%.

Effect of feed rate on experimental delamination factors

The same concept is done for the experimental delamination factors in regards to feed rate; as shown in Figure 6.8, as the increase in feed rate leads to the rise of delamination factors. Delamination increases drastically when feed rate is over 500mm/min especially when the feed rate reaches 1250 mm/min. This indicates feed rate has more effect on delamination than the effect of spindle speed due to the highly correlation increase of thrust force with the increase of feed rate, which plays a significant role in delamination when drilling composite materials.

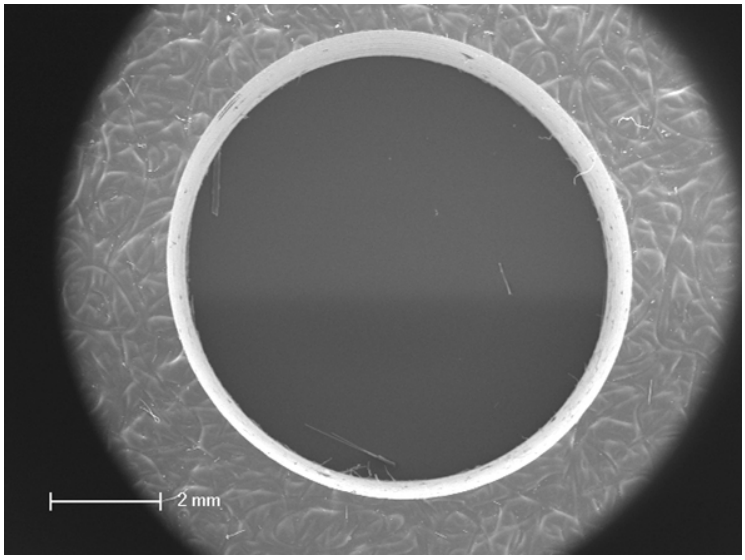

1(a)

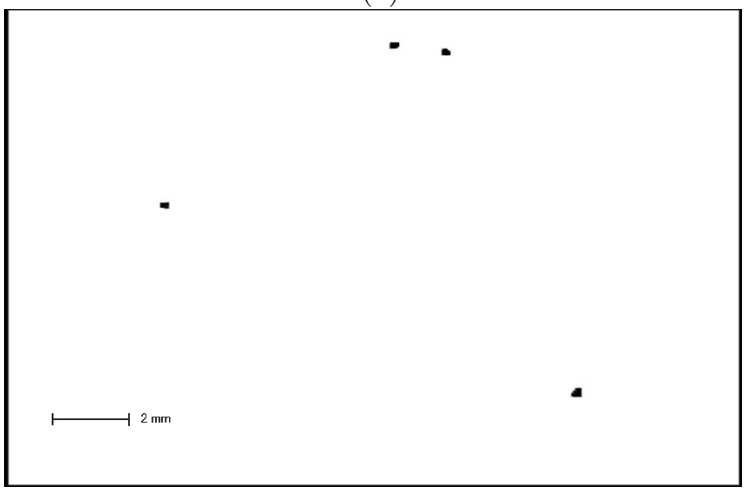

1(b)

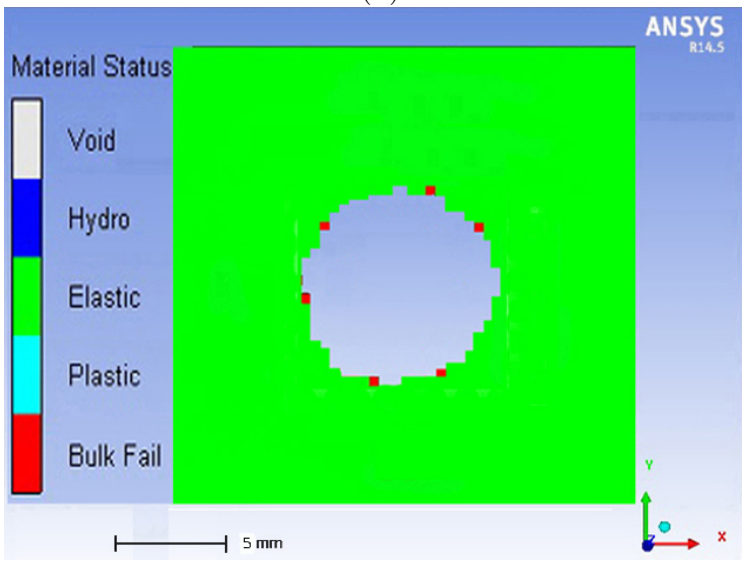

1(c)

(PCD twist drill) (Spindle speed: 7500 rpm) (Feed rate: 125 mm/min)

Figure 6.6: Delamination analysis for drill entry (a) SEM image processing. (b) Experimental delamination areas. (c) Finite element delamination.

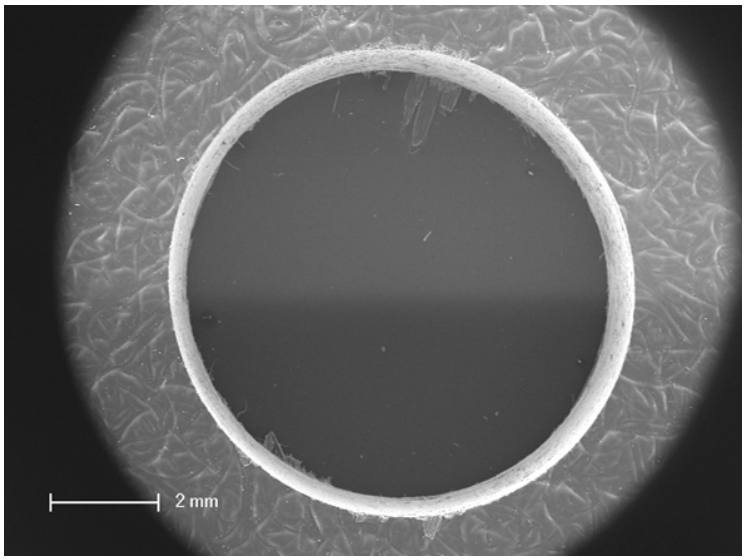

2(a)

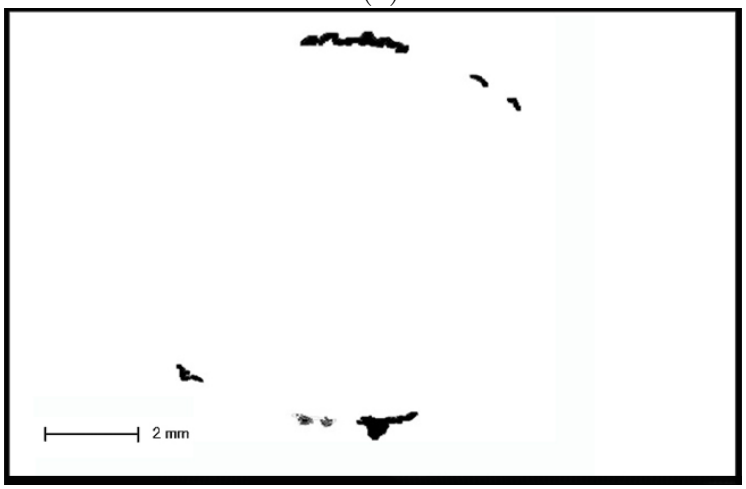

2(b)

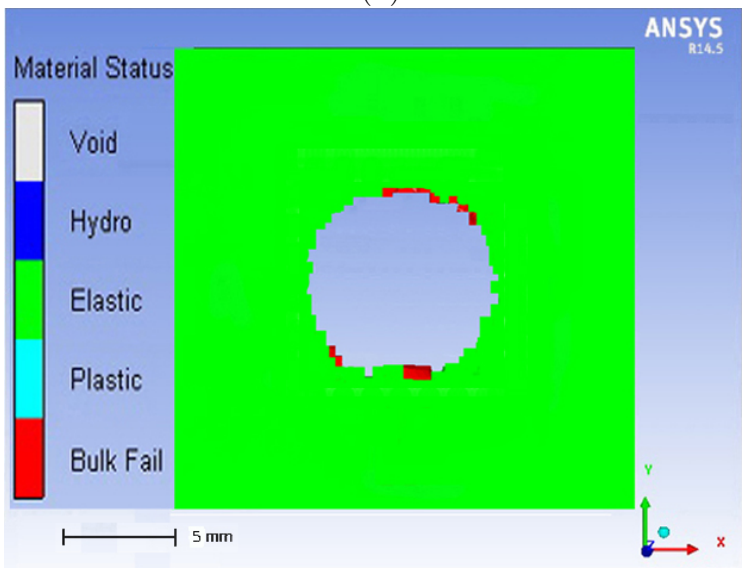

2(c)

(PCD twist drill) (Spindle speed: 7500 rpm) (Feed rate: 500 mm/min)

Figure 6.6: Delamination analysis for drill entry (a) SEM image processing. (b) Experimental delamination areas. (c) Finite element delamination.

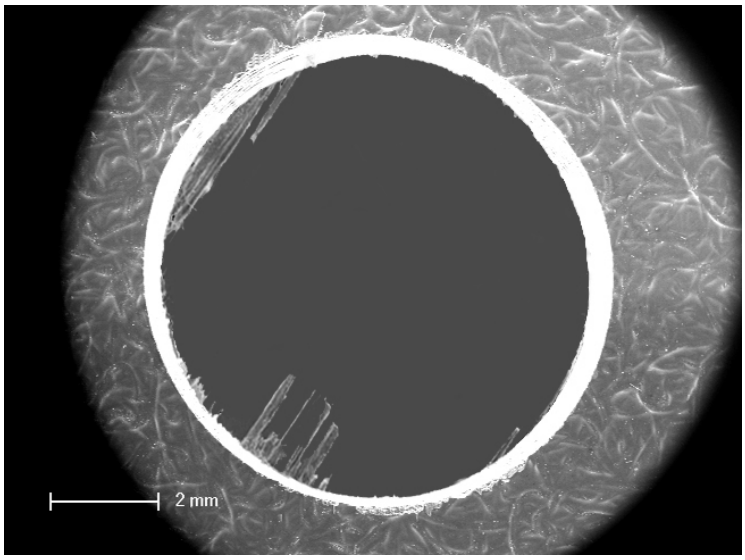

3(a)

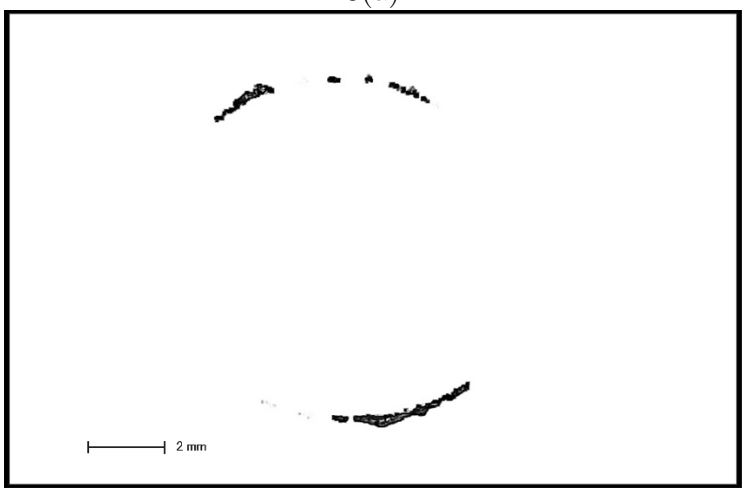

3(b)

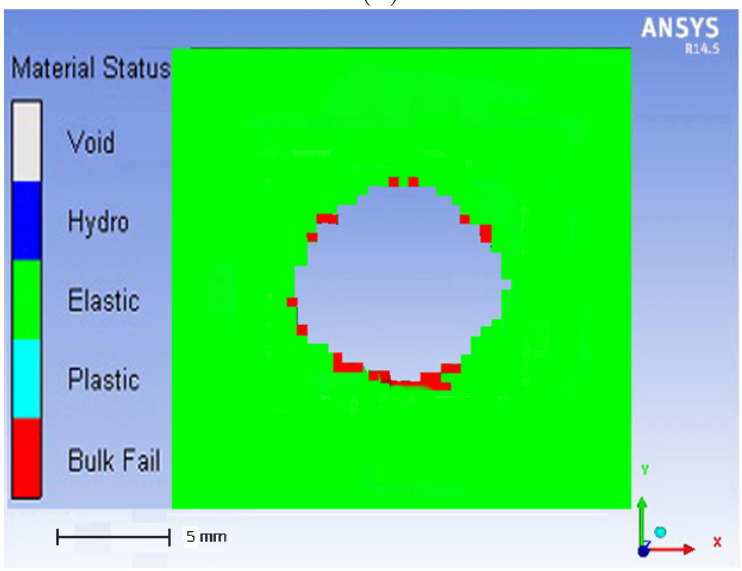

3(c)

(PCD twist drill) (Spindle speed: 7500 rpm) (Feed rate: 1250 mm/min)

Figure 6.6: Delamination analysis for drill entry (a) SEM image processing. (b) Experimental delamination areas. (c) Finite element delamination.

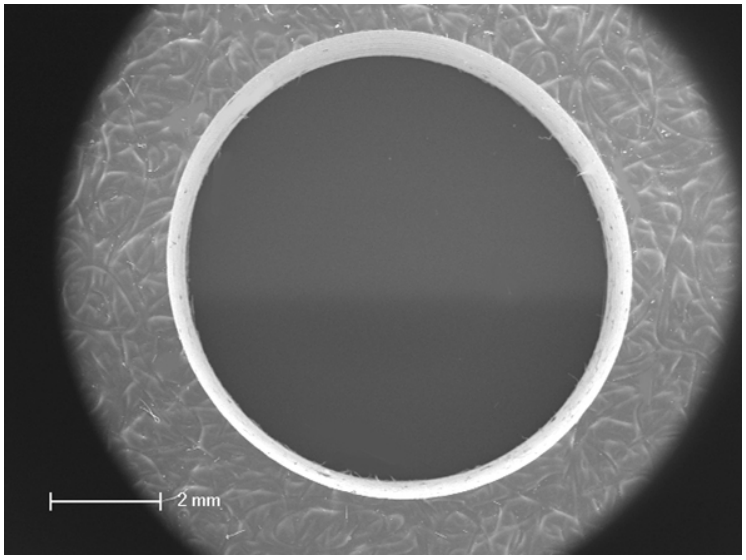

4(a)

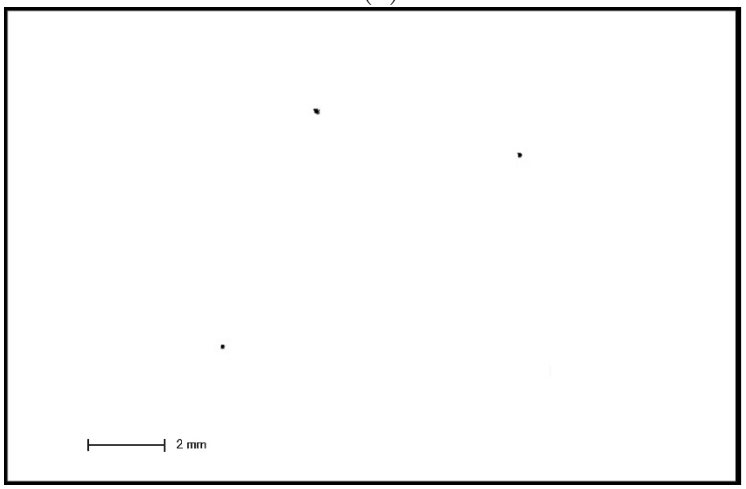

4(b)

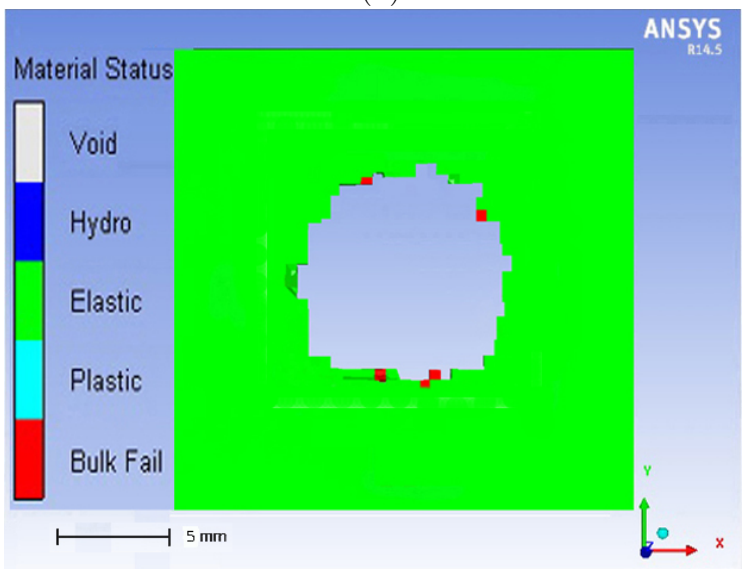

4(c)

(PCD twist drill) (Spindle speed: 10000 rpm) (Feed rate: 125 mm/min)

Figure 6.6: Delamination analysis for drill entry (a) SEM image processing. (b) Experimental delamination areas. (c) Finite element delamination.

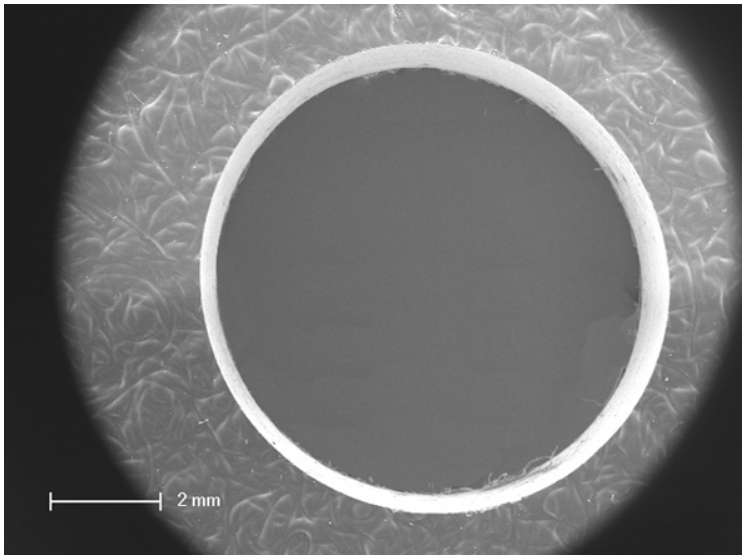

5(a)

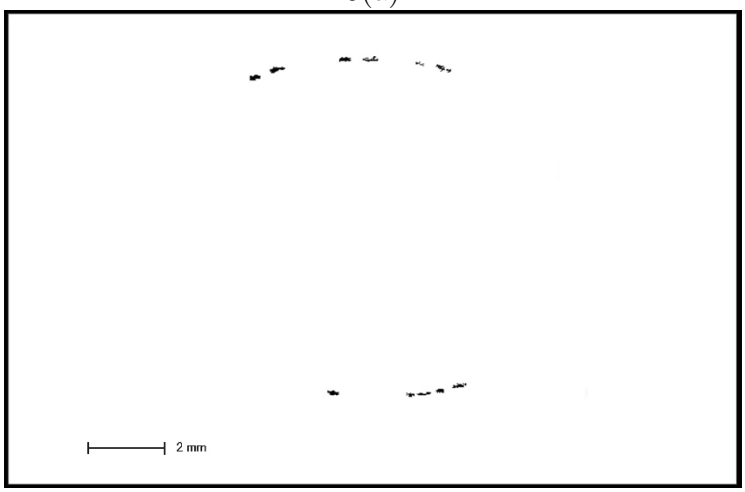

5(b)

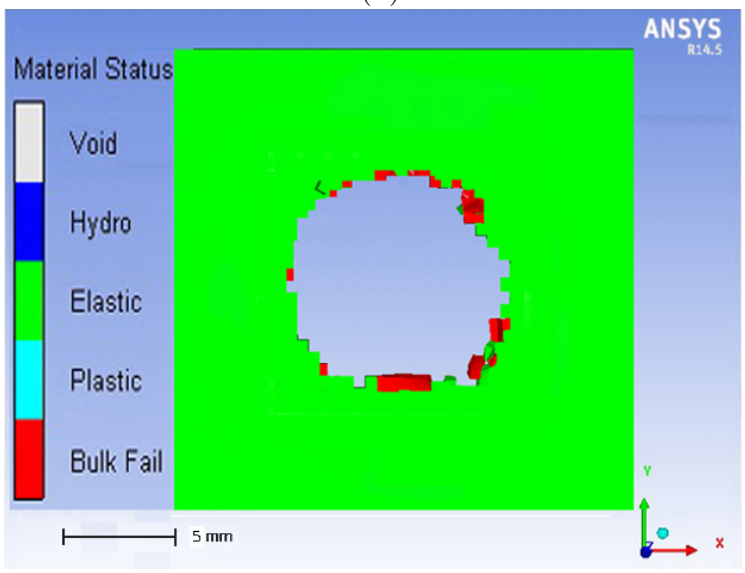

5(c)

(PCD twist drill) (Spindle speed: 10000 rpm) (Feed rate: 500 mm/min)

Figure 6.6: Delamination analysis for drill entry (a) SEM image processing. (b) Experimental delamination areas. (c) Finite element delamination.

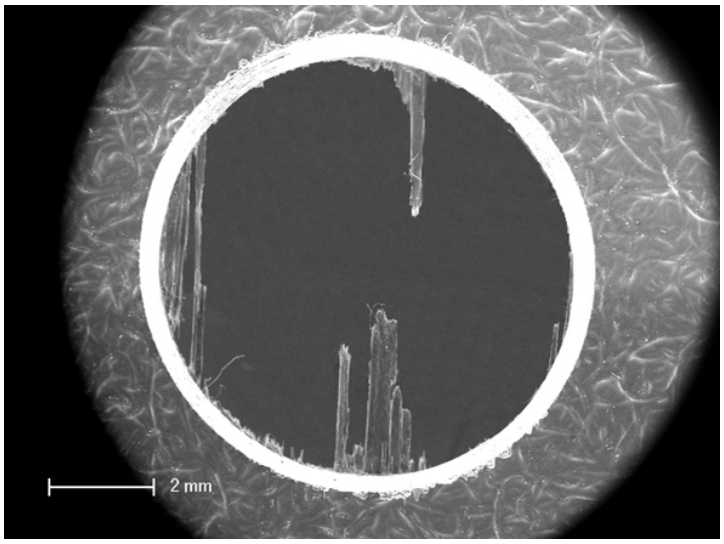

6(a)

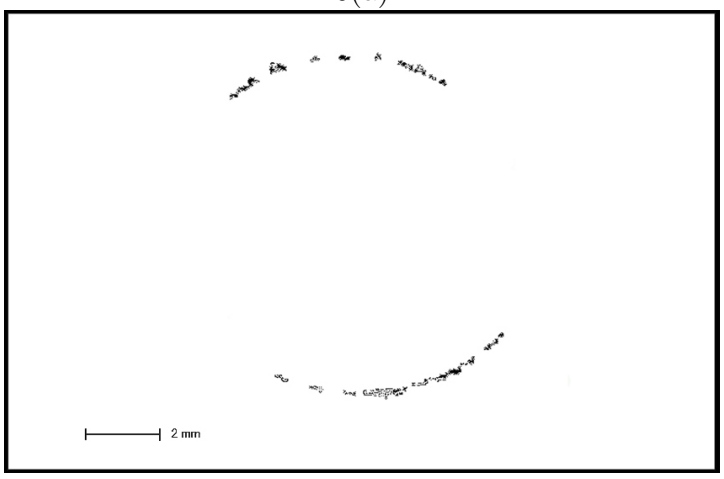

6(b)

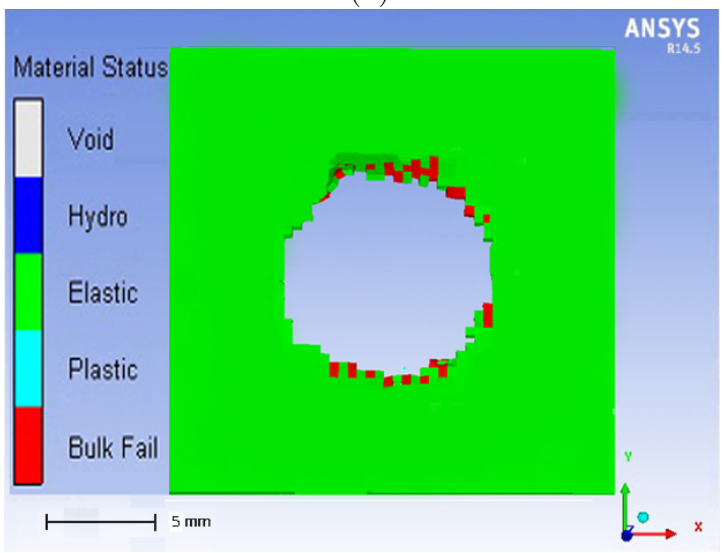

6(c)

(PCD twist drill) (Spindle speed: 10000 rpm) (Feed rate: 1250 mm/min)

Figure 6.6: Delamination analysis for drill entry (a) SEM image processing. (b) Experimental delamination areas. (c) Finite element delamination.

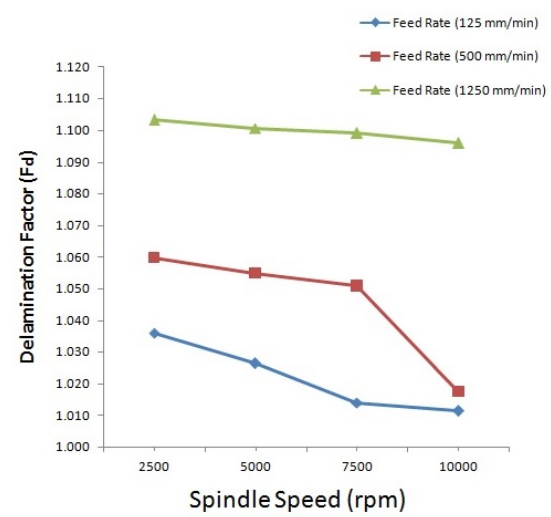

(a)

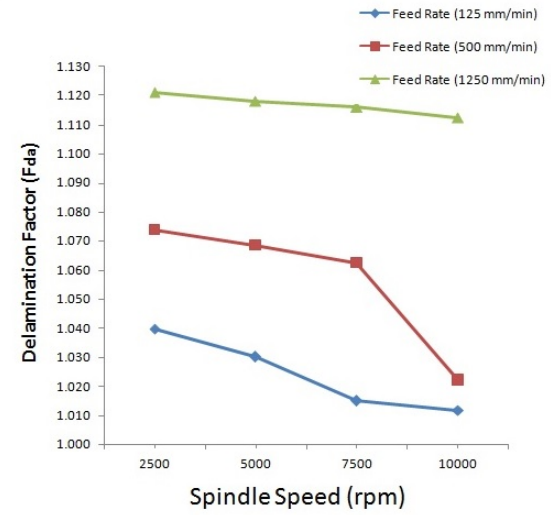

(b)

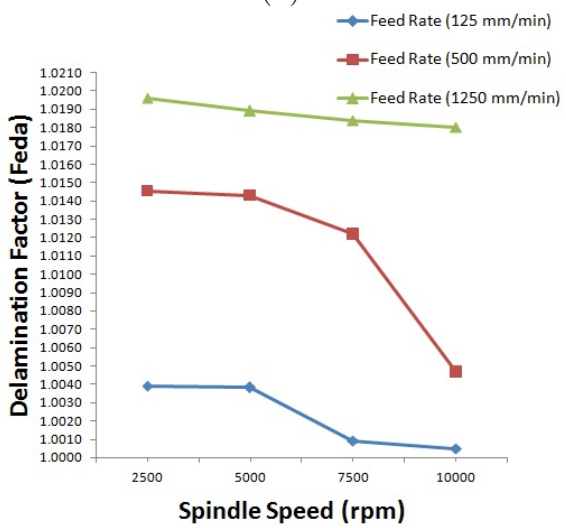

(c)

Figure 6.7: Effect of PCD twist drill spindle speed on experimental delamination factors (a) Conventional delamination factor F_d (b) Adjusted delamination factor F_{da} (c) Equivalent adjusted delamination factor F_{eda}.

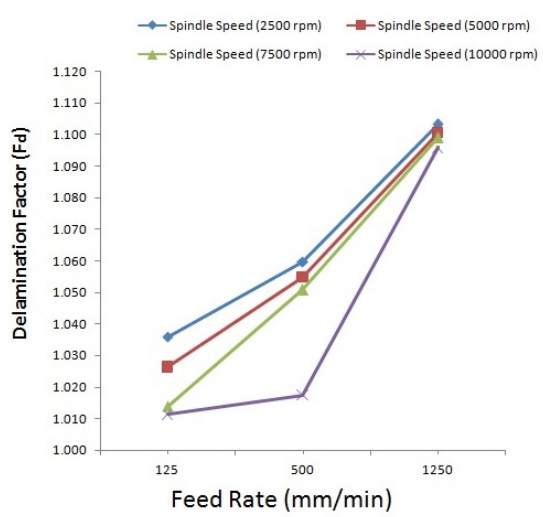

(a)

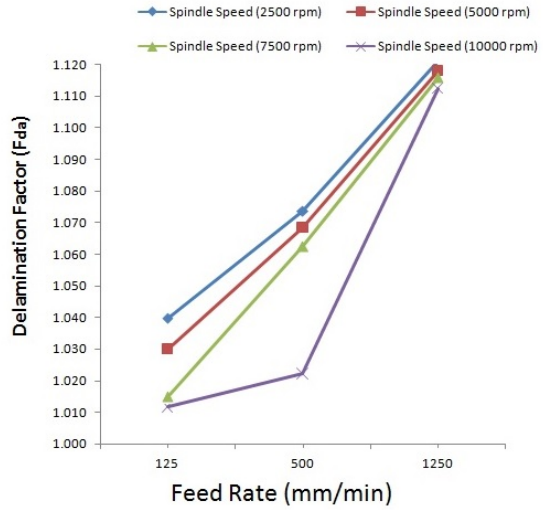

(b)

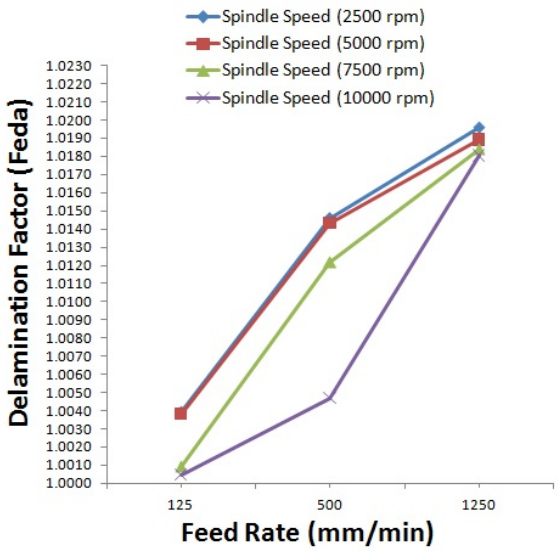

(c)

Figure 6.8: Effect of PCD twist drill feed rate on experimental delamination factors (a) Conventional delamination factor F_d (b) Adjusted delamination factor F_{da} (c) Equivalent adjusted delamination factor F_{eda}.

Effect of feed rate on FE delamination factors at constant spindle speed (7500rpm)

To validate simulation results, the delamination factors F_d, F_{da} and F_{eda} were calculated and compared for spindle speed of 7500 rpm and feed rates of 125 mm/min, 500 mm/min and 1250 mm/min, as shown in Table 6.6 and Figure 6.9, results show that trend of delamination factors is similar to the trend of experimental results, as F_d, F_{da} and F_{eda} increased 8.8%, 22.4% and 12.9% respectively with the increase of feed rate from 125 mm/min to 1250 mm/min. The difference in results between experiment and FE simulation ranges from 4.15% to 4.54% for F_d, 4.82% to 16.69% for F_{da} and 0.72% to 11.76% for F_{eda} which is a good correlation of output results.

It can be seen from the results in Table 6.6 that F_d and F_{da} have close values to each other whereas the F_{eda} has much lower values due to the effect of F_{ed}, it also shows that F_{eda} and F_{da} have better discrimination values than F_d. It also shows the percentage of errors between the experiment and FEA for F_{eda} is less than F_{da}.

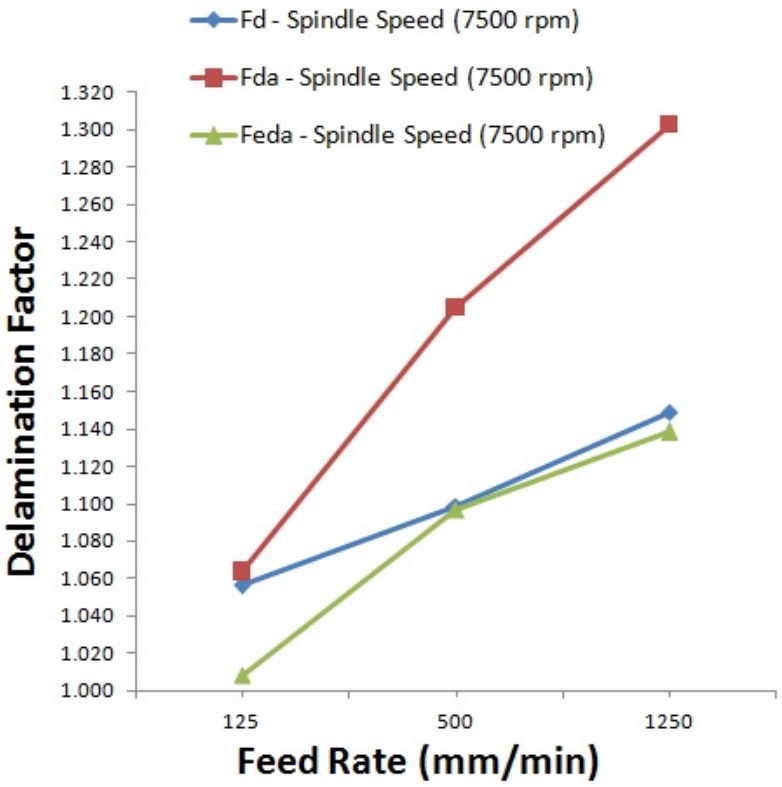

Figure 6.9: Effect of PCD twist drill feed rate on FE delamination factors.

Table 6.6: Twist drill delamination factors for experimental and FEA at drill entry for 7500 rpm.

Cutting parameters		Experimental			FEA			% Errors		
Spindle speed (rpm)	Feed rate (mm/min)	F_d	F_{da}	F_{eda}	F_d	F_{da}	F_{eda}	F_d	F_{da}	F_{eda}
7500	125	1.014	1.015	1.001	1.056	1.064	1.008	4.150	4.820	0.726
7500	500	1.051	1.062	1.012	1.098	1.205	1.097	4.540	13.374	8.379
7500	1250	1.099	1.116	1.018	1.149	1.302	1.138	4.540	16.695	11.764

Effect of feed rate on FE delamination factors at constant spindle speed (10000rpm)

Also another validation of the FE simulation results have been done as F_{eda} was calculated and then compared at spindle speed of 10000 rpm and different feed rates of 125 mm/min, 500 mm/min and 1250 mm/min. The results in Table 6.7 shows the similarity in trend for delamination factors of FE simulation and experiment drilling, it also shows that F_{eda} has increased 12.7% for FE simulation when feed rate increased from 125 mm/min to 1250 mm/min. The difference between the experiment and FE simulation results approximately ranges from 0.73% to 11.57%, this leads to a clear correlation of result output.

Table 6.7: Twist drill delamination factors for experimental and FEA at drill entry for 10000 rpm

Cutting parameters		Experimental	FE	% Errors
Spindle speed (rpm)	Feed rate (mm/min)	F_{eda}	F_{eda}	F_{eda}
10000	125	1.001	1.008	0.739
10000	500	1.005	1.068	6.304
10000	1250	1.018	1.136	11.570

6.1.3 Stress analysis

Figure 6.10 shows the FE stress distribution and onset damage respectively on the first ply when the twist drill has started penetrating the unidirectional carbon fibre reinforced composite workpiece for spindle speed of 10000 rpm and feed rates of 1250 mm/min. As mentioned earlier, the workpiece will act and deform as orthotropic homogeneous elastic according to the fibre orientation through a defined local coordinate system.

As shown in Figure 6.10(a) the von Mises stress obtained from the FE simulation is

52.71 MPa which is higher than the 90^0 failure tensile strength (40.00 MPa) listed in the VTM264 CFRP specification sheet shown in appendix (A), which indicates the tensile matrix mode being dominant failure mode as shown in Figure 6.10(b), the Hashin failure modes with elements failing will be removed when they reach the value of 1, also it can be observed that the highest stresses are induced around the centre of hole, this indicates that the stress analysis is correct and can be concluded as verified.

The distribution of stress, effective strain and pressure for the PCD twist drill when the twist drill has started penetrating the unidirectional carbon fibre reinforced composite workpiece for spindle speed of 10000 rpm and feed rates of 1250 mm/min are shown in Figure 6.11, Figure 6.12 and Figure 6.13 respectively. The simulation of the von Mises stress distribution shows that there are high stress concentrations along the chisel and cutting edge due to the applied forces, values range up to 206 MPa at chisel edge and gradually decrease going up to the drill body. From the effective strain, it's evident that it reflects the same distribution as the von Mises distribution along the chisel and cutting edge due to the stress concentration. For the pressure distribution, it shows the maximum pressure is at the cutting edge, which indicates the reason at the experimental stage for the drill bits to start being damaged after drilling many holes.

6.1.4 Workpiece displacement analysis

Many researchers have used a back-up plate when drilling composite materials in their studies and not many have examined the affect of back-up plate absence, therefore to highlight this effect, we have removed the back-up plate in this study when drilling the unidirectional CFRP experimentally and in the FEM simulation.

Capello [57] has investigated the difference in delamination mechanism in supported and unsupported back-up plate in drilling composite material, he acknowledged that the delamination mechanism in unsupported drilling is more complex especially when the dynamics of the workpiece acts as an inflected beam and the drill acts as a punch on the laminate when using high feed rates. Also, Klotz et al [127] [128] has highlighted the importance and effect of clamping system and it's affect on CFRP specimen deflection during the drilling process, their studies concluded that the highest speed of deflection occurs at the beginning of the drilling process, also another conclusions from their study states that the surface damage at the top side stabilizes at a constant level with increasing deflection of workpiece.

Fig. 6.14 shows the displacement distribution of twist drill at first ply failure for

spindle speed of 10000 rpm and feed rate of 1250 mm/min, it can been seen from the figure that the highest deflection is in the middle and decreases going to the sides of the workpiece and this will highly effect the delamination around the hole especially when there is no back-up plate.

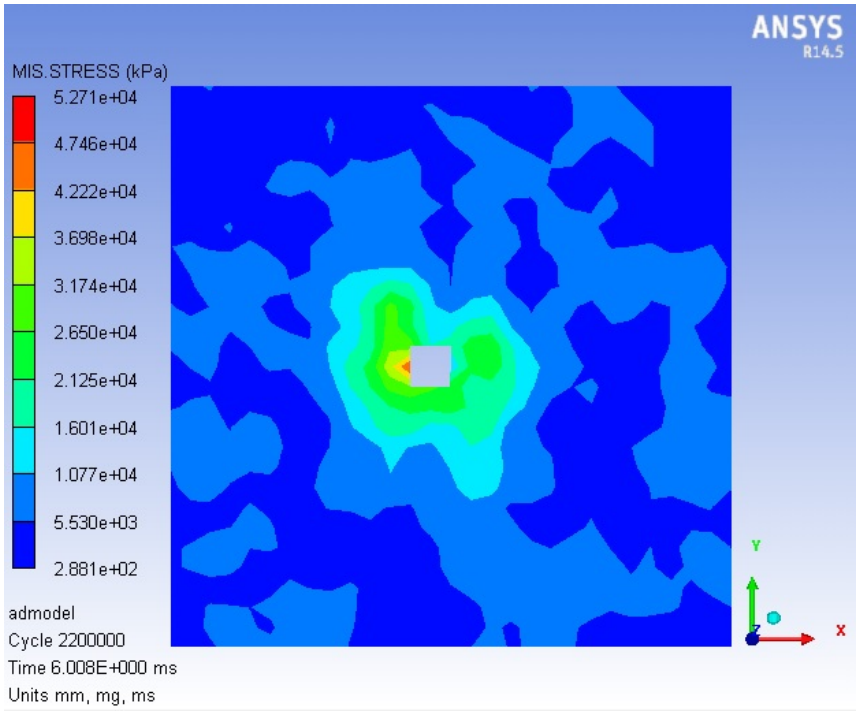

(a)

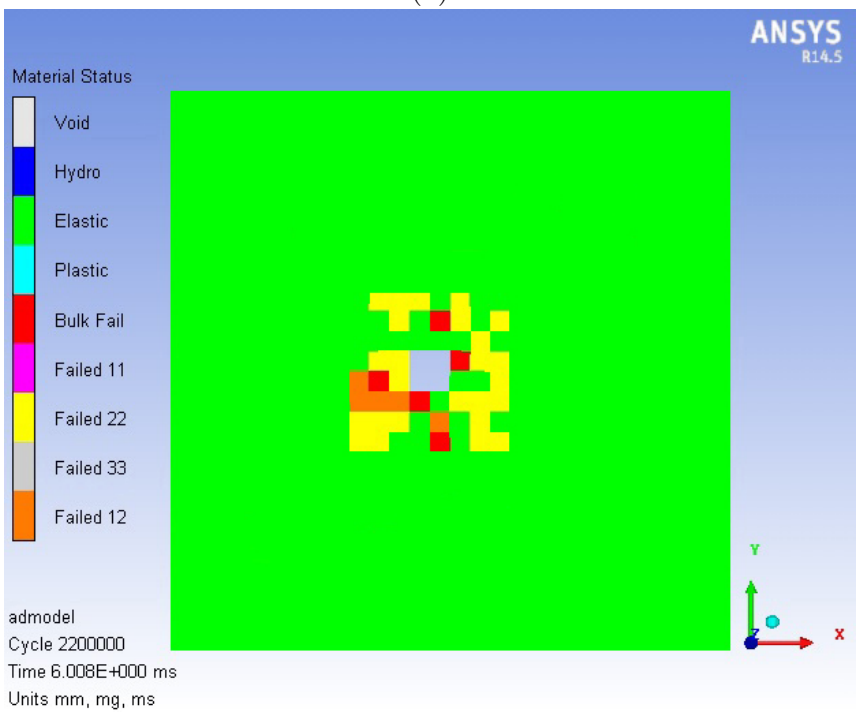

(b)

Figure 6.10: PCD twist drilling of first Ply (a) Von Mises stress distribution. (b) Hashin Failure modes.

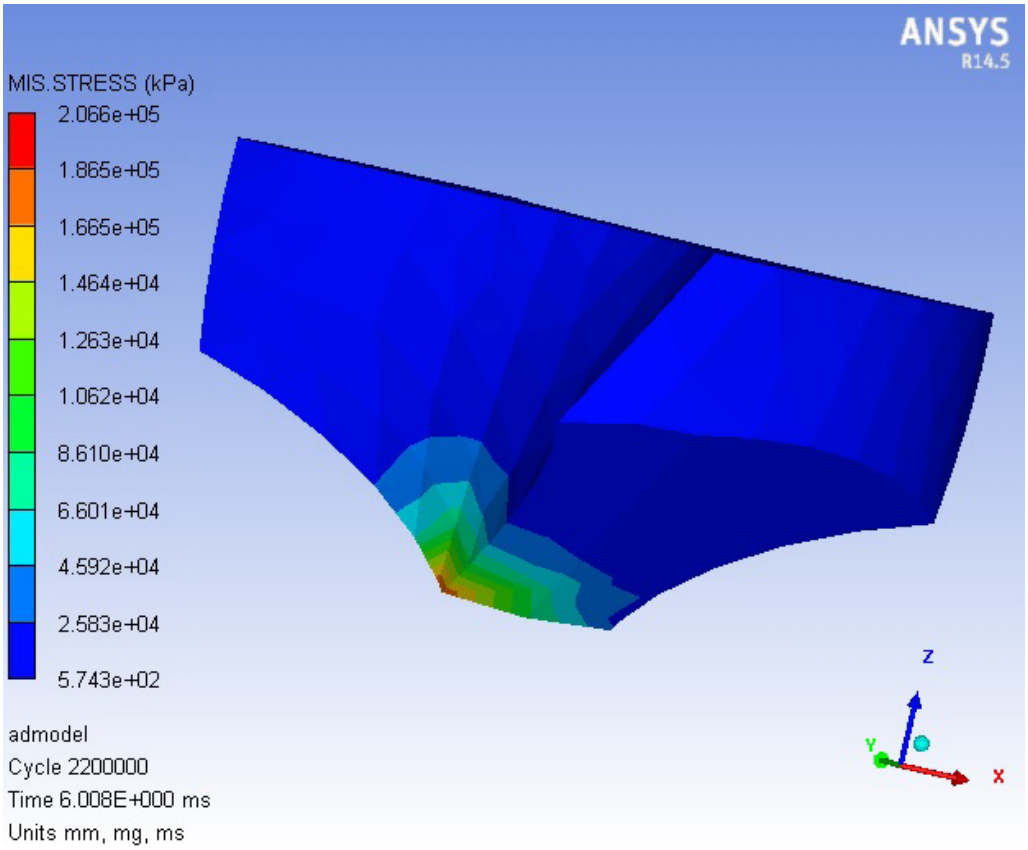

Figure 6.11: von Mises stress distribution for PCD twist drill at first ply failure

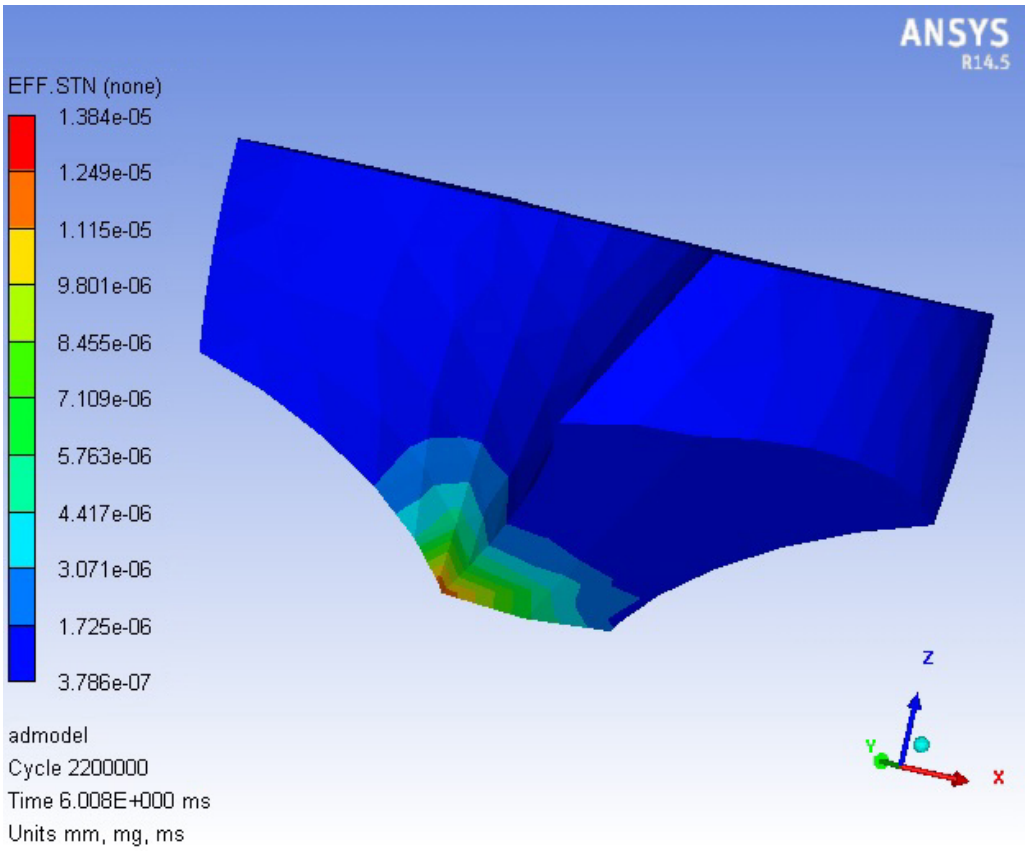

Figure 6.12: Effective strain distribution for PCD twist drill at first ply failure

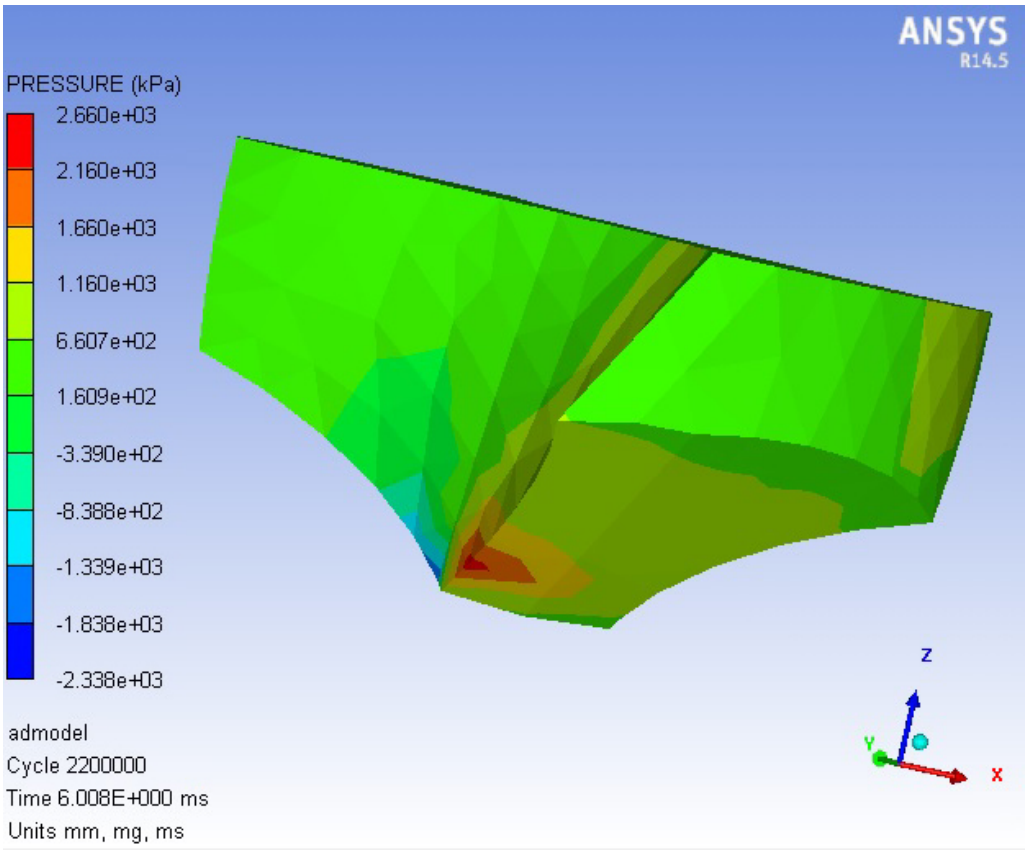

Figure 6.13: Pressure distribution for PCD twist drill at first ply failure

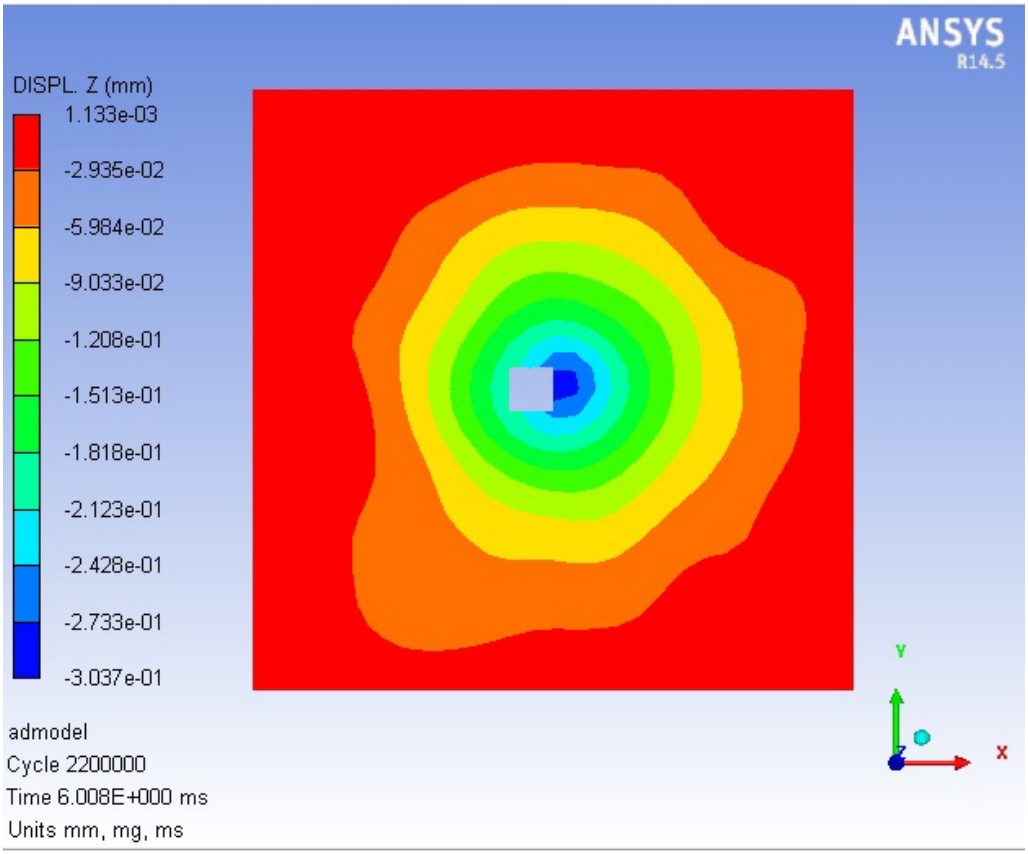

Figure 6.14: Displacement distribution of PCD twist drill at first ply failure

6.2 Double point angle drill analysis

6.2.1 FE model validation

Thrust force and torque (5000rpm - 500mm/min)

In this section, the double point angle drill will be analyzed, as thrust force and torque measured in the drilling experiments are calculated and were compared with the results obtained from the new FEA model.

Table 6.8 shows drilling force and torque of experiment and FEA simulation when spindle speed is 5000 rpm and feed rate 500 mm/min. It can be seen that the average thrust force measured in the experiment was 127.96 N, whereas the FE result showed 134.86 N; the experiment torque was 0.62 N.m and FE torque result was 0.53 N.m., the deviation in results ranges approximately between 5% to 15%.

Table 6.8: Experimental and FEA force and torque measurements for spindle speed 5000 rpm and feed rate 500 mm/min

Drill type	Exp.	FE	%Errors	Exp.	FE	%Errors
	Thrust force (N)	Thrust force (N)		Torque (N.m)	Torque (N.m)	
Diamond coated double point angle drill	127.96	134.86	5.39	0.62	0.53	14.52

Thrust force and torque (10000rpm - 1250mm/min)

Table 6.9 shows drilling force and torque of experiment and FE simulation at spindle speed of 10000 rpm and feed rate of 1250 mm/min, the experimental thrust force measured was 136.88 N whereas the FE result showed 132.76 N; the experimental torque was 0.55 N.m and FE torque was 0.53 N.m, the difference in results approximately ranges between 3% to 4%.

The accuracy between the experiment and the FE simulation results for both validations are concluded close and within acceptable range, which indicates the FE model is accurate.

Table 6.9: Experimental and FEA force and torque measurements for spindle speed of 10000 rpm and feed rate of 1250 mm/min

Drill type	Exp.	FE	%Errors	Exp.	FE	%Errors
	Thrust force (N)	Thrust force (N)		Torque (N.m)	Torque (N.m)	
Diamond coated double point angle drill	136.88	132.76	3.10	0.55	0.53	3.77

To provide a bigger picture of %errors, Figure 6.15 shows a statistical comparison of the %errors for other cutting conditions used in this study for thrust force and torque using double point angle drill.

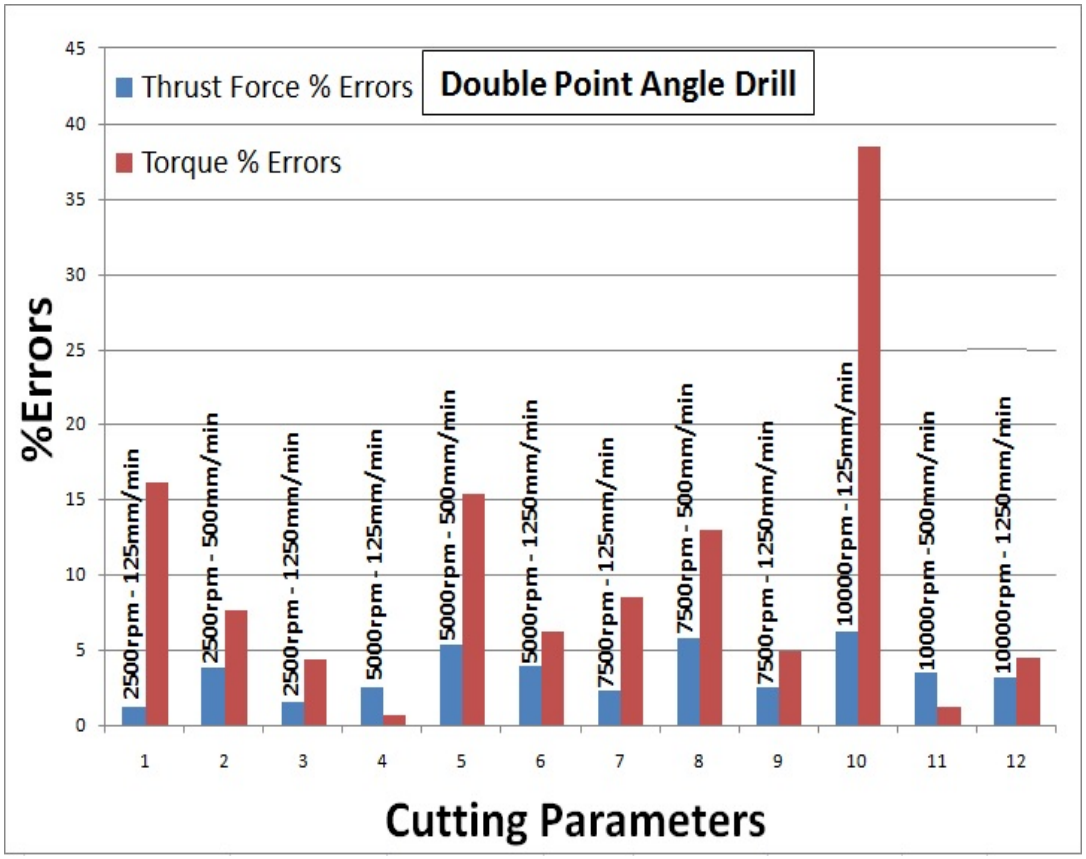

Figure 6.15: Statistical comparison of the %errors for thrust force and torque using double point angle drill.

Effect of feed rate on thrust force and torque

Feed rate is one of the major parameters that affect drilling of composite materials, as shown in Figures 6.16(a) and 6.16(b) show the thrust force and torque analysis for double point angle drill, with the same trend as the twist drill, the thrust force and torque went up with the increase of feed rate when spindle speed was constant 10000rpm. Thrust force in the experiment was 54.51 N at 125 mm/min feed rate, the highest was 136.88 N at 1250 mm/min feed rate, whereas the minimum of FE simulation was 51.32 N at 125 mm/min feed rate, the highest was 132.76 N at 1250 mm/min feed rate. Whilst the torque in the experiment was 0.28 N.m at 125 mm/min feed rate, the highest was 0.55 N.m at 1250 mm/min feed rate, whereas the FE estimated 0.2 N.m at 125 mm/min feed rate, the highest was 0.53 N.m at 1250 mm/min feed rate.

Effect of feed rate and spindle speed on thrust force and torque

In order to predict the effects of feed rate and spindle speed on thrust force and torque in the drilling process, and by using the validated FE model, a combination of drill feed rate and spindle speed were chosen from Table 6.5. The overall results (Figure 6.17) show that thrust force and torque increase with the increase in drill feed rate and decrease with the increase in spindle speed. Thrust force increased by 158% when the drill feed rate increased from 125 mm/min to 1250 mm/min at spindle speed of 10000 rpm, torque increased by 159%. Also thrust force decreased by 63% when spindle speed increased from 2500 rpm to 10000 rpm at 125 mm/min, and the torque decreased by 63% as well.

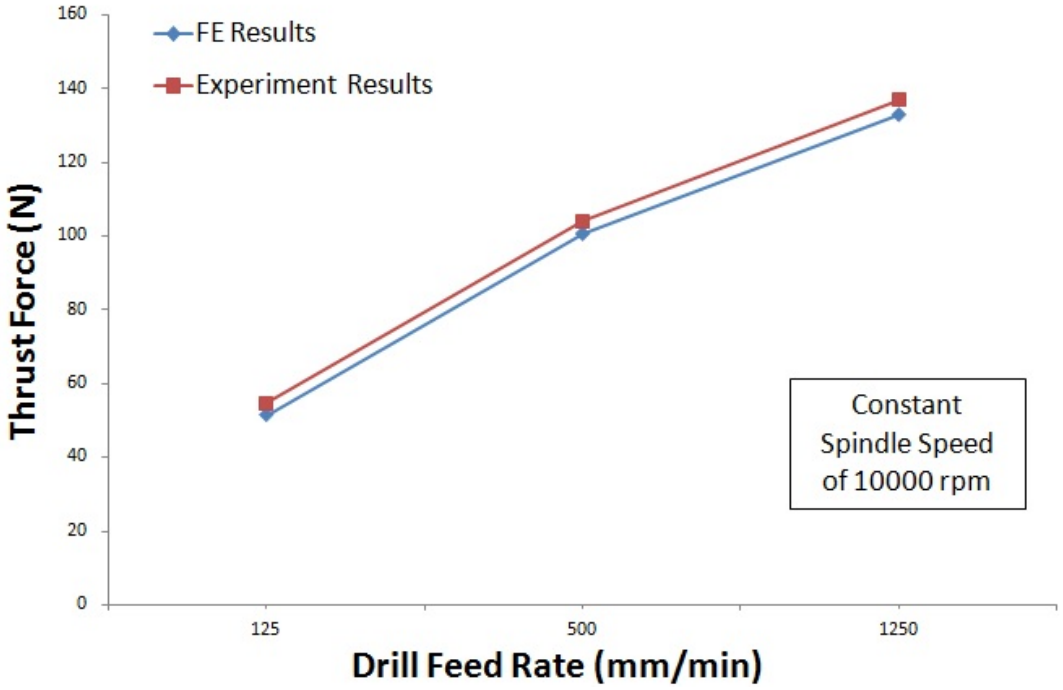

(c)

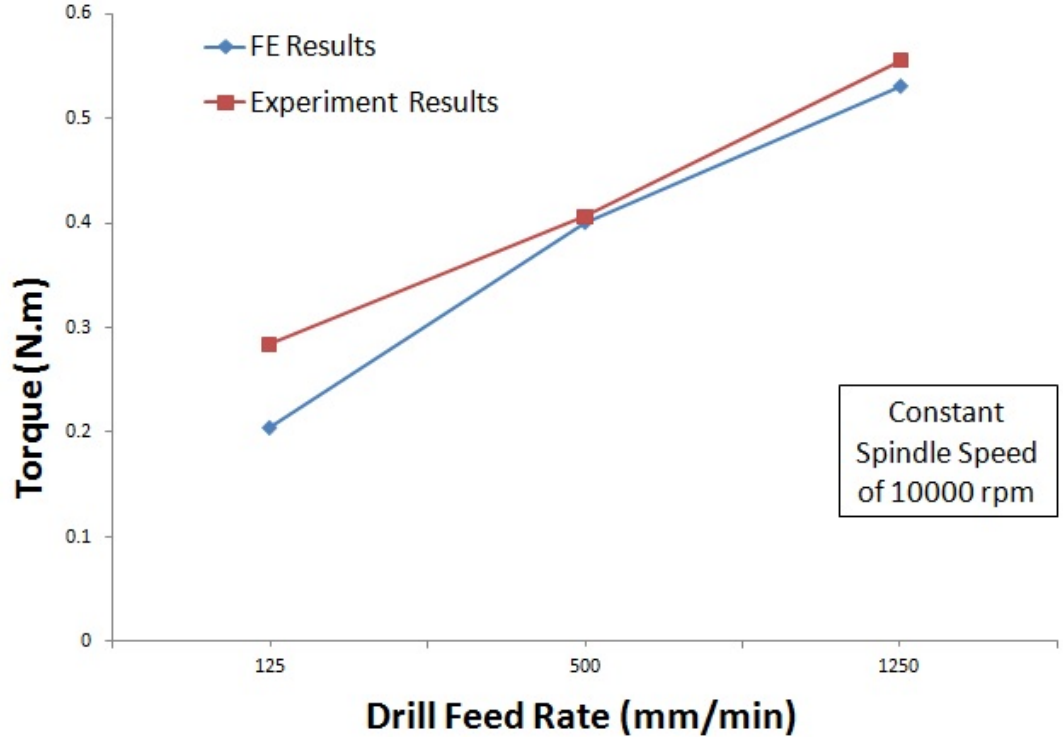

(d)

Figure 6.16: Double point angle drill (a) Thrust force analysis (Experiment and FE) (b) Torque analysis (Experiment and FE).

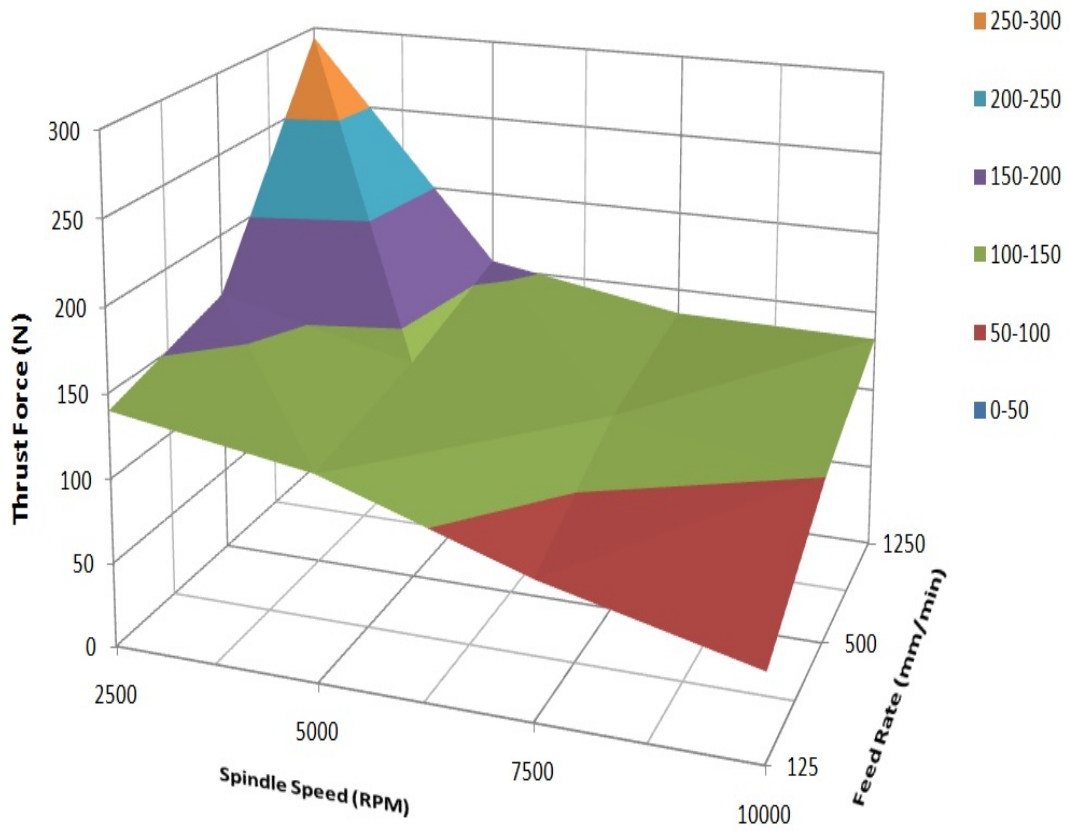

(c)

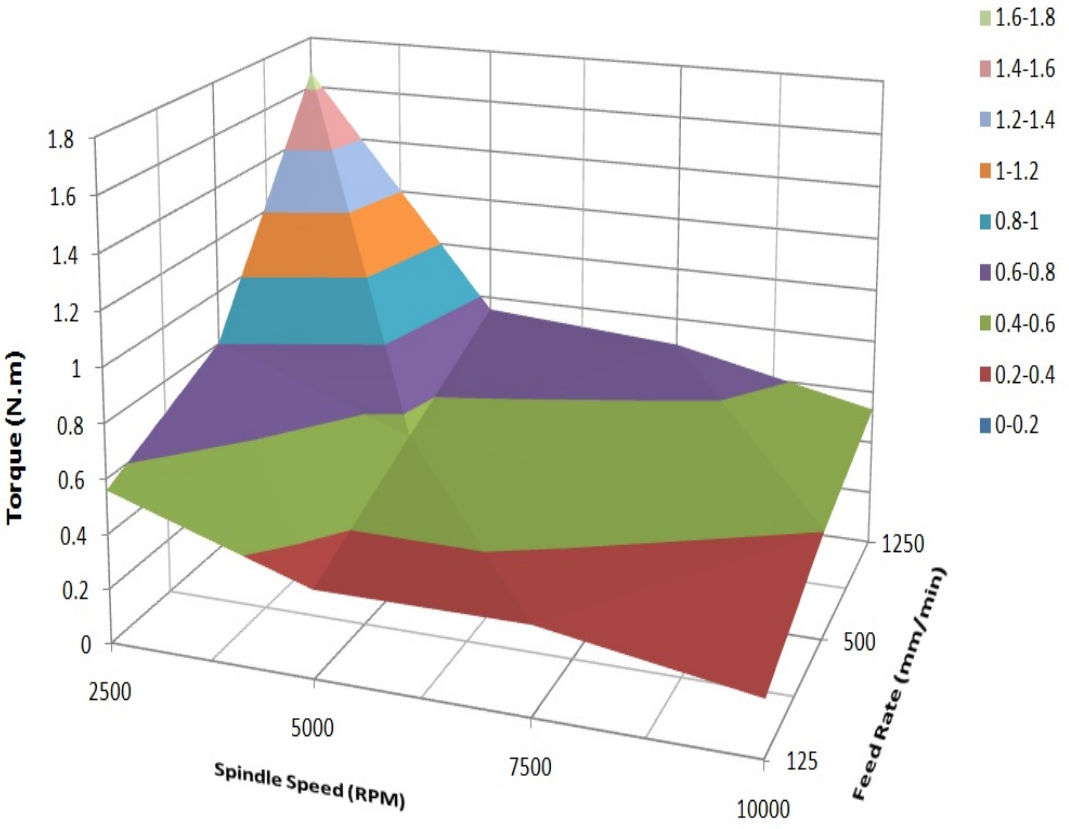

(d)

Figure 6.17: Double point angle drill (a) Effect of drill feed rate and spindle speed on thrust force. (b) Effect of drill feed rate and spindle speed on torque.

6.2.2 Delamination factor analysis

To investigate the effect of operating parameters for double point angle drill on the drilling induced damage, the delamination factors obtained in the experimental drilling and finite element analysis were calculated and compared.

Figure 6.18 shows results of delamination occurred on the drilled hole entrance peripheral at different cutting parameters. Again Figures in (a) illustrate the images for experimental drilling with the noises inside the holes filtered, Figures in (b) show the acquired delamination areas of Figures in (a) after they were processed with Image J. Figures in (c) show the FEA simulation results of drilling induced damage. By comparing (b) and (c), it can be seen that the FEA prediction was well estimated and the general delamination trend is very similar to the experiment results.

Effect of spindle speed on experimental delamination factors

The experimental delamination factor F_d, the adjusted delamination factor F_{da} and the equivalent adjusted delamination factor F_{eda} are calculated against the spindle speed and compared in each case; the results are shown in Figure 6.19. From these results it can be seen that F_{da} is highest value of the delamination factors, and due to the increase of number of cutting action in the cutting edges at each stage of feed, the trend of delamination factors decreases with the increase in spindle speed except when it reaches 7500 rpm, as there is a sudden huge increase in delamination factor when it reaches 10000 rpm, this indicates spindle speed after 7500 rpm is not suitable for double point drill. It can be noted that when spindle speed increased 200% F_d decreased between 0.31% to 30.8%, F_{da} decreased between 0.45% to 32.35% while F_{eda} decreased between 0.15% to 4.25%. While if the spindle speed increased 300% F_d increases between 2.79% to 48.53%, F_{da} increased between 4.14% to 53.34% while F_{eda} increased between 2.60% to 6.62%.

Effect of feed rate on experimental delamination factors

The same concept is done for the experimental delamination factors in regards to feed rate (Figure 6.20), as the increase in feed rate leads to the rise of delamination factors. Delamination increases drastically when feed rate is over 500mm/min for spindle speed 2500 rpm and 5000 rpm. As mentioned earlier, this indicates that feed rate has more effect on delamination than the effect of spindle speed, due to the highly correlation increase of thrust force with the increase of feed rate, which plays a significant role in delamination when drilling composite materials.

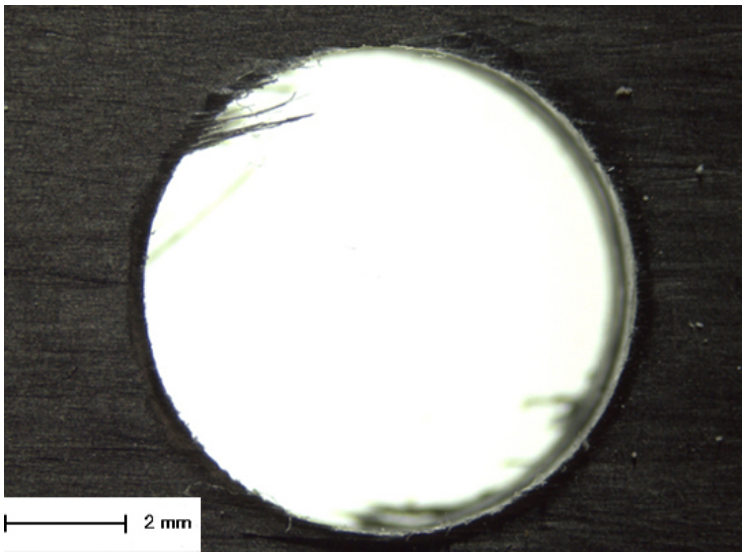

1(a)

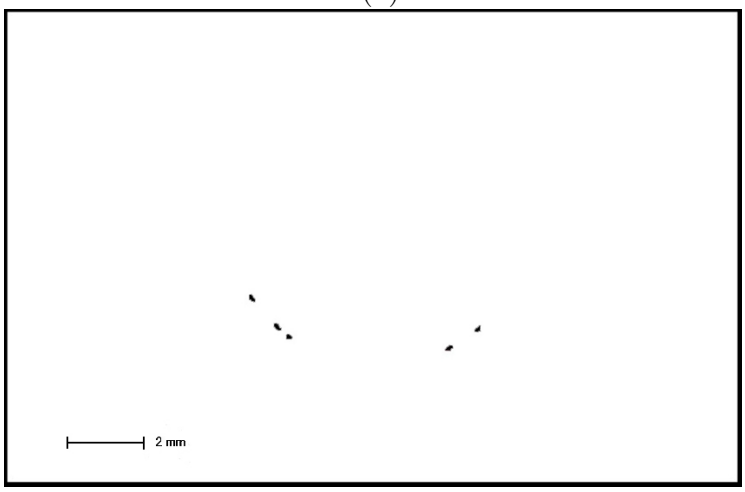

1(b)

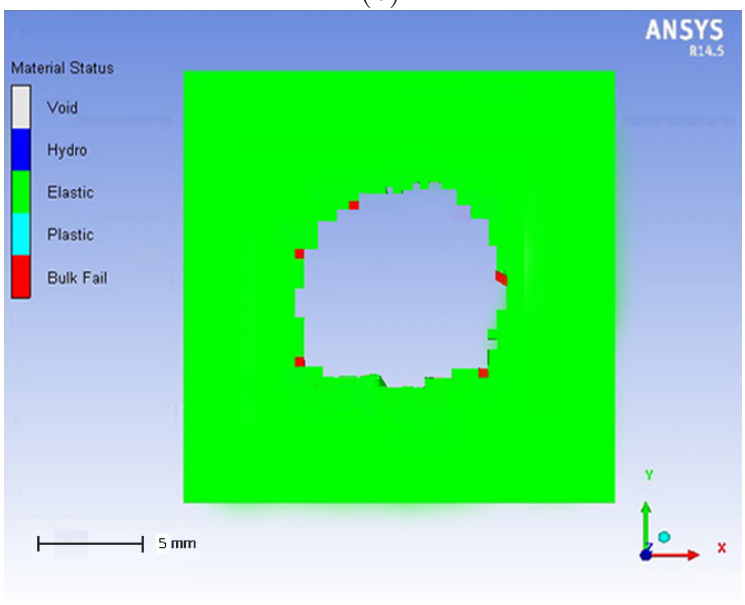

1(c)

(Double point angle drill) (Spindle speed: 7500 rpm) (Feed rate: 125 mm/min)
Figure 6.18: Delamination analysis for drill entry (a) Hole images (b) Experimental delamination areas (c) Finite element delamination.

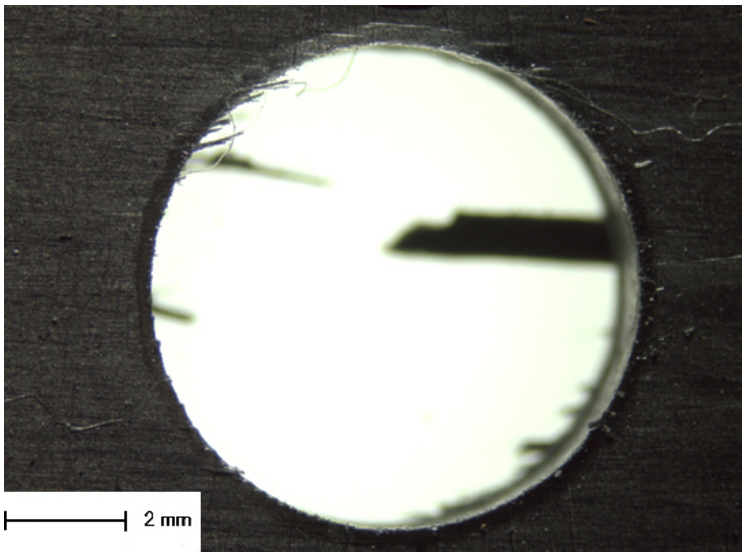

2(a)

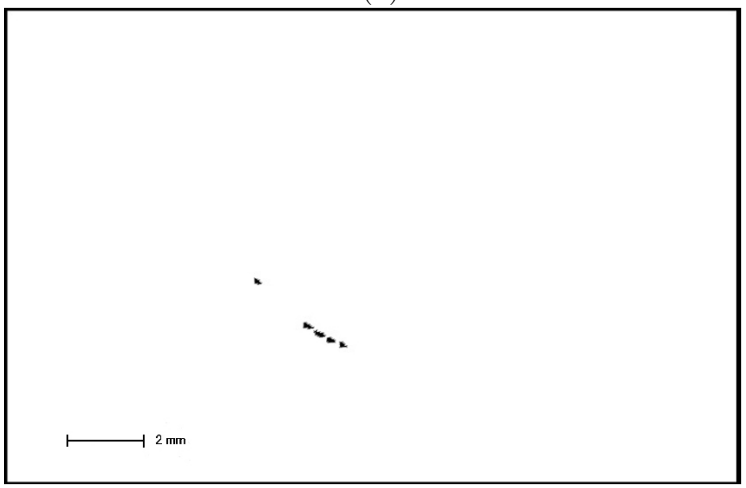

2(b)

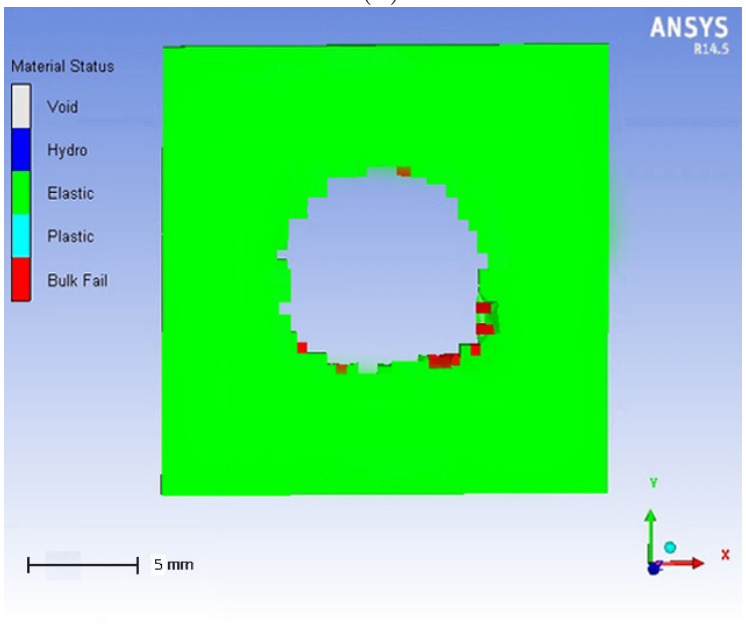

2(c)

(Double point angle drill) (Spindle speed: 7500 rpm) (Feed rate: 500 mm/min)
Figure 6.18: Delamination analysis for drill entry (a) Hole images (b) Experimental delamination areas (c) Finite element delamination.

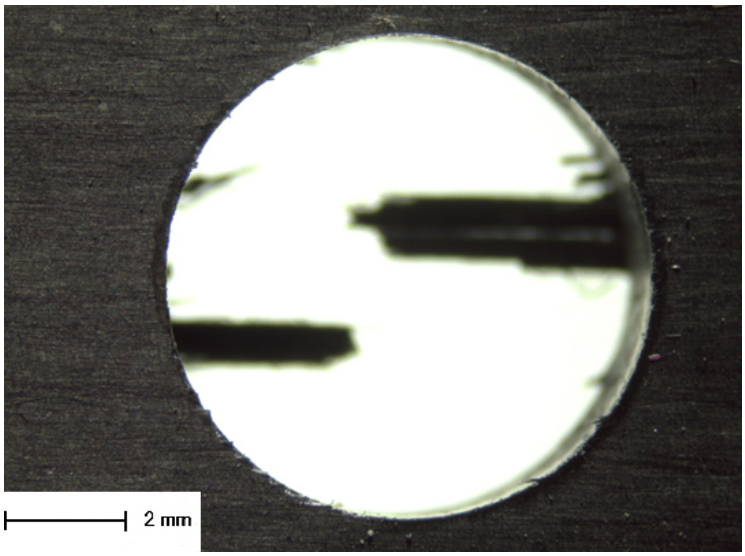

3(a)

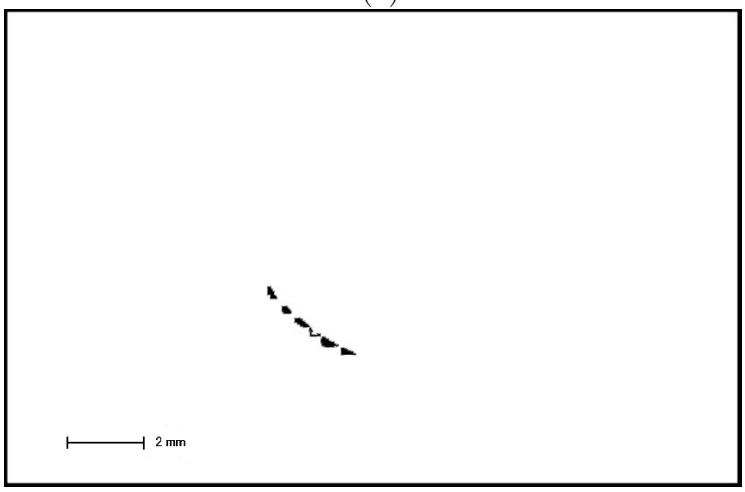

3(b)

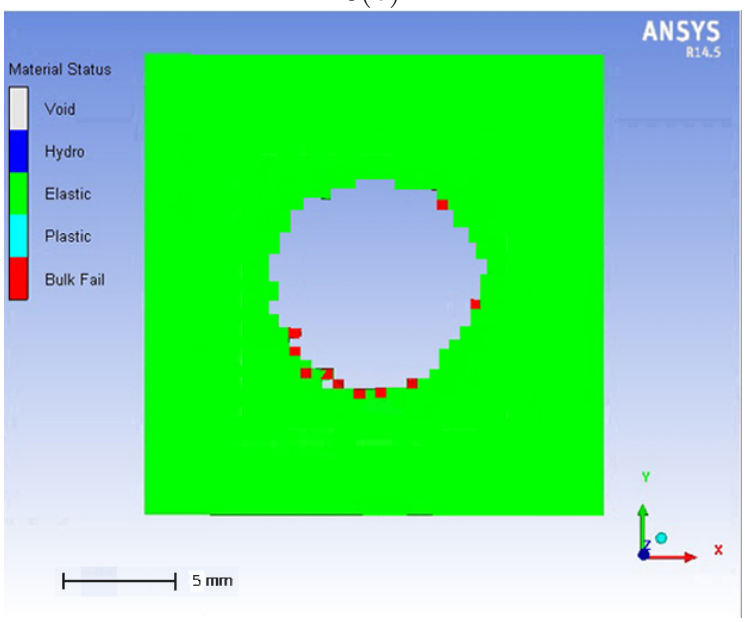

3(c)

(Double point angle drill) (Spindle speed: 7500 rpm) (Feed rate: 1250 mm/min)
Figure 6.18: Delamination analysis for drill entry (a) Hole images (b) Experimental delamination areas (c) Finite element delamination.

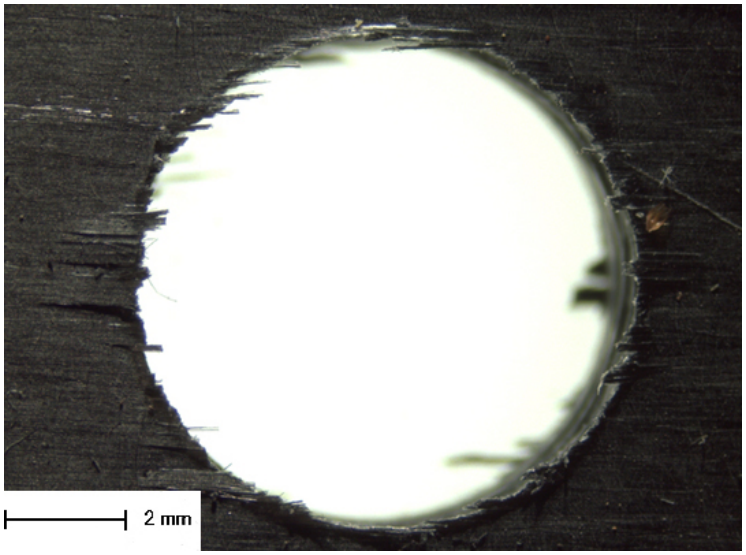

4(a)

4(b)

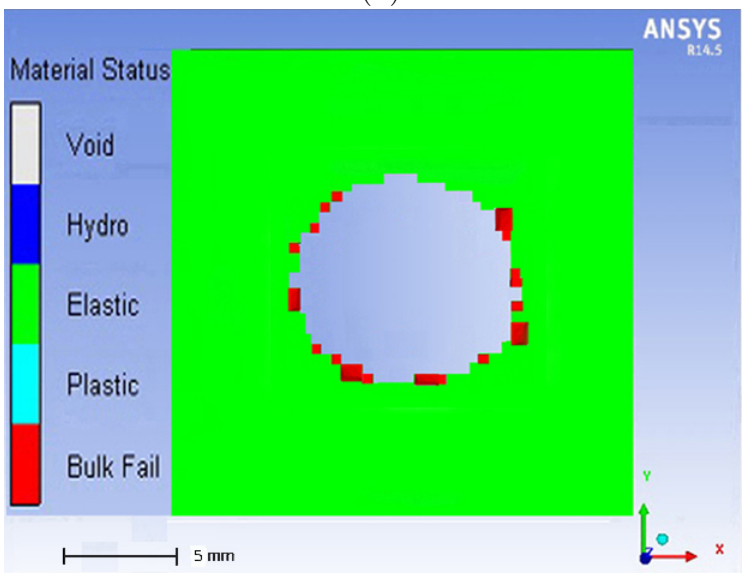

4(c)

(Double point angle drill) (Spindle speed: 10000 rpm) (Feed rate: 125 mm/min)
Figure 6.18: Delamination analysis for drill entry (a) Hole images (b) Experimental delamination areas (c) Finite element delamination.

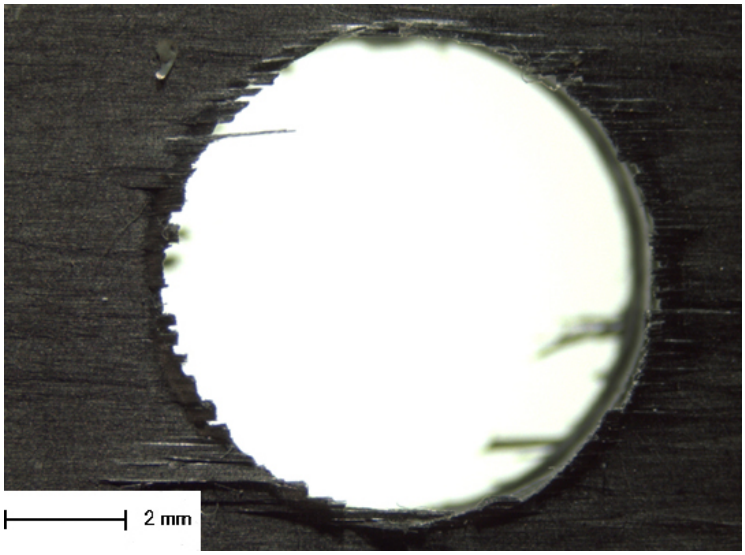

5(a)

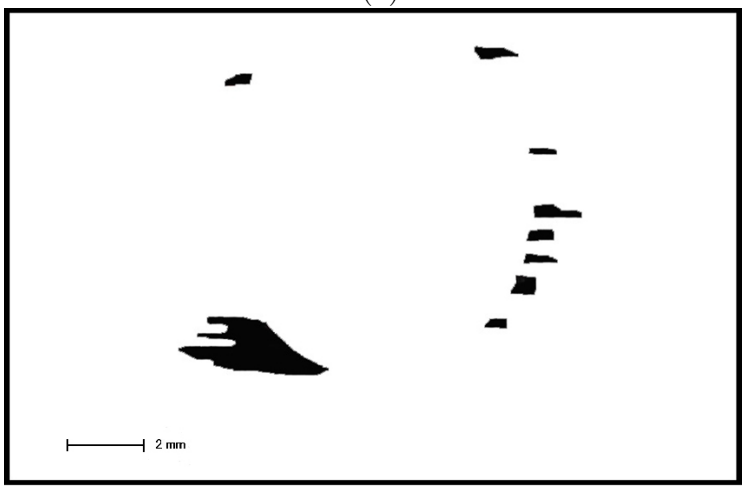

5(b)

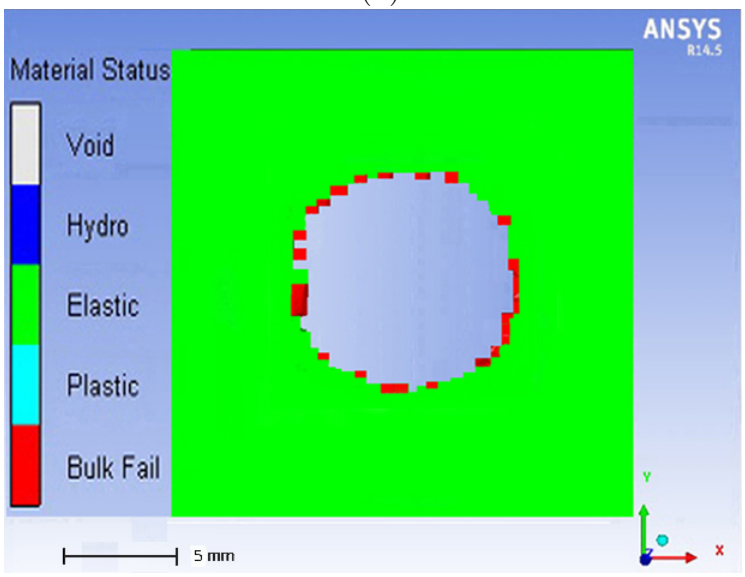

5(c)

(Double point angle drill) (Spindle speed: 10000 rpm) (Feed rate: 500 mm/min)
Figure 6.18: Delamination analysis for drill entry (a) Hole images (b) Experimental delamination areas (c) Finite element delamination.

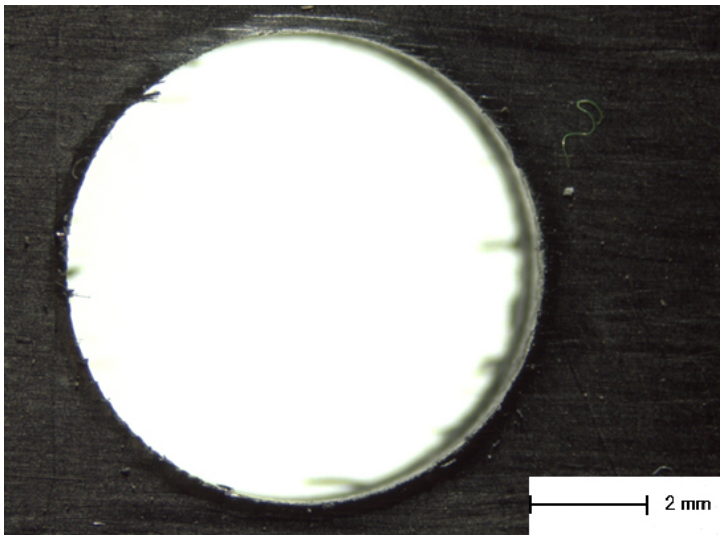

6(a)

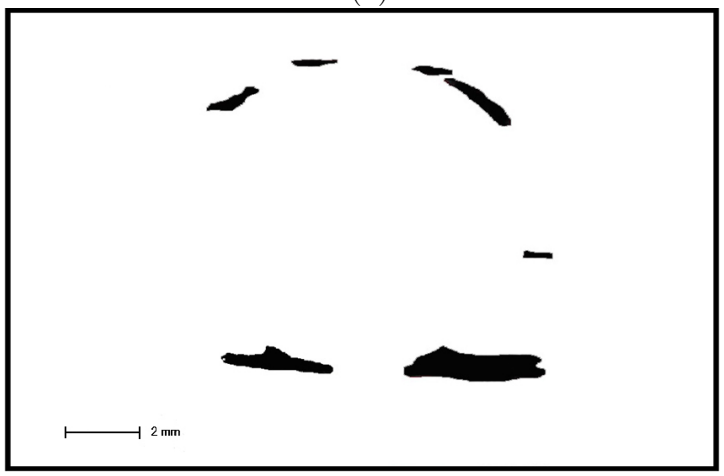

6(b)

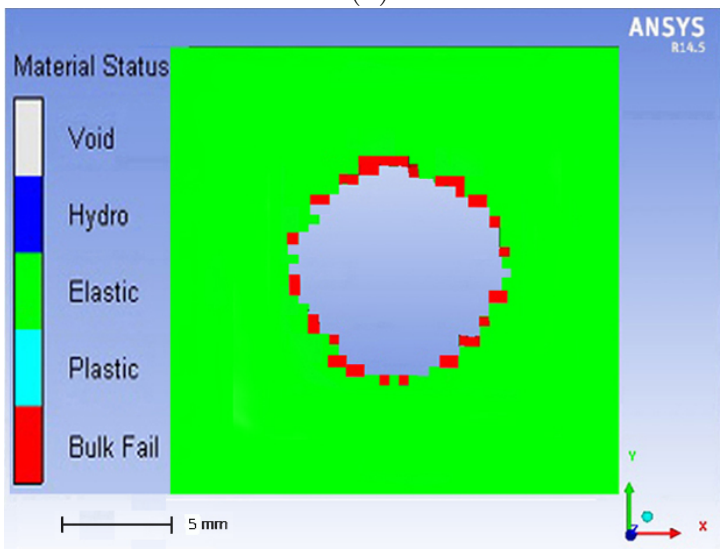

6(c)

(Double point angle drill) (Spindle speed: 10000 rpm) (Feed rate: 1250 mm/min)

Figure 6.18: Delamination analysis for drill entry (a) Hole images (b) Experimental delamination areas (c) Finite element delamination.

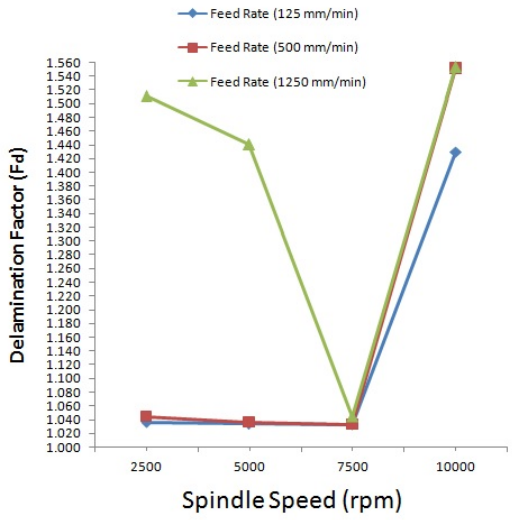

(a)

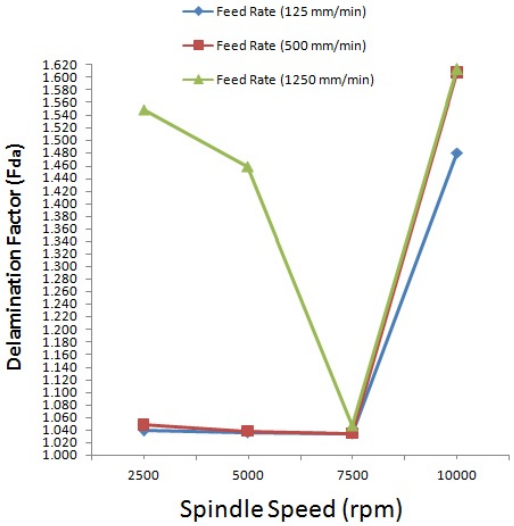

(b)

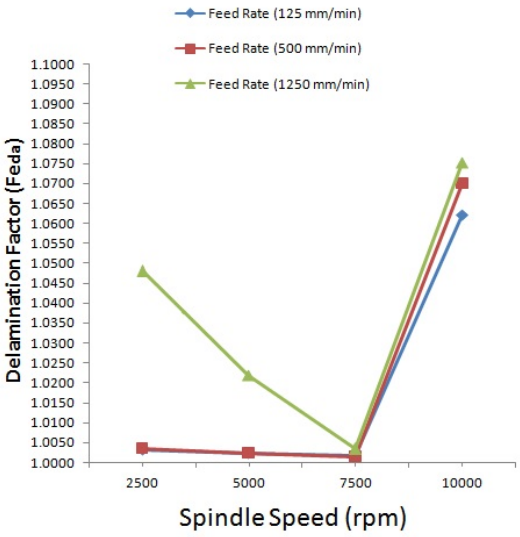

(c)

Figure 6.19: Effect of double point angle drill spindle speed on experimental delamination factors (a) Conventional delamination factor F_d (b) Adjusted delamination factor F_{da} (c) Equivalent adjusted delamination factor F_{eda}.

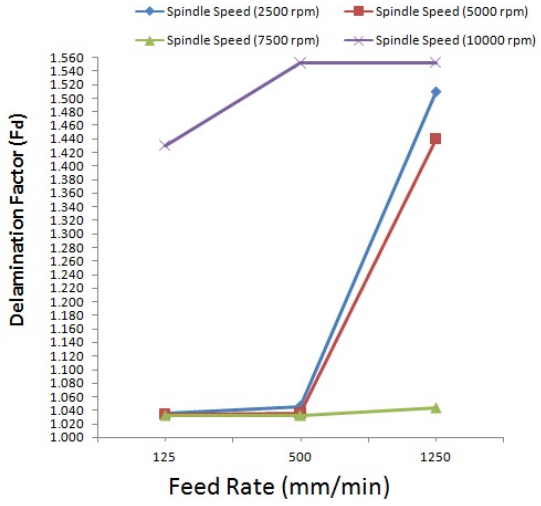

(a)

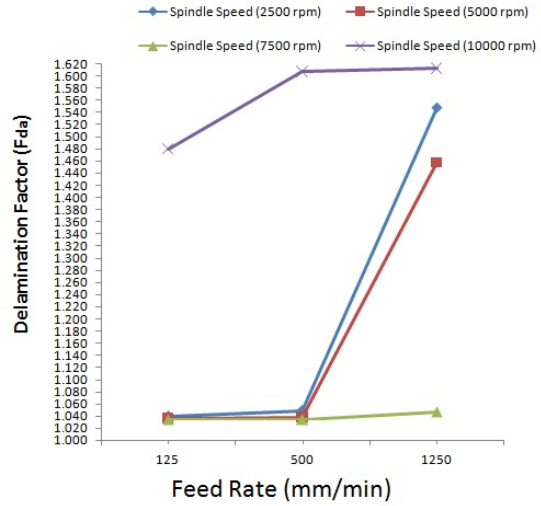

(b)

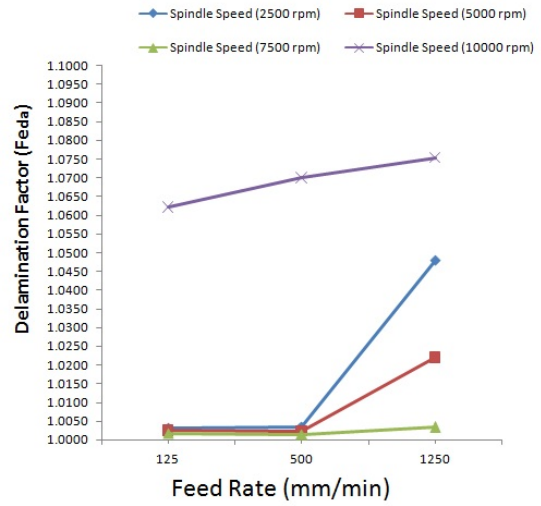

(c)

Figure 6.20: Effect of double point angle drill feed rate on experimental delamination factors (a) Conventional delamination factor F_d (b) Adjusted delamination factor F_{da} (c) Equivalent adjusted delamination factor F_{eda}.

Effect of feed rate on FE delamination factors at constant spindle speed (7500rpm)

To validate simulation results, F_d, F_{da} and F_{eda} were calculated and compared for spindle speed of 7500 rpm and feed rates of 125 mm/min, 500 mm/min and 1250 mm/min, as shown in Table 6.10 and Figure 6.21, the same trend for the delamination factors is experienced, as F_d, F_{da} and F_{eda} increased nearly 1%, 2.37% and 1.54% respectively with the increase of feed rate from 125 mm/min to 1250 mm/min. The difference in results between experiment and FEA simulation ranges from 4.54% to 4.67% for F_d, 5.6% to 6.98% for F_{da} and 1.19% to 2.71% for F_{eda}, which again is a good correlation of output results.

It can be seen from the results in Table 6.10 that F_d and F_{da} have close values to each other whereas the F_{eda} has much lower values due to the effect of F_{ed}, it also shows that F_{eda} and F_{da} have better discrimination values than F_d. It also shows the percentage of errors between the experiment and FEA for F_{eda} is less than F_d and F_{da}.

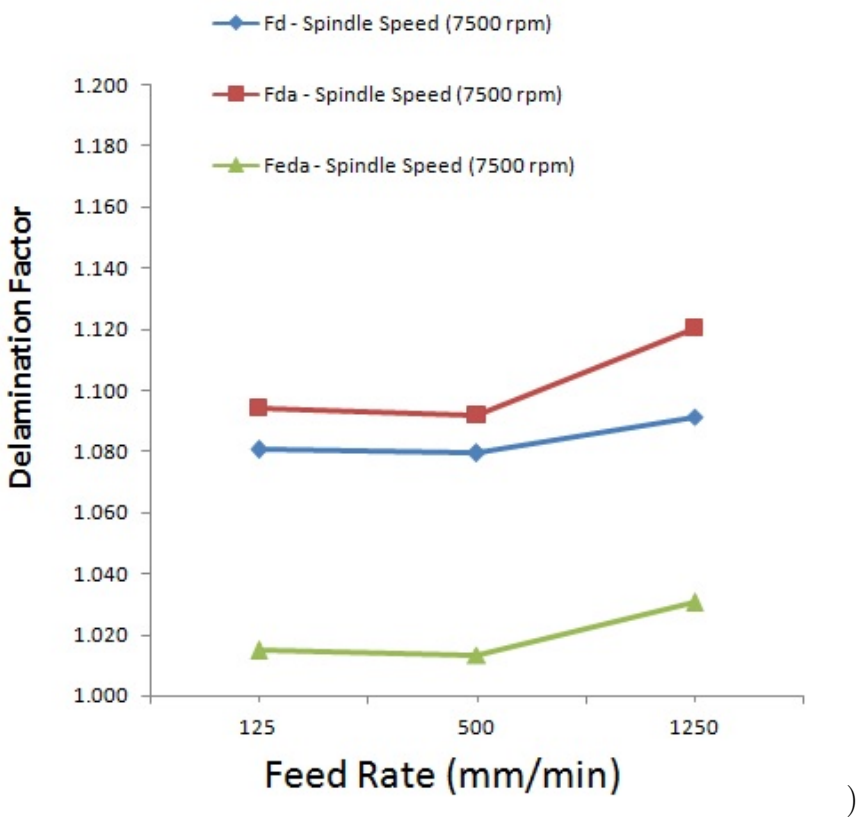

Figure 6.21: Effect of double point angle drill feed rate on FE delamination factors.

Table 6.10: Double point angle drill delamination factors for experimental and FEA at drill entry for 7500 rpm.

Cutting parameters		Experimental			FEA			% Errors		
Spindle speed (rpm)	Feed rate (mm/min)	F_d	F_{da}	F_{eda}	F_d	F_{da}	F_{eda}	F_d	F_{da}	F_{eda}
7500	125	1.032	1.034	1.002	1.081	1.094	1.015	4.675	5.850	1.315
7500	500	1.033	1.034	1.001	1.079	1.092	1.013	4.540	5.607	1.196
7500	1250	1.044	1.047	1.003	1.091	1.120	1.031	4.540	6.986	2.712

Effect of feed rate on FE delamination factors at constant spindle speed (10000rpm)

Also another validation of the FE simulation results have been done as F_{eda} was calculated and then compared at spindle speed of 10000 rpm and different feed rates of 125 mm/min, 500 mm/min and 1250 mm/min. The results in Table 6.11, shows the similarity in trend for delamination factors of FE simulation and experiment drilling, F_{eda} increased nearly 15.7% for FE simulation when the feed rate increased from 125 mm/min to 1250 mm/min. The difference between the experiment and FE simulation results approximately ranges from 2.04% to16.57% for F_{eda}, which again is a clear correlation of result output.

Table 6.11: Double point angle drill delamination factors for experimental and FEA at drill entry for 10000 rpm.

Cutting parameters		Experimental	FE	% Errors
Spindle speed (rpm)	Feed rate (mm/min)	F_{eda}	F_{eda}	F_{eda}
10000	125	1.062	1.083	2.047
10000	500	1.070	1.156	8.056
10000	1250	1.075	1.253	16.577

6.2.3 Stress analysis

Figure 6.22 shows the stress distribution and onset damage respectively on the first ply when the double point angle drill has started penetrating the unidirectional carbon fibre reinforced composite workpiece for spindle speed of 10000 rpm and feed rates of 1250 mm/min. The workpiece will act and deform as orthotropic homogeneous elastic according to the fibre orientation through a defined local coordinate system.As shown in Figure 6.22(a) the von Mises stress is 57.72 MPa which is higher

than the 90^0 failure tensile strength, which indicates the tensile matrix mode being dominant failure mode as shown in Figure 6.22(b), the Hashin failure modes with elements failing will be removed when they reach the value of 1.

The distribution of stress, effective strain and pressure for the double point angle drill when the drill has started penetrating the unidirectional carbon fibre reinforced composite workpiece for spindle speed of 10000 rpm and feed rates of 1250 mm/min are shown in Figure 6.23, Figure 6.24 and Figure 6.25 respectively. The simulation of the von Mises stress distribution shows that there are high stress concentrations along the chisel and cutting edge due to the applied forces, values range up to 237 MPa at chisel edge and gradually decrease going up to the drill body. From the effective strain, it's evident that it reflects the same distribution as the von Mises distribution along the chisel and cutting edge due to the stress concentration. For the pressure distribution, it shows the maximum pressure is at the cutting edge, which indicates the reason at the experimental stage for the drill bits to start being damaged after drilling many holes.

6.2.4 Workpiece displacement analysis

Fig. 6.26 shows the displacement distribution of double point angle drill at first ply failure for spindle speed of 10000 rpm and feed rate of 1250 mm/min, it can been seen from the figure that the highest deflection is in the middle and decreases going to the sides of the workpiece and this will highly effect the delamination around the hole especially when there is no back-up plate.

The results show that the double point angle drill has similar pattern to twist drill and close results around the drilled hole periphery, it also shows the double point angle drill has wider displacement distribution pattern due to being the point angle of double point angle drill is bigger than the twist drill.

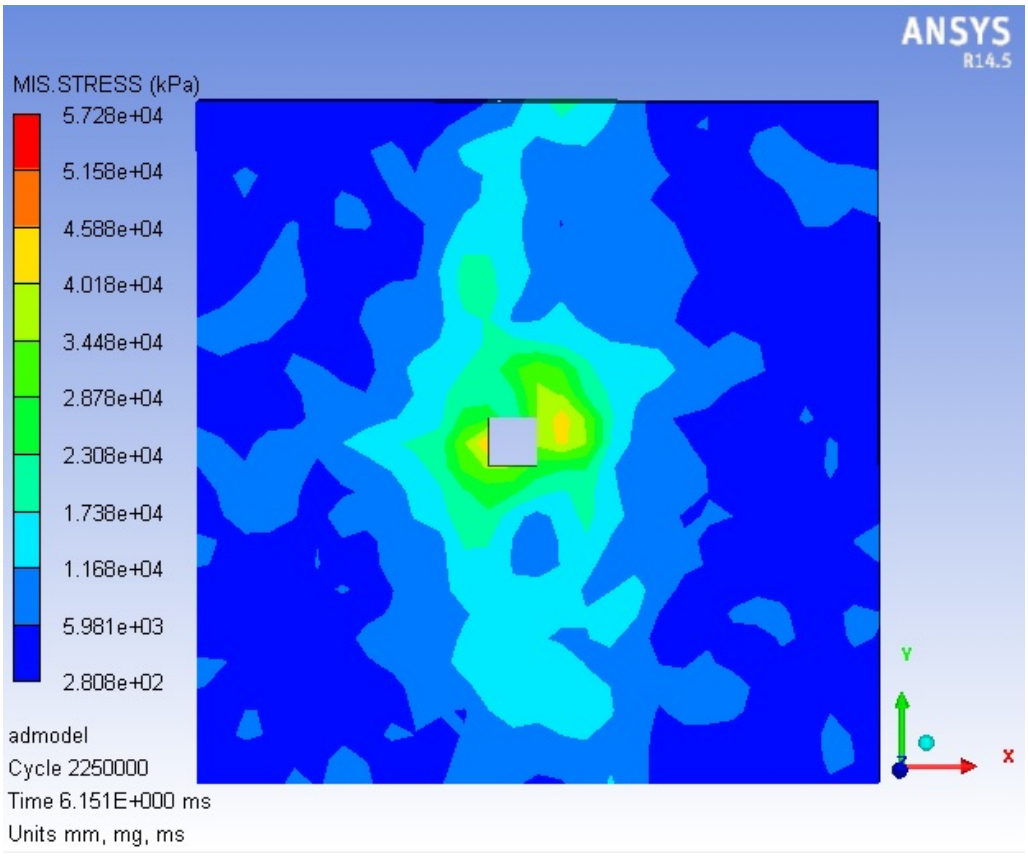

(a)

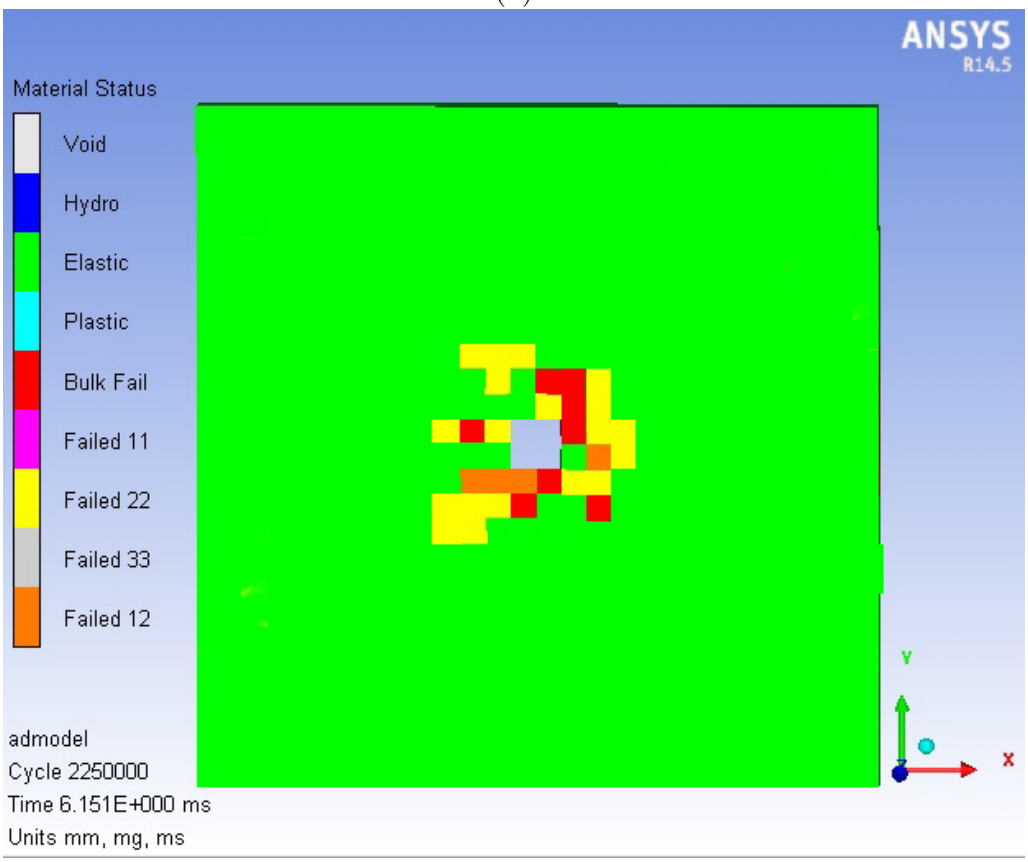

(b)

Figure 6.22: Double point angle drill first Ply (a) Von Mises stress distribution. (b) Hashin Failure modes.

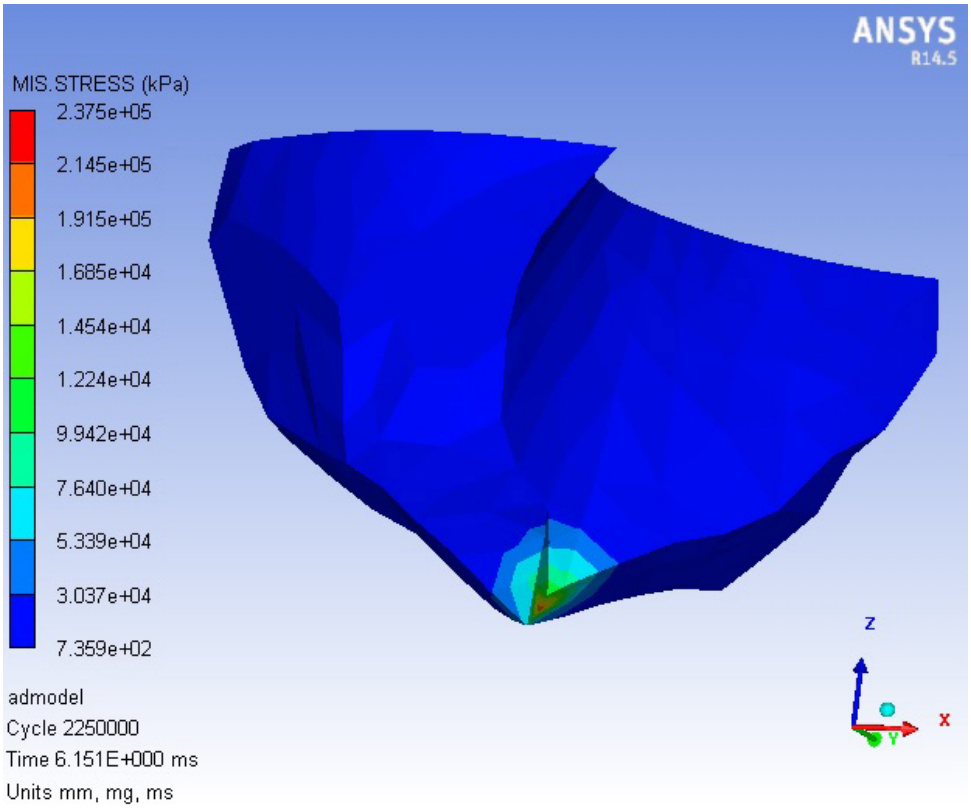

Figure 6.23: von Mises stress distribution for double point angle drill at first ply failure

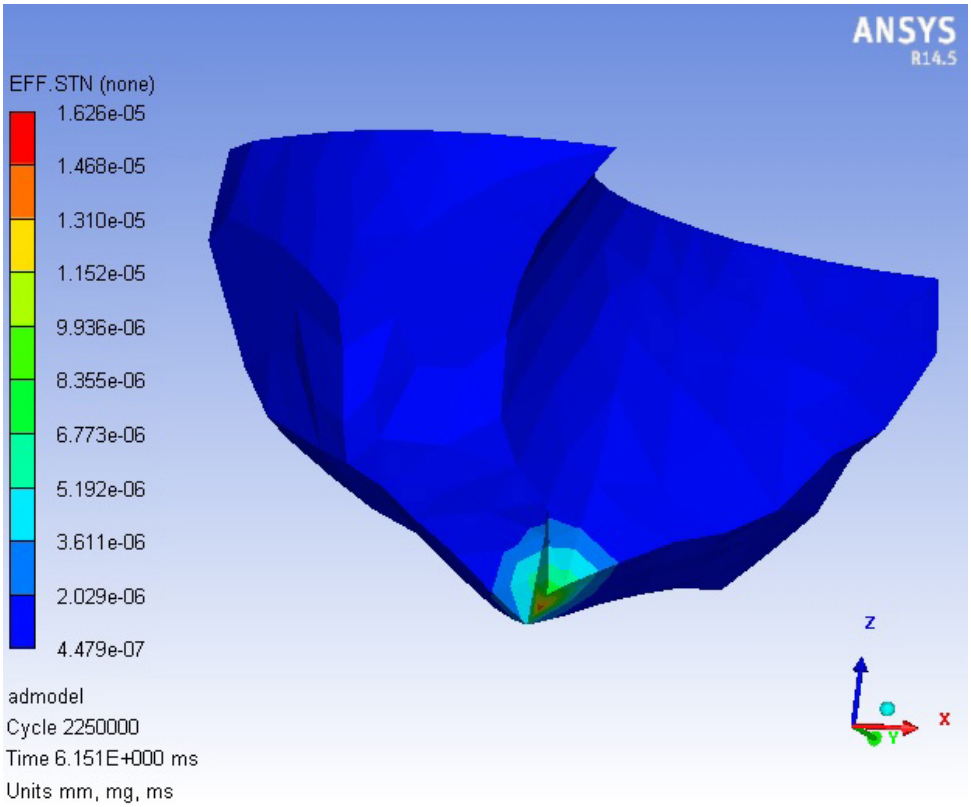

Figure 6.24: Effective strain distribution for double point angle drill at first ply failure

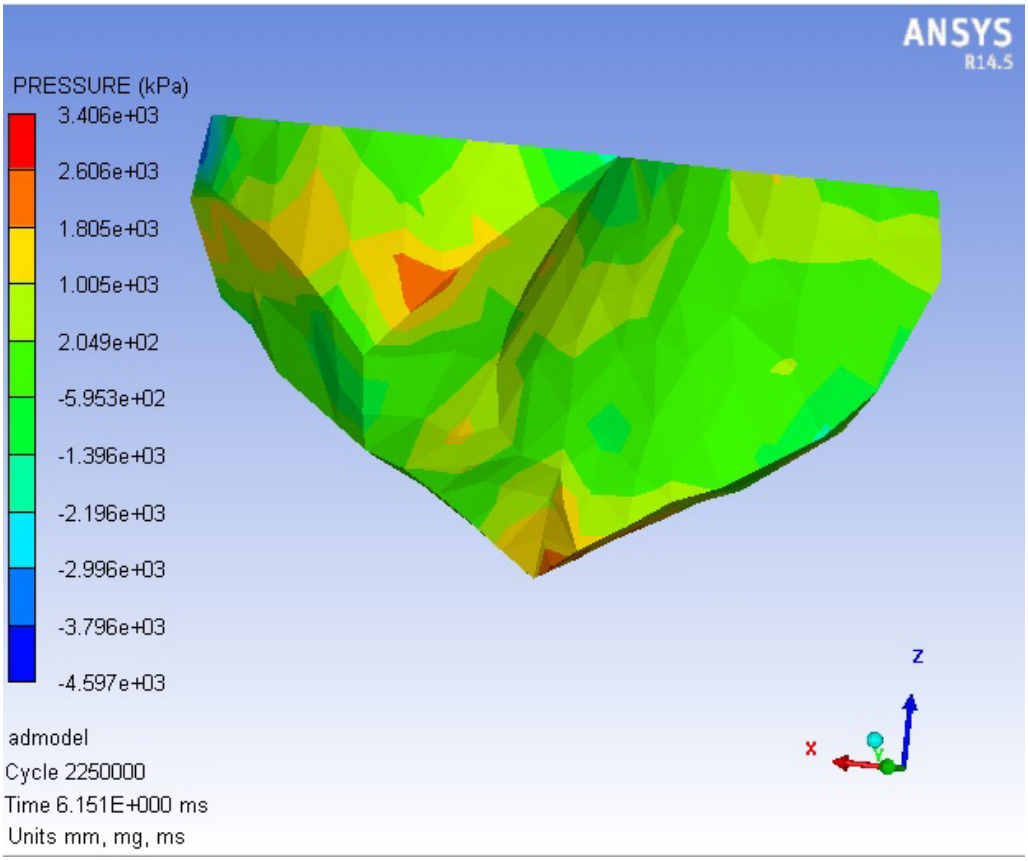

Figure 6.25: Pressure distribution for double point angle drill at first ply failure

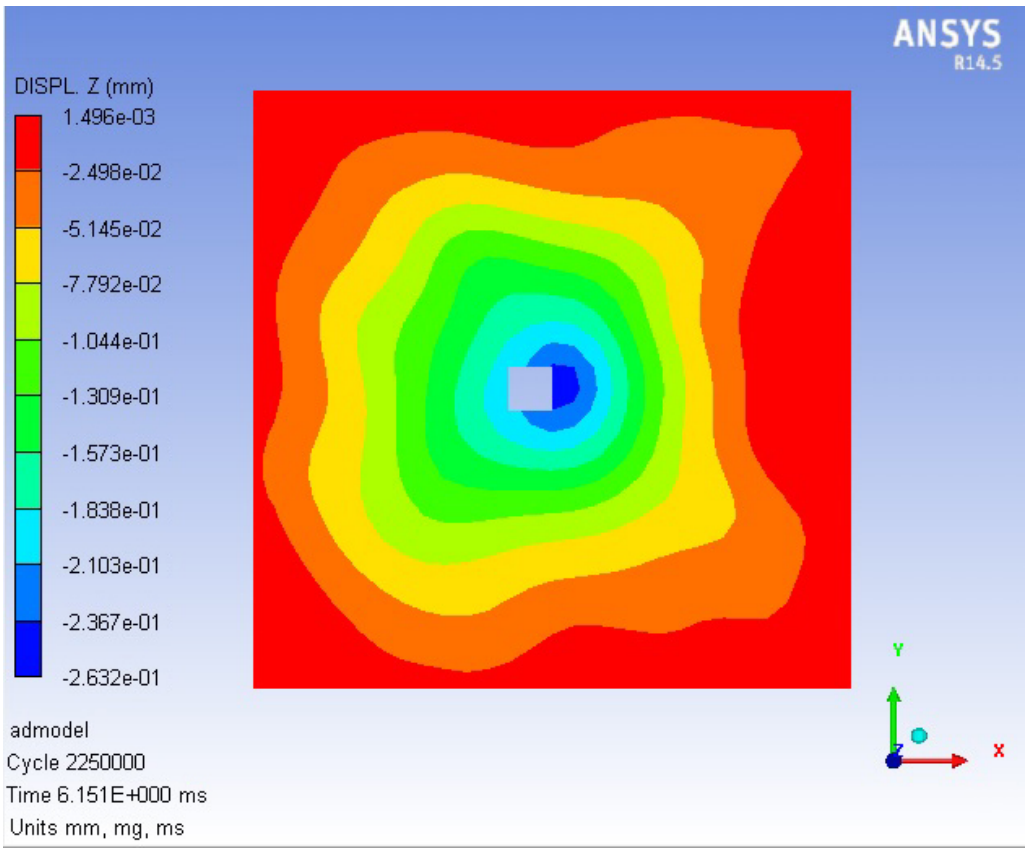

Figure 6.26: Displacement distribution of double point angle drill at first ply failure

6.3 Critical thrust force analysis

It is necessary to establish the relationship between thrust force and delamination factor to obtain the critical thrust force at the onset of delamination during the drilling process, hence delamination free holes can be obtained when critical thrust force is predicted if the applied thrust force does not exceed the critical thrust force.

Figure 6.27 shows the effect of thrust force on the equivalent adjusted delamination factor F_{eda} using the twist and double point angle drill, it can be seen that the delamination factor increases with the increase of thrust force.

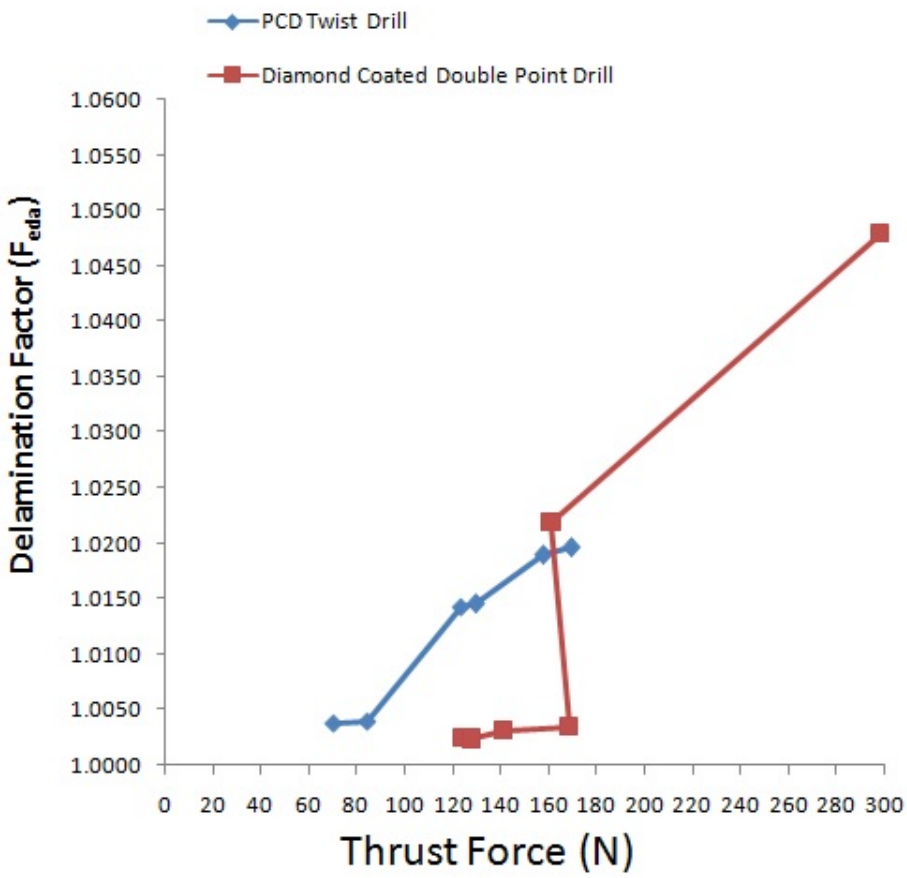

Figure 6.27: Effect of thrust force on F_{eda} using twist drill and double point drill.

By using the polynomial function to fit the graphs for each drill bit, we can calculate the critical thrust forces from the below shown equations:

$$F_{tt} = 0.98243746 + 0.00033289 * F_{tt1} - 6.56881045 * 10^{-7} F_{tt1}^2 \quad (6.1)$$

$$F_{dd} = 0.62114214 + 0.00634414 * F_{tt2} - 3.3625575 * 10^{-5} F_{tt2}^2 + 5.75112352 * 10^{-8} F_{tt2}^3 \quad (6.2)$$

Where F_{tt} is the critical thrust force for twist drill; F_{dd} is the critical thrust force for double point angle drill; F_{tt1} is the thrust force for twist drill and F_{tt2} is the thrust force for double point angle drill.

When defining the F_{tt}=1 and F_{dd}=1, then the critical thrust forces for twist drill and double point angle drill will be 59.82 N, 123.34 N respectively, this indicates that the double point angle drill has a higher safety free-delamination factor approximately 2.1 times the twist drill despite the double point drill generates higher thrust force than twist drill in most occasions.

Also, by calculating the ratio of thrust force and critical force as shown in equation below, we can define the effect of thrust force on delamination factor.

$$\eta = (F_{tt} - F_{critical}) / F_{critical} \quad (6.3)$$

By applying as an example the critical force and thrust forces values for spindle speed of 5000 rpm and feed rates of 125 mm/min, the calculated ratios of twist drill and double point drill are 17.44% and 0.51% respectively, this leads to the double point drill generates smaller ratios and therefore results in lower delamination factors.

Chapter 7

Conclusion

The innovation and main contributions made in this research are concluded in this chapter. Also, suggestions for future research work are recommended.

7.1 Contributions

A great deal of interest has been received lately for progressive damage modeling of polymer matrix composites as predictive capabilities for the complex nonlinear behaviour of these materials are sought. Analyzing delamination and evaluating its damage on the CFRP workpiece is very important in determining the structural integrity of the machined part. 3D finite element analysis can be used to evaluate and compare different point angles for drills and finding its effect on delamination, hence defects can be controlled with selecting the optimum cutting parameters and drill geometry.

In this research, a new FEA model and new delamination factor called the equivalent adjusted delamination factor F_{eda} is developed for drilling UDCFRP without using a back-up plate to study delamination and it's effecting parameters of cutting speed and feed rate at drilled hole entrance. The study is based on utilizing PCD twist drill and diamond coated double point angle drill in the experiment and finite element analysis. And by using the FEA results can be evaluated to optimize delamination and parameters can be predicted so further machining and delamination can be prevented.

Through FE simulation and experimental analysis, it was found that the thrust force and torque increased with the increase in feed rate and decreased with the increase in spindle speed. Both drills showed the percentage of increase of thrust force and torque when feed rate is increased are much higher than the percentage of decrease when spindle speed is increased. Also results showed delamination increases with the increase of feed rate and decreases with the spindle speed, as delamination increased drastically when feed rate is over 500 mm/min, this leads to being feed rate has more effect than spindle speed on hole entry delamination, it also indicates low feed rates are appropriate for CFRP drilling and the importance of reducing feed rate leads to reducing the axial thrust force to achieve less onset delamination and with better results.

In this study the adjusted delamination factor F_{da} was refined to create an equivalent adjusted delamination factor F_{eda} and was able to discriminate the damage areas and to overcome the null minimal and maximal delamination areas. The trend of variation for F_{eda} is similar to F_d and F_{da}, but F_{eda} had lower percentage error values obtained between the experiment and FEA, all this indicates that the mathe-

matical approach proposed is suitable for characterizing delamination when drilling composites.

Both drills resulted a higher F_{da} than F_d and F_{eda}, as the trend of delamination factors decrease with the increase in spindle speed except for double point angle drill when it reaches over 7500 rpm, as the study showed by using spindle speed of 10000 rpm and different feed rates for both drills, delamination results showed double point angle drill has higher delamination results when using twist drill, this indicates that double point angle drill is not suitable at these drilling conditions.

Drill geometry such as point angle and helix angle have high importance in effecting delamination when drilling CFRP, small point angle and low helix angle are preferred for good hole entrance, in this study both drills have the same helix angle while the double point angle drill has a primary point angle of 130^o which is larger than the twist drill of 120^o, which resulted in a higher thrust force in most occasions and was evident in the double point angle drill. Results showed in the double point angle drill had less delamination than the twist drill, this is mainly due to its critical thrust force as it possess higher values than the critical thrust force for twist drill, this means the double point angle drill was highly affected by the critical thrust force and made it better suited for composite drilling as it has a higher safety free-delamination factor approximately 2.1 times the twist drill.

Ply-based modeling based on Meso-scale is an outstanding base material design and for analyzing mechanisms of composite material behavior and its degradation which are difficult to analyze, while using shell elements reduces the computational time of the simulation process, hence provides an option to model the cutting tool as a flexible body to capture and predict the dynamic effect of machining parameters on the CFRP workpiece . The model was found to be accurate as results of simulations were verified against experimental data, good correlation with experiments has been revealed in terms of predicted delamination area and qualitative representation of external damage.

The majority of researches have used the backing plate when drilling composite materials in their study, while in this study we have eliminated the backing plate in order to assess the delamination and to treat the drilling operation close to production conditions as possible, as using a backing plate will most likely reduce the delamination further. Finite element simulation has showed that when drilling the CFRP without the backing plate the drilling operation tends to work as punching operation in the beginning instead of cutting operation and this will increase the load on the periphery of the drilled hole edges and hence affecting the delamination.

The FE distribution of von mises stress, effective strain, pressure distribution, dis-

placement distribution and Hashin failure mode when the drill has started penetrating the UDCFRP composite workpiece has been presented. The stress distribution and onset damage on the first ply when using the PCD twist drill and double point angle drill shows that von Mises stress is higher than the 90^0 failure tensile strength, which indicates the tensile matrix mode being the dominant failure mode. The simulation of the von Mises stress for both drills shows that there are high stress concentrations along the chisel and cutting edge due to the applied forces, values are higher at the chisel edge and gradually decrease going up to the drill body, from the effective strain, it's evident that it reflects the same distribution as the von Mises distribution along the chisel and cutting edge due to the stress concentration, For the pressure distribution, it shows the maximum pressure is at the cutting edge, which indicates the reason at the experimental stage for the drill bits to start being damaged after drilling many holes. At spindle speed of 10000 rpm and feed rate 1250 mm/min for both drills, FE simulation showed the big effect of drill geometry as double point angle drill showed higher values in von Mises stress, strain, pressure and displacement than the values when using PCD twist drill.

Due to the widely usage of CFRP in various applications, polycrystalline diamond and coated diamond drill bits are the most preferable drills used especially when there are hundreds of holes to be drilled due to it's special properties, such as being one of the hardest material, it also has high stiffness, high thermal conductivity, low coefficient of friction and low thermal expansion. All of these properties are important in drilling CFRP which increases tool life and improves hole quality thereby reducing tool changes and increasing production and tool value.

7.2 Future work

From this study and based on the observations and outcomes, the following recommendations for future work are presented.

This research was based on drilling CFRP using pollycrystalline diamond and diamond coated drills with different point angles, hence more work should be done on comparative study of other different drill materials with different geometries and studying their effect on the drilling induced damage.

The next step in the research efforts in this direction can be the optimization of drill point geometry by simultaneously considering all the geometric parameters of drill and studying their effect on the drilling induced damage. An optimized drill geometry can be developed which may help in making damage free holes in fibrous composites.

Hashin failure criteria has been implemented in this study, determining the deformation behavior of workpiece using different constitutive models and failure criteria is a next step in the right direction in selecting the best failure criteria for a better finite element model.

Investigating the affect of other fibre stacking sequence such as [0/45/90] degrees on cutting parameters and tool wear.

To compare the study with a backing plate in order to assess and evaluate the delamination under different supporting conditions.

Appendix A

VTM260 Series

VTM®260 series

VTM®260 series resins are toughened, 65 to 120°C (149 to 248°F) curing temperature epoxy resin matrices specifically developed for oven vacuum bag processing of large structures. These resins are particularly suited to the marine and industrial markets

Features

- Outstanding vacuum only processing capability on a wide range of reinforcements
- Flexible curing capability
- Up to 30 days out life at 21°C (70°F)
- 12 months storage at -18°C (0°F)
- Service temperature up to 100°C (212°F)
- Available in ZPREG® selective impregnation formats
- Suitable for component and tooling manufacture
- Fully co-curable with the VTM260 range of adhesives, surfacing films and syntactic plies

Product variants

- VTM263: High viscosity, low flow variant - suitable for selective impregnation of fabrics or full impregnation of lightweight fabric reinforcements
- VTM264: Intermediate viscosity and tack - suitable for full impregnation of light and medium weight unidirectional and fabric reinforcements
- VTM266: Low viscosity - suitable for the full impregnation of heavyweight fabric reinforcements up to 2400g/m²
- VTM267: Controlled tack for sided impregnation and film infusion
- VTM267FRB and VTM264FRB: Flame-retarded resin systems are also available, see (PDS1180)

Related documents

- Recommendations for manufacturing large marine mould tools from LTF/VTM260 series materials (TDS1011)
- De-bulking guidelines (TDS1036)
- Oven vacuum bag processing – lay-up and bagging guidelines (TDS1041)

Related products

- VTA260 adhesive film (PDS1174)
- VTS263 syntactic film (PDS1165)
- VTF261 surfacing ply (PDS1194)
- VTF266 surface improvement film (PDS1255)
- FS201 lightweight syntactic filler (PDS1015)
- VTM264-1 prepreg (PDS1268)
- VTM264S-1 prepreg (PDS1268)
- VTM264FRB prepreg (PDS1180)
- VTM267FRB prepreg (PDS1180)

Cure cycle

Vacuum bag pressure	Minimum of 980mbar (29"Hg)*
Ramp rate	0.5 to 2°C (0.9 to 3.6°F)/minute
Minimum temperature cure cycle	16 hours at 65°C (149°F)
Cool down	Maximum of 3°C (5.4°F)/minute to room temperature

*This is the ideal vacuum level, however, it is recognised that it is not always possible to attain. If in doubt, please contact our technical support staff for advice.

Alternative cure cycles

Temperature	Duration
80°C (176°F)	5 hours
100°C (212°F)	2 hours
120°C (248°F)	1 hour

Post-cure

In applications demanding maximum temperature or environmental resistance, it is essential that the component is post-cured to fully develop the glass transition temperature.

Ramp rate	0.3°C (0.5°F)/minute
Post-cure cycle	Minimum of 1 hour at 120°C -0/+2°C (248°F-0/+4°F)*
Cool down	Maximum of 3°C (5.4°F)/minute to 60°C (140°F)

* Temperature must be measured by the lagging thermocouple attached to the part.

Notes:

- Parts may be loaded into a pre-heated oven or heated at 3°C (5.4°F)/minute to the initial cure temperature.
- Large components should be adequately supported to avoid distortion.
- Alternative post-cures are possible. Please contact our technical support staff for advice.

Physical properties

Resin selector guide

Resin	Tack at 15°C (60°F)	Tack at 21°C (70°F)	Glass UD	Carbon UD	Glass woven	Carbon woven
VTM263	low	low/medium	N/A	N/A	<300 g/m^2	<300 g/m^2
VTM264	low	medium	<400 g/m^2	<600 g/m^2	<900 g/m^2	<900 g/m^2
VTM266	medium	high	<600 g/m^2	<600 g/m^2	>900 g/m^2	>900 g/m^2
VTM267	very low	low	differential coating of heavy reinforcements			

Test	Sample cure conditions		Results
Cured resin density	1 hour at 120°C (248°F)		1.20 g/cm^3
DMA E' onset Tg	16 hours at 65°C (149°F), dry 5 hours at 80°C (176°F), dry 2 hours at 100°C (212°F), dry 1 hour at 120°C (248°F), dry	All variants	80°C (176°F) 95°C (203°F) 115°C (239°F) 120°C (248°F)

Dynamic viscosity at 2°C (3.6°F)/minute

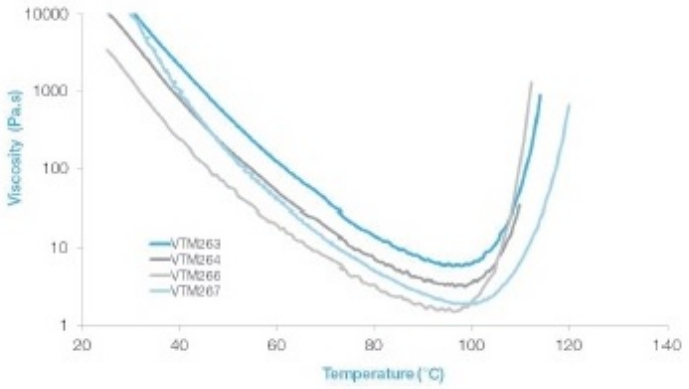

Mechanical properties

Material: VTM264/CF0302*-42%
Cure cycle: 5 hours at 80°C (176°F), oven vacuum bag cure
Test conditions: Room temperature, dry

Property	Test method	Units	Results
0° Tensile strength	ASTM D3039	MPa (ksi)	700 (102)
0° Tensile modulus		GPa (msi)	60.0 (8.70)
90° Tensile strength		MPa (ksi)	745 (108)
90° Tensile modulus		GPa (msi)	60.5 (8.77)
0° Compressive strength	ASTM D3410	MPa (ksi)	540 (78.3)
0° Compressive modulus		GPa (msi)	54.0 (7.83)
90° Compressive strength		MPa (ksi)	560 (81.2)
90° Compressive modulus		GPa (msi)	53.0 (7.69)
In-plane shear strength (IPSS)	ASTM D3518	MPa (ksi)	95.0 (13.8)
In-plane shear modulus (IPSM)		GPa (msi)	3.90 (0.57)
0° Interlaminar shear strength (ILSS)	ASTM D2344	MPa (ksi)	71.0 (10.3)

Data normalised to 55%Vf except for ILSS and IPSS & IPSM.

*CF0302 is a 2x2 twill, 199 g/m^2 fabric with 3k FT300B 40B fibres.

Material: VTM264/T700-35%
Cure cycle: 5 hours at 80°C (176°F), oven vacuum bag cure
Test conditions: Room temperature, dry

Property	Test method	Units	Results
0° Tensile strength	ASTM D3039	MPa (ksi)	2575 (374)
0° Tensile modulus		GPa (msi)	131 (19.0)
90° Tensile strength		MPa (ksi)	40 (5.80)
90° Tensile modulus		GPa (msi)	9.1 (1.32)
0° Compressive strength	ASTM D695 (MOD)	MPa (ksi)	1235 (179)
0° Compressive modulus		GPa (msi)	118 (17.1)
90° Compressive strength		MPa (ksi)	182 (26.4)
90° Compressive modulus		GPa (msi)	-
In-plane shear strength (IPSS)	ASTM D3518	MPa (ksi)	85.7 (12.4)
In-plane shear modulus (IPSM)		GPa (msi)	3.94 (0.57)
0° Interlaminar shear strength (ILSS)	ASTM D2344	MPa (ksi)	88.6 (12.9)

Data normalised to 60%Vf except for ILSS and IPSS & IPSM.

Availability

VTM260 series prepregs are available in a wide range of reinforcing fabrics and unidirectional tapes including glass, carbon, aramid and hybrids. Materials can also be supplied in full and ZPREG selectively impregnated formats.

Storage

Out life* at 21°C (70°F)	VTM263 VTM264 VTM266	30 days
	VTM267	21 days
Storage at -18°C (0°F)	12 months from date of manufacture	

*Out life refers to accumulated time out of the freezer before the part is cured

Note:
The actual freezer storage life and out life are dependent on a number of factors, including fibre type, format and application. For certain formats, it may be possible for the storage life and out life to be longer than stated. Please contact our technical support staff for advice.

Exotherm

VTM260 prepregs are reactive formulations which can undergo severe exothermic heat up during the initial curing process if incorrect curing procedures are followed.

Great care must be taken to ensure that safe heating rates, dwell temperatures and lay-up/bagging procedures are adhered to, especially when moulding solid laminates in excess of 10mm (0.4in) thickness. The risk of exotherm increases with lay-up thickness and increasing cure temperature. It is strongly recommended that trials, representative of all the relevant circumstances, are carried out by the user to allow a safe cure cycle to be specified. It is also important to recognise that the model or tool material and its thermal mass, combined with the insulating effect of breather/bagging materials can affect the risk of exotherm in particular cases.

Please contact our technical department for further information on exotherm behaviour of these systems.

Health & safety

VTM260 series resin systems contain epoxy resins which can cause allergic reaction on prolonged or repeated skin contact. Avoid contact with the skin. Gloves and protective clothing must be worn.

Wash skin thoroughly with soap and water or resin removing cream after handling. Do not use solvents for cleaning the skin.

Use mechanical exhaust ventilation when heat curing the resin system. Exhaust from vacuum pumps should be vented to external atmosphere and not into the work place.

For further information, consult Cytec Safety Data Sheet numbers:

VTM263	SDS 350
VTM264	SDS 338
VTM266	SDS 339
VTM267	SDS 483

Bibliography

[1] DeFu Liu, YongJun Tang, and W.L. Cong. "A review of mechanical drilling for composite laminates". In: *Composite Structures* 94.4 (2012), pp. 1265–1279.

[2] Ruizhen Yang, Yunze He, and Hong Zhang. "Progress and trends in nondestructive testing and evaluation for wind turbine composite blade". In: *Renewable and Sustainable Energy Reviews* 60 (2016), pp. 1225–1250.

[3] C Red. "Wind turbine blades: Big and getting bigger". In: *Composites Technology* 6 (2008), pp. 42–47.

[4] Vaibhav A Phadnis et al. "Drilling in carbon/epoxy composites: Experimental investigations and finite element implementation". In: *Composites Part A: Applied Science and Manufacturing* 47.0 (2013), pp. 41–51.

[5] C C Tsao, H Hocheng, and Y C Chen. "Delamination reduction in drilling composite materials by active backup force". In: *CIRP Annals - Manufacturing Technology* 61.1 (2012), pp. 91–94.

[6] Jaroslav Mackerle. "Finite-element analysis and simulation of machining: a bibliography (1976–1996)". In: *Journal of Materials Processing Technology* 86.1–3 (1998), pp. 17–44.

[7] Richard Garrick. "Drilling Advanced Aircraft Structures with PCD (Polycrystalline Diamond) Drill". In: *Precorp Inc* (2007).

[8] Yiğit Karpat, Onur Bahtiyar, and Burak Değer. "Mechanistic force modeling for milling of unidirectional carbon fiber reinforced polymer laminates". In: *International Journal of Machine Tools and Manufacture* 56.0 (2012), pp. 79–93.

[9] Chinmaya R Dandekar and Yung C Shin. "Modeling of machining of composite materials: A review". In: *International Journal of Machine Tools and Manufacture* 57.0 (2012), pp. 102–121.

[10] L C Zhang. "Cutting composites: A discussion on mechanics modelling". In: *Journal of Materials Processing Technology* 209.9 (2009), pp. 4548–4552.

[11] R El Alaiji, L Lasri, and A Bouayad. "3D finite element modeling of chip formation and induced damage in machining fiber reinforced composites". In: *American Journal of Engineering Research (AJER)* 4.7 (2015), pp. 123–132.

[12] George H Staab. *Laminar composites*. Butterworth-Heinemann, 1999. ISBN: 1-281-07144-7.

[13] Flake C Campbell. *Structural composite materials*. ASM International, 2010. ISBN: 9781615030378.

[14] Salar Bagherpour. "Fibre reinforced polyester composites". In: *Edited by Hosam El-Din M. Saleh* (2012), p. 167.

[15] A Kukner and B S Sarioglu. "Composite sructure design in passenger ship using multi-objective optimization algorithm". In: *Proceedings of a meeting held 4-5 November 2014, Makassar, Indonesia (ICSOT 2014): Development in Ship Design and Construction*. 2014.

[16] Stuart M Lee and Knovel, eds. *Handbook of composite reinforcements*. New York: VCH, 1993.

[17] Hexcel Corporation, ed. *Publication No. FGU 017c*. 2013.

[18] A A Baker, Donald Kelly, and Stuart Dutton. *Composite materials for aircraft structures*. 2nd ed. American Institute of Aeronautics and Astronautics, 2004.

[19] Luís Miguel P Durão et al. "Damage evaluation of drilled carbon/epoxy laminates based on area assessment methods". In: *Composite Structures* 96.0 (2013), pp. 576–583.

[20] A M Abrão et al. "Drilling of fiber reinforced plastics: A review". In: *Journal of Materials Processing Technology* 186.1–3 (2007), pp. 1–7.

[21] P K Rakesh et al. "Delamination in fiber reinforced plastics: a finite element approach". In: *Engineering* 03.05 (2011), p. 549.

[22] J S Strenkowski, C C Hsieh, and A J Shih. "An analytical finite element technique for predicting thrust force and torque in drilling". In: *International Journal of Machine Tools and Manufacture* 44.12–13 (2004), pp. 1413–1421.

[23] Merlin Barschke et al. "Finite element modeling of composite materials using kinematic constraints". In: *Ingeniería y ciencia* 10 (2009), pp. 133–153.

[24] Luís Miguel P Durão et al. "Comparative analysis of drills for composite laminates". In: *Journal of Composite Materials* 46.14 (2012), pp. 1649–1659.

[25] Li Zhou et al. “Finite element and experimental studies of the cutting process of SiCp/Al composites with PCD tools”. English. In: *The International Journal of Advanced Manufacturing Technology* 52.5-8 (2011), pp. 619–626.

[26] Erik Persson, Ingvar Eriksson, and Leif Zackrisson. “Effects of hole machining defects on strength and fatigue life of composite laminates”. In: *Composites Part A: Applied Science and Manufacturing* 28.2 (1997), pp. 141–151.

[27] U A Khashaba et al. “Drilling analysis of woven glass fiber-reinforced/epoxy composites”. In: *Journal of Composite Materials* 47.2 (2013), pp. 191–205.

[28] C C Tsao. “Prediction of thrust force of step drill in drilling composite material by Taguchi method and radial basis function network”. English. In: *The International Journal of Advanced Manufacturing Technology* 36.1-2 (2008), pp. 11–18.

[29] Marta Fernandes and Chris Cook. “Drilling of carbon composites using a one shot drill bit. Part II: empirical modeling of maximum thrust force”. In: *International Journal of Machine Tools and Manufacture* 46.1 (2006), pp. 76–79.

[30] Miao Chao et al. “Integrated design and analysis of diamond-coated drills”. In: *Computer-Aided Design & Applications (Computer-Aided Design & Applications)* 6.2 (2009), pp. 195–205.

[31] S V Muthukrishna Selvam and C Sujatha. “Twist drill deformation and optimum drill geometry”. In: *Computers & Structures* 57.5 (1995), pp. 903–914.

[32] E Abele and M Fujara. “Simulation-based twist drill design and geometry optimization”. In: *CIRP Annals - Manufacturing Technology* 59.1 (2010), pp. 145–150.

[33] Yiğit Karpat, Burak Değer, and Onur Bahtiyar. “Drilling thick fabric woven CFRP laminates with double point angle drills”. In: *Journal of Materials Processing Technology* 212.10 (2012), pp. 2117–2127.

[34] Xin Wang et al. “Tool wear of coated drills in drilling CFRP”. In: *Journal of Manufacturing Processes* 15.1 (2013), pp. 127–135.

[35] Kyung-Hee Park et al. “Tool wear in drilling of composite/titanium stacks using carbide and polycrystalline diamond tools”. In: *Wear* 271.11–12 (2011), pp. 2826–2835.

[36] Ali Faraz, Dirk Biermann, and Klaus Weinert. “Cutting edge rounding: An innovative tool wear criterion in drilling CFRP composite laminates”. In: *International Journal of Machine Tools and Manufacture* 49.15 (2009), pp. 1185–1196.

[37] Sanjay Rawat and Helmi Attia. “Wear mechanisms and tool life management of WC–Co drills during dry high speed drilling of woven carbon fibre composites”. In: *Wear* 267.5–8 (2009), pp. 1022–1030.

[38] S C Lin and I K Chen. “Drilling carbon fiber-reinforced composite material at high speed”. In: *Wear* 194.1 (1996), pp. 156–162.

[39] Wen-Chou Chen. “Some experimental investigations in the drilling of carbon fiber-reinforced plastic (CFRP) composite laminates”. In: *International Journal of Machine Tools and Manufacture* 37.8 (1997), pp. 1097–1108.

[40] D Iliescu et al. “Modeling and tool wear in drilling of CFRP”. In: *International Journal of Machine Tools and Manufacture* 50.2 (2010), pp. 204–213.

[41] F Klocke and C Wurtz. “PCD in the machining of fibre-reinforced materials”. In: *IDR. Industrial diamond review* 59.580 (1999).

[42] J Paulo Davim and C A Conceição António. “Optimal drilling of particulate metal matrix composites based on experimental and numerical procedures”. In: *International Journal of Machine Tools and Manufacture* 41.1 (2001), pp. 21–31.

[43] Farhad Nabhani. “Machining of aerospace titanium alloys”. In: *Robotics and Computer-Integrated Manufacturing* 17.1–2 (2001), pp. 99–106.

[44] R Teti. “Machining of composite materials”. In: *CIRP Annals - Manufacturing Technology* 51.2 (2002), pp. 611–634.

[45] M Ramulu, P Young, and H Kao. “Drilling of graphite/bismaleimide composite material”. In: *Journal of Materials Engineering and Performance* 8.3 (1999), pp. 330–338.

[46] D Samuel Raj and L Karunamoorthy. “Study of the effect of tool wear on hole quality in drilling cfrp to select a suitable drill for multi-criteria hole quality”. In: *Materials and Manufacturing Processes* (2015), null–null.

[47] Jinyang Xu, Qinglong An, and Ming Chen. “A comparative evaluation of polycrystalline diamond drills in drilling high-strength T800S/250F CFRP”. In: *Composite Structures* 117.0 (2014), pp. 71–82.

[48] Eshetu D Eneyew and Mamidala Ramulu. “Experimental study of surface quality and damage when drilling unidirectional CFRP composites”. In: *Journal of Materials Research and Technology* 3.4 (2014), pp. 354–362.

[49] I S Shyha et al. “Hole quality assessment following drilling of metallic-composite stacks”. In: *International Journal of Machine Tools and Manufacture* 51.7–8 (2011), pp. 569–578.

[50] E Brinksmeier, S Fangmann, and R Rentsch. “Drilling of composites and resulting surface integrity”. In: *CIRP Annals - Manufacturing Technology* 60.1 (2011), pp. 57–60.

[51] Luís Miguel P Durão et al. “Drilling tool geometry evaluation for reinforced composite laminates”. In: *Composite Structures* 92.7 (2010), pp. 1545–1550.

[52] T J Grilo et al. “Experimental delamination analyses of CFRPs using different drill geometries”. In: *Composites Part B: Engineering* 45.1 (2013), pp. 1344–1350.

[53] V N Gaitonde et al. “A study aimed at minimizing delamination during drilling of CFRP composites”. In: *Journal of Composite Materials* 45.22 (2011), pp. 2359–2368.

[54] Andreas Haeger et al. “Non-destructive detection of drilling-induced delamination in cfrp and its effect on mechanical properties”. In: *Procedia Engineering* 149 (2016), pp. 130–142.

[55] Z Li et al. “Detection and evaluation of damage in aircraft composites using electromagnetically coupled inductors”. In: *Composite Structures* 140 (2016), pp. 252–261.

[56] J Babu et al. *Delamination in composite materials: Measurement, assessment and prediction*. Vol. 4, pp. 139–162.

[57] Edoardo Capello. “Workpiece damping and its effect on delamination damage in drilling thin composite laminates”. In: *Journal of Materials Processing Technology* 148.2 (2004), pp. 186–195.

[58] C C Tsao and H Hocheng. “Effects of exit back-up on delamination in drilling composite materials using a saw drill and a core drill”. In: *International Journal of Machine Tools and Manufacture* 45.11 (2005), pp. 1261–1270.

[59] V A Phadnis, A Roy, and V V Silberschmidt. “Finite element analysis of drilling in carbon fiber reinforced polymer composites”. In: *Journal of Physics: Conference Series*. Vol. 382. 1. IOP Publishing, 2012, p. 12014.

[60] Brett A Bednarcyk et al. “Meso- and micro-scale modeling of damage in plain weave composites”. In: *Composite Structures* 121 (2015), pp. 258–270.

[61] Jaroslav Mackerle. “Finite-element analysis and simulation of machining: a bibliography (1976–1996)”. In: *Journal of Materials Processing Technology* 86.1–3 (1999), pp. 17–44.

[62] J Mackerle. “Finite element analysis and simulation of machining: an addendum: A bibliography (1996–2002)”. In: *International Journal of Machine Tools and Manufacture* 43.1 (2003), pp. 103–114.

[63] S. L. Soo and D. K. Aspinwall. “Developments in modelling of metal cutting processes”. In: *Proceedings of the Institution of Mechanical Engineers* 221 (Oct. 2007), pp. 197–211.

[64] S M Athavale and J S Strenkowski. “Finite element modeling of machining: from proof-of-concept to engineering applications”. In: *Machining Science and Technology* 2.2 (1998), pp. 317–342.

[65] Ozden Isbilir and Elaheh Ghassemieh. “Finite element analysis of drilling of carbon fibre reinforced composites”. English. In: *Applied Composite Materials* 19.3-4 (2012), pp. 637–656.

[66] Ozden Isbilir and Elaheh Ghassemieh. “Numerical investigation of the effects of drill geometry on drilling induced delamination of carbon fiber reinforced composites”. In: *Composite Structures* 105.0 (2013), pp. 126–133.

[67] Chinmaya R Dandekar and Yung C Shin. “Multiphase finite element modeling of machining unidirectional composites: prediction of debonding and fiber damage”. In: *Journal of Manufacturing Science and Engineering* 130.5 (2008), p. 51016.

[68] Bo-Lin Hsu. *Computer simulations for burr formation study*. 2002.

[69] O C Zienkiewicz, R L Taylor, and J Z Zhu. “18 - Multiscale modelling*”. In: *The Finite Element Method Set (Sixth Edition)*. Oxford: Butterworth-Heinemann, 2005, pp. 547–589.

[70] Wing Kam Liu et al. “Preface: special issue of computational mechanics on “Connecting Multiscale Mechanics to Complex Material Design””. In: *Computational Mechanics* 57.3 (2016), pp. 355–357.

[71] Leon Mishnaevsky. “Mesoscale level in the mechanics of materials”. In: *Computational Mesomechanics of Composites*. John Wiley & Sons, Ltd, 2007, pp. 13–36.

[72] T Niezgoda and A Derewońko. “Multiscale composite FEM modeling”. In: *Procedia Engineering* 1.1 (2009), pp. 209–212.

[73] Aleksandr Cherniaev and Igor Telichev. “Meso-scale modeling of hypervelocity impact damage in composite laminates”. In: *Composites Part B: Engineering* 74.0 (2015), pp. 95–103.

[74] B Stier, J W Simon, and S Reese. “Comparing experimental results to a numerical meso-scale approach for woven fiber reinforced plastics”. In: *Composite Structures* 122.0 (2015), pp. 553–560.

[75] G Lubineau, P Ladevèze, and D Violeau. “Durability of CFRP laminates under thermomechanical loading: A micro–meso damage model”. In: *Composites Science and Technology* 66.7–8 (2006), pp. 983–992.

[76] Min-Gu Han and Seung-Hwan Chang. “Failure analysis of a Type III hydrogen pressure vessel under impact loading induced by free fall”. In: *Composite Structures* 127 (2015), pp. 288–297.

[77] P Nali and E Carrera. “A numerical assessment on two-dimensional failure criteria for composite layered structures”. In: *Composites Part B: Engineering* 43.2 (2012), pp. 280–289.

[78] Jamal Echaabi, Franclois Trochu, and Raymond Gauvin. “Review of failure criteria of fibrous composite materials”. In: *Polymer Composites* 17.6 (1996), pp. 786–798.

[79] Vaibhav A Phadnis et al. “Experimental and numerical investigations in conventional and ultrasonically assisted drilling of cfrp laminate”. In: *Procedia CIRP* 1 (2012), pp. 455–459.

[80] Vaibhav A Phadnis, Anish Roy, and Vadim V Silberschmidt. “A finite element model of ultrasonically assisted drilling in carbon/epoxy composites”. In: *Procedia CIRP* 8 (2013), pp. 141–146.

[81] Jinyang Xu and Mohamed El Mansori. “Cutting modeling of hybrid CFRP/Ti composite with induced damage analysis”. In: *Materials* 9.1 (2016), p. 22.

[82] L Lasri, M Nouari, and M El Mansori. “Modelling of chip separation in machining unidirectional FRP composites by stiffness degradation concept”. In: *Composites Science and Technology* 69.5 (2009), pp. 684–692.

[83] J Limido et al. “SPH method applied to high speed cutting modelling”. In: *International Journal of Mechanical Sciences* 49.7 (2007), pp. 898–908.

[84] R Izamshah RA, John P T Mo, and Songlin Ding. “Hybrid deflection prediction on machining thin-wall monolithic aerospace component”. In: *Journal of Engineering Manufacture* 226.4 (), pp. 592–605.

[85] V E Panin et al. “Physical mesomechanics of materials”. English. In: *Russian Physics Journal* 41.9 (1998), pp. 856–884.

[86] K I Tserpes, P Papanikos, and Th Kermanidis. “Progressive fatigue damage modeling of CFRP laminates at the mesoscale level”. In: *Proceedings of the International Symposium of Multiscaling Mechanics, Messini, Greece*. 2002.

[87] H A Israr et al. “Finite element simulation of 0/90 CFRP laminated plates subjected to crushing using a free-face-crushing concept”. In: *Composites Part A: Applied Science and Manufacturing* 62 (2014), pp. 16–25.

[88] P Ladeveze and G Lubineau. “On a damage mesomodel for laminates: micro–meso relationships, possibilities and limits”. In: *Composites Science and Technology* 61.15 (2001), pp. 2149–2158.

[89] Vladimir S Sokolinsky, Kyle C Indermuehle, and Juan A Hurtado. “Numerical simulation of the crushing process of a corrugated composite plate”. In: *Composites Part A: Applied Science and Manufacturing* 42.9 (2011), pp. 1119–1126.

[90] A Needleman. “Computational mechanics at the mesoscale”. In: *Acta Materialia* 48.1 (2000), pp. 105–124.

[91] C J Mitchell et al. “A discrete mesoscopic finite element model used as a design tool for textile composite structures”. In: *Proceedings of the American Society for Composites: Twenty-ninth Technical Conference on Composite Materials*. 2014.

[92] Ing Ulrich Stelzmann and Ing Matthias Hörmann. “Ply-based composite modeling with the new* ELEMENT_SHELL_COMPOSITE keyword”. In: *Proceedings of the 8th European LS-DYNA Users Conference, Strasbourg*. 2011.

[93] ANSYS. *ANSYS composite preppost user’s guide. Release 15.0 edn.* Canonsburg, United States of America, 2013.

[94] N Feito et al. “Numerical prediction of delamination in CFRP drilling”. In: *Composite Structures* 108.0 (2014), pp. 677–683.

[95] N Feito et al. “Numerical analysis of the influence of tool wear and special cutting geometry when drilling woven CFRPs”. In: *Composite Structures* 138 (2016), pp. 285–294.

[96] L M P Durao, M F S F de Moura, and A T Marques. “Numerical prediction of delamination onset in carbon/epoxy composites drilling”. In: *Engineering Fracture Mechanics* 75.9 (2008), pp. 2767–2778.

[97] L M P Durao, M F S F de Moura, and A T Marques. “Numerical simulation of the drilling process on carbon/epoxy composite laminates”. In: *Composites Part A: Applied Science and Manufacturing* 37.9 (2006), pp. 1325–1333.

[98] I Singh, N Bhatnagar, and P Viswanath. “Drilling of uni-directional glass fiber reinforced plastics: Experimental and finite element study”. In: *Materials & Design* 29.2 (2008), pp. 546–553.

[99] L A Burns et al. “Strength improvement to composite T-joints under bending through bio-inspired design”. In: *Composites Part A: Applied Science and Manufacturing* 43.11 (2012), pp. 1971–1980.

[100] N Sato, M Hojo, and M Nishikawa. “Intralaminar fatigue crack growth properties of conventional and interlayer toughened CFRP laminate under mode I loading”. In: *Composites Part A: Applied Science and Manufacturing* 68 (2015), pp. 202–211.

[101] Robert M Jones. *Mechanics of composite materials*. 2nd. Taylor and Francis, 1999.

[102] R Roos, G Kress, and P Ermanni. “A post-processing method for interlaminar normal stresses in doubly curved laminates”. In: *Composite Structures* 81.3 (2007), pp. 463–470.

[103] Z Hashin. “Failure criteria for unidirectional fiber composites”. In: *Journal of Applied Mechanics* 47.2 (1980), pp. 329–334.

[104] Pedro P Camanho and Carlos G Dávila. “Mixed-mode decohesion finite elements for the simulation of delamination in composite materials”. In: *NASA/TM-2002-211737* (2002).

[105] Cytex Industrial Materials, ed. *Publication No. PDS1154 07.13 Issue9a*. 2013.

[106] Seco Tools, ed. *Publication No. 2012-06-29*. 2012.

[107] J Paulo Davim et al. “Finite element simulation and experimental analysis of orthogonal cutting of an aluminium alloy using polycrystalline diamond tools”. In: *International Journal of Materials and Product Technology* 37.1-2 (2009), pp. 46–59.

[108] Haruyo Fukui et al. “Cutting performance of DLC coated tools in dry machining aluminum alloys”. In: *Surface and Coatings Technology* 187.1 (2004), pp. 70–76.

[109] C H Shen. “The importance of diamond coated tools for agile manufacturing and dry machining”. In: *Surface and Coatings Technology* 86 (1996), pp. 672–677.

[110] Kistler, ed. *Quartz 3-component dynamometer type 9257B instruction manual*.

[111] Kistler, ed. *Multi-channel charge amplifier type 5070A instruction manual*.

[112] Songmei Yuan et al. “Development of a cutting force prediction model based on brittle fracture for carbon fiber reinforced polymers for rotary ultrasonic drilling”. In: *The International Journal of Advanced Manufacturing Technology* 81.5 (2015), pp. 1223–1231.

[113] Chenwei Shan et al. “Three-dimensional numerical simulation for drilling of 2.5D carbon/carbon composites”. In: *The International Journal of Advanced Manufacturing Technology* (2017).

[114] Nagaraja Shetty et al. “A review on finite element method for machining of composite materials”. In: *Composite Structures* 176 (2017), pp. 790–802.

[115] H Hocheng and C C Tsao. “The path towards delamination-free drilling of composite materials”. In: *Journal of Materials Processing Technology* 167.2 (2005), pp. 251–264.

[116] J Sedláček and A Humár. “Analysis of fracture mechanisms and surface quality in drilling of composite materials”. In: *Strength of Materials* 40.1 (2008), pp. 40–43.

[117] Hou Jiang Zhang et al. “Assessment of the exit defects in carbon fibre-reinforced plastic plates caused by drilling”. In: *Key Engineering Materials* 196 (2001), pp. 43–52.

[118] H Hocheng and C C Tsao. “The path towards delamination-free drilling of composite materials”. In: *Journal of Materials Processing Technology* 167.2 (2005), pp. 251–264.

[119] António T Marques et al. “Delamination analysis of carbon fibre reinforced laminates: Evaluation of a special step drill”. In: *Composites Science and Technology* 69.14 (2009), pp. 2376–2382.

[120] M R Vaziri Sereshk and H Mohmmadi Bidhendi. “Evaluation of revealing and quantifying techniques available for drilling delamination in woven carbon fiber-reinforced composite laminates”. In: *Journal of Composite Materials* 50.10 (2015), pp. 1377–1385.

[121] Ozden Isbilir and Elaheh Ghassemieh. “Delamination and wear in drilling of carbon-fiber reinforced plastic composites using multilayer TiAlN/TiN PVD-coated tungsten carbide tools”. In: *Journal of Reinforced Plastics and Composites* 31.10 (2012), pp. 717–727.

[122] A Soni M Mehta T Reinhart. “Effect of fastener hole drilling anomalies on structural integrity of PMR-15/Gr composite laminates”. In: *Proceedings of the Machining Composite Materials Symposium, ASM Materials Week* (1992), pp. 113–126.

[123] J Paulo Davim, J Campos Rubio, and A M Abrao. “A novel approach based on digital image analysis to evaluate the delamination factor after drilling composite laminates”. In: *Composites Science and Technology* 67.9 (2007), pp. 1939–1945.

[124] J Babu et al. “Examination and modification of equivalent delamination factor for assessment of high speed drilling”. In: *Journal of Mechanical Science and Technology* 30.11 (2016), pp. 5159–5165.

[125] C C Tsao, K L Kuo, and I C Hsu. “Evaluation of a novel approach to a delamination factor after drilling composite laminates using a core–saw drill”. In: *The International Journal of Advanced Manufacturing Technology* 59.5 (2012), pp. 617–622.

[126] V A Nagarajan, S Sundaram, and J S Rajadurai. “A novel approach based on digital image analysis to evaluate refined delamination factor for E-Glass 21xK43 Gevetex/LY556/DY063 epoxy composite laminates”. In: *Proceedings of the Institution of Mechanical Engineers, Part B: Journal of Engineering Manufacture* 225.10 (2011), pp. 1977–1982.

[127] Stefan Klotz et al. “Influence of clamping systems during drilling carbon fiber reinforced plastics”. In: *Procedia CIRP* 13.Supplement C (2014), pp. 208–213. ISSN: 2212-8271.

[128] Stefan Klotz et al. “Experimental investigation of clamping systems and the resulting change of cutting conditions while drilling carbon fiber reinforced plastics”. In: *Procedia CIRP* 62.Supplement C (2017), pp. 15–20. ISSN: 2212-8271.